

RL-TR-95-269  
Final Technical Report  
January 1996



# ENHANCED CAPABILITIES OF ADVANCED AIRBORNE RADAR SIMULATION

The MITRE Corporation

V.N. Suresh Babu and J.A. Torres

19960206 124

*APPROVED FOR PUBLIC RELEASE; DISTRIBUTION UNLIMITED.*

DTIC QUALITY INSPECTED 1

Rome Laboratory  
Air Force Materiel Command  
Rome, New York

This report has been reviewed by the Rome Laboratory Public Affairs Office (PA) and is releasable to the National Technical Information Service (NTIS). At NTIS, it will be releasable to the general public, including foreign nations.

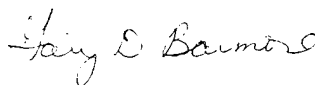
RL-TR-95- 269 has been reviewed and is approved for publication.

APPROVED:



JOHN V. MCNAMARA  
Project Engineer

FOR THE COMMANDER:



GARY D. BARMORE, Major, USAF  
Deputy Director of Surveillance & Photonics

If your address has changed or if you wish to be removed from the Rome Laboratory mailing list, or if the addressee is no longer employed by your organization, please notify Rome Laboratory/ ( OCSA ), Rome NY 13441. This will assist us in maintaining a current mailing list.

Do not return copies of this report unless contractual obligations or notices on a specific document require that it be returned.

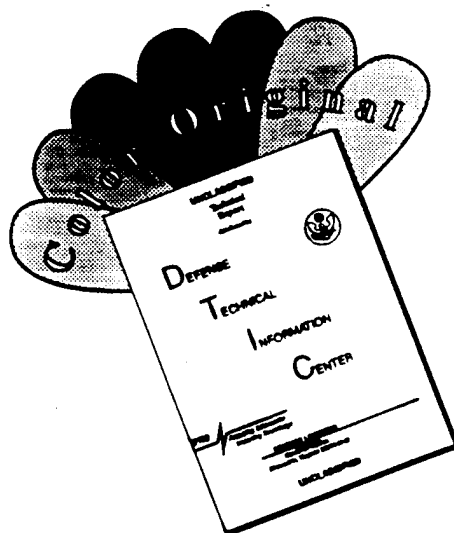
# REPORT DOCUMENTATION PAGE

Form Approved  
OMB No. 0704-0188

Public reporting burden for this collection of information is estimated to average 1 hour per response, including the time for reviewing instructions, searching existing data sources, gathering and maintaining the data needed, and completing and reviewing the collection of information. Send comments regarding this burden estimate or any other aspect of this collection of information, including suggestions for reducing this burden, to Washington Headquarters Services, Directorate for Information Operations and Reports, 1215 Jefferson Davis Highway, Suite 1204, Arlington, VA 22202-4302, and to the Office of Management and Budget, Paperwork Reduction Project (0704-0188), Washington, DC 20503.

1. AGENCY USE ONLY (Leave Blank)		2. REPORT DATE January 1996		3. REPORT TYPE AND DATES COVERED Final Oct 93 - Sep 94	
4. TITLE AND SUBTITLE ENHANCED CAPABILITIES OF ADVANCED AIRBORNE RADAR SIMULATION				5. FUNDING NUMBERS C - F19628-94-C-0001 PE - 62702F PR - 4506 TA - PR WU - OJ	
6. AUTHOR(S) B.N. Suresh Babu and J.A. Torres					
7. PERFORMING ORGANIZATION NAME(S) AND ADDRESS(ES) The MITRE Corporation Burlington Road Bedford MA 01730-0208				8. PERFORMING ORGANIZATION REPORT NUMBER  N/A	
9. SPONSORING/MONITORING AGENCY NAME(S) AND ADDRESS(ES) Rome Laboratory/OCSA 26 Electronic Pky Rome NY 13441-4514				10. SPONSORING/MONITORING AGENCY REPORT NUMBER  RL-TR-95-269	
11. SUPPLEMENTARY NOTES Rome Laboratory Project Engineer: John V. McNamara/OCSA/(315) 330-4441					
12a. DISTRIBUTION/AVAILABILITY STATEMENT Approved for public release; distribution unlimited.				12b. DISTRIBUTION CODE	
13. ABSTRACT (Maximum 200 words) MITRE has enhanced the capabilities of the Advanced Airborne Radar Simulation, a flexible end-to-end steady-state simulation that can be used to evaluate the critical issues affecting the performance of advanced airborne radars that use adaptive antenna techniques, i.e., space-time processing (STP), for both jamming and clutter suppression. For a large phased-array antenna, the limitations of a practical implementation of optimal STP will generally require suboptimal adaptive array architectures, such as element space, beam space, and subarrays. The simulation was modified to augment these suboptimal architectures with spatial degrees of freedom in elevation. The received signal models, i.e., target, jamming, and clutter, were modified to include the effects of near-field scattering using a multiple point scatterer model.					
14. SUBJECT TERMS Advanced airborne radar simulation, Steady-state simulation, space-time processing, suboptimal adaptive array architectures, subarrays, near-field scattering				15. NUMBER OF PAGES 116	
				16. PRICE CODE	
17. SECURITY CLASSIFICATION OF REPORT UNCLASSIFIED	18. SECURITY CLASSIFICATION OF THIS PAGE UNCLASSIFIED	19. SECURITY CLASSIFICATION OF ABSTRACT UNCLASSIFIED	20. LIMITATION OF ABSTRACT UL		

# DISCLAIMER NOTICE



THIS DOCUMENT IS BEST QUALITY AVAILABLE. THE COPY FURNISHED TO DTIC CONTAINED A SIGNIFICANT NUMBER OF COLOR PAGES WHICH DO NOT REPRODUCE LEGIBLY ON BLACK AND WHITE MICROFICHE.

## ABSTRACT

MITRE has enhanced the capabilities of the Advanced Airborne Radar Simulation, a flexible end-to-end steady-state simulation that can be used to evaluate the critical issues affecting the performance of advanced airborne radars that use adaptive antenna techniques (i.e., space-time processing (STP)) for both jamming and clutter suppression. For a large phased-array antenna, the limitations of a practical implementation of optimal STP will generally require suboptimal adaptive array architectures such as element space, beam space, and subarrays. The simulation was modified to augment these suboptimal architectures with spatial degrees of freedom in elevation. The received signal models (i.e., target, jamming, and clutter) were modified to include the effects of near-field scattering using a multiple point scatterer model. The simulation was interfaced with the NEC BSC geometric theory of diffraction (GTD) ray-tracing simulation to provide a more accurate model of antenna-aircraft interactions for the received clutter signal. The simulation was modified to allow the capability to read additional elemental taper weights. This capability allows modeling of non-dispersive antenna errors, beam spoiling techniques, predictive-nulling and alternative non-adaptive aperture weighting, and any antenna aperture configurable within a planar grid such as an elliptical array. The supporting documentation provides a global view of all of the simulation features, a description of the simulation inputs and outputs, and a set of typical examples showing how to run the enhanced simulation. An illustrative example is provided to show how the simulation can be used to create performance benchmarks for the Rome Laboratory's Multichannel Airborne Radar Measurements (MCARM) Program.

## **ACKNOWLEDGMENTS**

We are indebted to Sheila A. Robertshaw for her expert typing.

## TABLE OF CONTENTS

SECTION	PAGE
1 Introduction	1
1.1 Background	1
1.2 Simulation Enhancements	3
1.2.1 Elevation Degrees of Freedom	3
1.2.2 Near-Field Scattering	5
1.2.3 Additional Elemental Tapering	7
1.3 Overview	7
1.4 Summary	7
2 Illustrative Examples	9
2.1 Elevation Degrees of Freedom	9
2.1.1 Sidelobe Jammer Nulling	9
2.1.2 Clutter Cancellation	12
2.2 Near-Field Point Scattering	12
2.2.1 Sidelobe Jammer Nulling	17
2.2.2 Clutter Cancellation	17
2.3 Additional Elemental Tapering	25
2.4 Illustrative MCARM Example	25
3 Description of Simulation Inputs and Outputs	47
3.1 Simulation Inputs	47
3.1.1 Radar Parameters	47
3.1.2 Antenna Parameters	48
3.1.3 Environmental Parameters	49
3.1.4 Processing Parameters	52
3.1.5 Miscellaneous Input Files	57
3.2 Simulation Outputs	57
3.2.1 Output File 10	57
3.2.2 Output File 11	58
3.2.3 Output File 13	58
3.2.4 Output Files 14 and 16	58
3.2.5 Output File 22	58
3.2.6 Output File 25	58
3.2.7 Output File 30	59
3.2.8 Output File 31	59

## TABLE OF CONTENTS (CONCLUDED)

SECTION	PAGE
4 Running the Advanced Airborne Radar Simulation	61
4.1 RCF UNIX-Based Machines	61
4.2 VMS-Based Sensor Center VAX	63
4.3 CPU Run Times	64
4.4 Bounds on Simulation Input Parameters	67
List of References	71
Appendix A Mathematical Details of Program Modifications	73
Appendix B Overview of Changes to Subroutines	79
Appendix C Input and Output Files for Illustrative Examples	83



## LIST OF FIGURES

FIGURE	PAGE
1      Jointly-Adaptive Space-Time Processing Architectures	2
2      Global Features of the Advanced Airborne Radar Simulation	4
3      Four Simulated Scattering Paths	6
4      Performance Measures for Cancelling a Sidelobe Jammer With Twenty Elevation Degrees of Freedom	10
5      Elevation Receive Antenna Gain Patterns for Cancelling a Sidelobe Jammer With Twenty Elevation Degrees of Freedom	11
6      Performance Measures for Clutter Cancellation With Eight Elevation Degrees of Freedom	13
7      Elevation Receive Antenna Gain Patterns for Clutter Cancellation With Eight Elevation Degrees of Freedom	14
8      Performance Measures for Clutter Cancellation With Eight Elevation Degrees of Freedom and Four Pulses	15
9      Elevation Receive Antenna Gain Patterns for Clutter Cancellation With Eight Elevation Degrees of Freedom and Four Pulses	16
10     Location of Eleven Near-Field Point Scatterers	18
11     Azimuth Receive Antenna Gain Patterns for Cancelling a Sidelobe Jammer, Without Near-Field Scattering	19
12     Performance Measures for Cancelling a Sidelobe Jammer, Without Near-Field Scattering	20
13     Azimuth Receive Antenna Gain Patterns for Cancelling a Sidelobe Jammer, With Near-Field Scattering	21
14     Performance Measures for Cancelling a Sidelobe Jammer, With Near-Field Scattering	22
15     Performance Measures for Cancelling Clutter, Without Near-Field Scattering	23

## LIST OF FIGURES (CONTINUED)

FIGURE	PAGE
16 Performance Measures for Cancelling Clutter, With Near-Field Scattering	24
17 Amplitude of Elemental Taper Weights for the Elliptical Array Example	26
18 Quiescent Clutter-Plus-Noise-to-Noise Ratio Versus Doppler and Range for the Elliptical Array Example	27
19 Non-Adapted Clutter-Plus-Noise-to-Noise Ratio Versus Doppler and Range for the MCARM Example—View 1	31
20 Non-Adapted Clutter-Plus-Noise-to-Noise Ratio Versus Doppler and Range for the MCARM Example—View 2	33
21 Non-Adapted Signal-to-Clutter-Plus-Noise Ratio Versus Doppler and Range for the MCARM Example—View 1	35
22 Non-Adapted Signal-to-Clutter-Plus-Noise Ratio Versus Doppler and Range for the MCARM Example—View 2	37
23 Adapted Clutter-Plus-Noise-to-Noise Ratio Versus Doppler and Range for the MCARM Example—View 1	39
24 Adapted Clutter-Plus-Noise-to-Noise Ratio Versus Doppler and Range for the MCARM Example—View 2	41
25 Adapted Signal-to-Clutter-Plus-Noise Ratio Versus Doppler and Range for the MCARM Example — View 1	43
26 Adapted Signal-to-Clutter-Plus-Noise Ratio Versus Doppler and Range for the MCARM Example—View 2	45
27 Illustrative CPU Run Times for RCF UNIX-Based Machine BAUHAUS	65
A-1 Illustrations to Understand How GTD Files are Read	78
C-1 Input File for Sidelobe Jammer Nulling With Elevation Degrees of Freedom	84

## LIST OF FIGURES (CONCLUDED)

FIGURE	PAGE
C-2 Output File 11 for Sidelobe Jammer Nulling With Elevation Degrees of Freedom	88
C-3 Input File for Clutter Cancellation With Elevation Degrees of Freedom	89
C-4 Output File 11 for Clutter Cancellation With Elevation Degrees of Freedom	93
C-5 Input File for Sidelobe Jammer Nulling With Near-Field Scattering	95
C-6 Output File 11 for Sidelobe Jammer Nulling With Near-Field Scattering	100
C-7 Input File for Clutter Cancellation With Near-Field Scattering	101
C-8 Output File 11 for Clutter Cancellation With Near-Field Scattering	106
C-9 Input File for Elliptical Array Example	107
C-10 Input File for Illustrative MCARM Example	112

## LIST OF TABLES

TABLE	PAGE
1 Input Parameters for the MCARM Example	28
2 Input Parameter Bounds	68

## SECTION 1

### INTRODUCTION

MITRE recently developed performance prediction models for airborne phased-array radars and algorithms using adaptive space-time processing (STP) to suppress interference signals received by these radars have not been adequately evaluated with measured data. Rome Laboratory's Multichannel Airborne Radar Measurements (MCARM) program is currently developing a testbed that will obtain this data. This program will tailor MITRE's in-house capability to create performance benchmarks for the Rome Laboratory's testbed for determining its potential performance and subsequently for analyzing the measured data. The objective of this report is to describe enhancements to MITRE's Advanced Airborne Radar Simulation and a set of typical examples illustrating the enhanced features.

#### 1.1 BACKGROUND

MITRE developed a simulation to evaluate the performance of advanced airborne radars using adaptive space-time processing (STP) techniques for detecting targets in noise, jamming and clutter [1-6]. MITRE's Advanced Airborne Radar Simulation is based upon the jointly-adaptive STP architectures shown in Figure 1. The architectures shown employ tapped-delay lines, with the taps spaced by one pulse repetition interval (PRI), on each element, subarray, or beam of an airborne phased-array radar. The adaptive weights for the tapped-delay lines are obtained by multiplying the inverse of the interference covariance matrix with a steering vector. Each weight is applied to the appropriate PRI tap (i.e., pulse), and the resulting weighted outputs are summed, providing a coherent combination of spatial and temporal information. The number of degrees of freedom for the jointly-adaptive STP architectures equals the number of pulses times the number of elements, subarrays, or beams. When the number of pulses is less than the number of PRI outputs to be coherently processed, Doppler processing following the STP summation provides further coherent gain for the target. The STP performance (i.e., signal-to-interference ratio) can be measured at the output of the summation and also at any Doppler filter output. Note that additional temporal taps spaced by a sampling rate interval can provide additional degrees of freedom [6]. In one mode, the individual steady-state covariance matrices of the received clutter, jamming, and

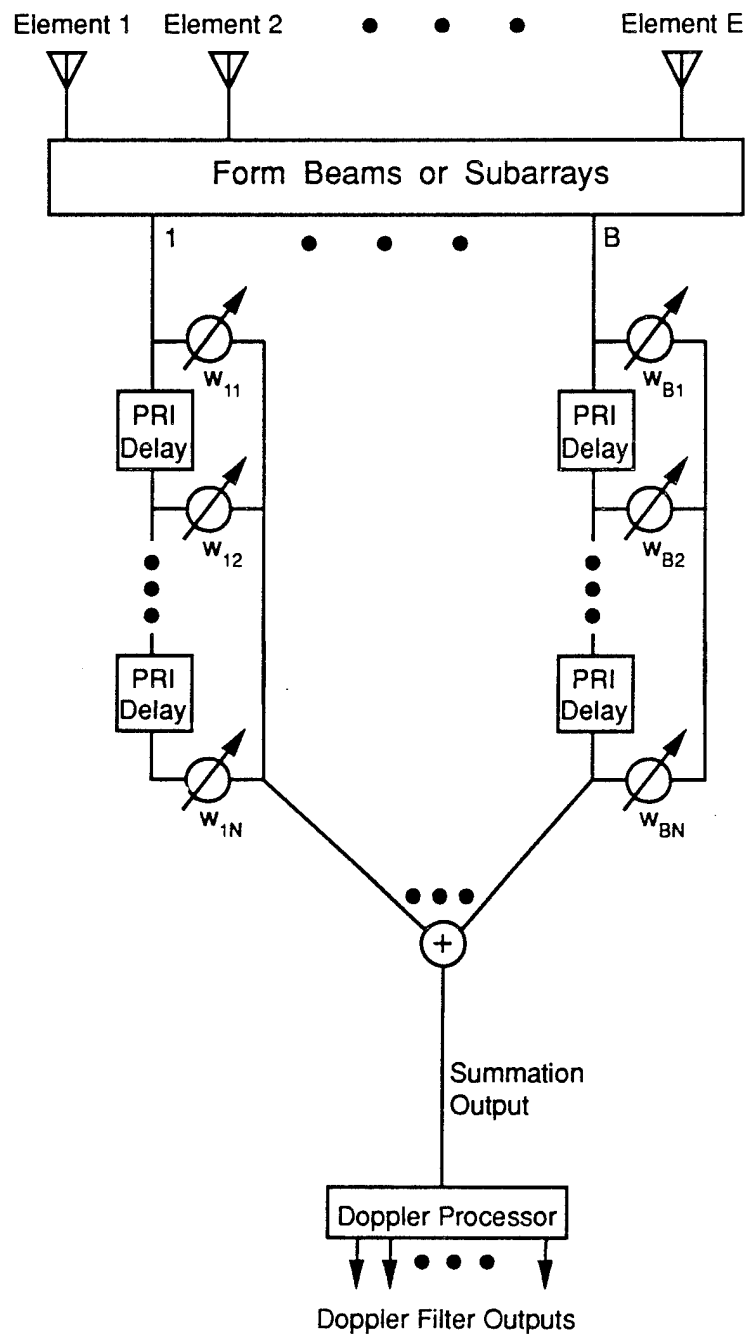


Figure 1. Jointly-Adaptive Space-Time Processing Architectures

thermal noise are calculated based on their modeled spatial and temporal correlation properties that include the effects of aircraft motion, crabbing, internal clutter motion, bandwidth, channel matching, and near-field scattering. Alternatively, the interference covariance matrix, calculated from measured or simulated elemental data, can be read from a file. Additional insight into performance can be obtained by calculating the eigenspectra of the interference covariance matrix and the adapted antenna gain patterns. The next section briefly describes the simulation enhancements.

## **1.2 SIMULATION ENHANCEMENTS**

Figure 2 shows the global features of the Advanced Airborne Radar Simulation, where the shaded portions indicate the enhancements. The enhanced steady-state simulation augments the jointly-adaptive STP architectures with spatial degrees of freedom in elevation, includes the effects of near-field scattering due to antenna-platform interactions, and allows additional elemental taper weights. Appendix A shows the mathematical details of the enhanced models. Appendix B briefly describes the new and modified subroutines of the enhanced simulation.

### **1.2.1 Elevation Degrees of Freedom**

Previously, the STP software employed a planar array to generate a free-space transmit antenna pattern, with the antenna elements having a specified gain pattern. On receive, a single non-adapted subarray output is calculated for each column of the planar array. The program can also calculate non-adaptive subarrays across the antenna columns in azimuth. The effects of azimuth subarraying on the performance of STP can be evaluated by adaptively processing the outputs of these receive subarrays. However, for medium and high-pulse repetition frequency (PRF) waveforms, the long-range target and short range clutter may compete with each other because of range folding. For these waveforms, the STP architecture may require additional spatial degrees of freedom in elevation to reduce the contributions of the short-range clutter. The simulation was enhanced to allow calculation of a variable number of non-adapted subarrays in elevation for each array column or azimuth subarray.

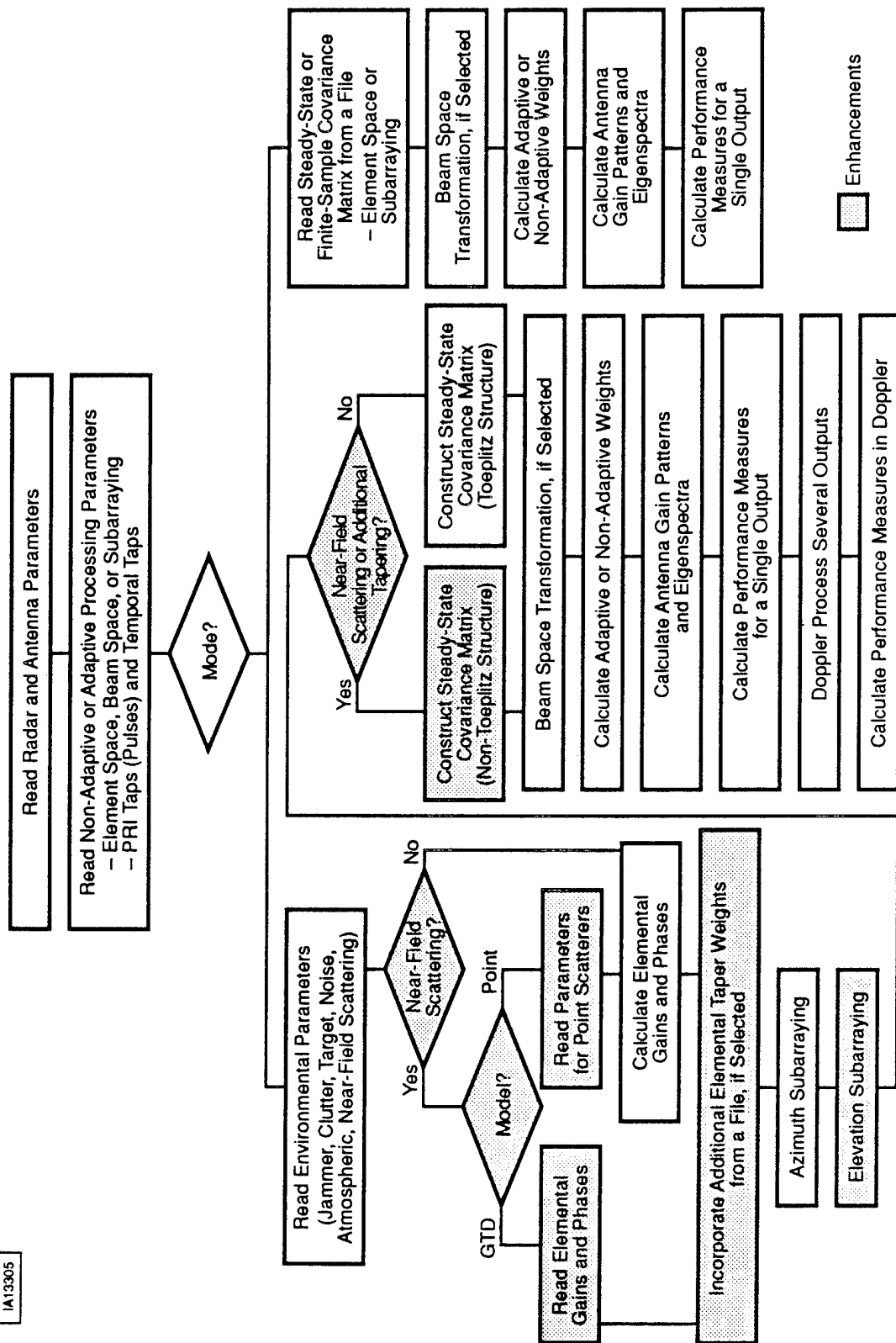


Figure 2. Global Features of the Advanced Airborne Radar Simulation



### **1.2.2 Near-Field Scattering**

The previous version of the simulation calculated the steady-state covariance matrix for the clutter received at an array in the absence of near-field scattering. The direct transmit and receive paths between the array and a far-field clutter scatterer are illustrated in Figure 3a. For each clutter scatterer, the software calculates an entry of the steady-state covariance matrix based on the radar range equation, the free-space transmit gain pattern of the array, and the linear phase terms due to the clutter's spatial (i.e., element-to-element) and temporal (i.e., tap-to-tap and pulse-to-pulse) correlation properties. In the absence of near-field scattering, the clutter steady-state covariance matrix is spatially and temporally stationary, and is constructed by calculating only a single row of entries and exploiting its Toeplitz structure. However, one of the critical factors that can limit the performance of STP is the near-field scattering effects due to the antenna-aircraft interactions. The modifications to include the near-field scattering effects in the simulation are described below.

#### **1.2.2.1 Point Scatterer Model**

The first modification represents the scattering effects by a small set of near-field point scatterers. This requires modeling the three additional scattering paths illustrated in Figures 3b through 3d. The one bounce path on transmit requires the calculation of the far-field transmit gain pattern in the presence of the near-field point scatterers. The one bounce path on receive requires augmenting the steady-state covariance matrix calculation with additional non-linear phase terms due to the nonstationary spatial correlation properties of the received clutter. The two bounce path is a composite of the one bounce paths on transmit and receive. These bounce paths result in a non-Toeplitz steady-state covariance matrix for the received clutter, where all entries of the matrix need to be calculated explicitly. Some of the mathematical details of this modification are briefly described in Appendix A.

#### **1.2.2.2 Integration of GTD Outputs**

The NEC BSC geometric theory of diffraction (GTD) ray-tracing simulation predicts the effects of electromagnetic interactions between the radar antenna and its aircraft platform on the signals received by the array antenna. The second modification uses the simulation to

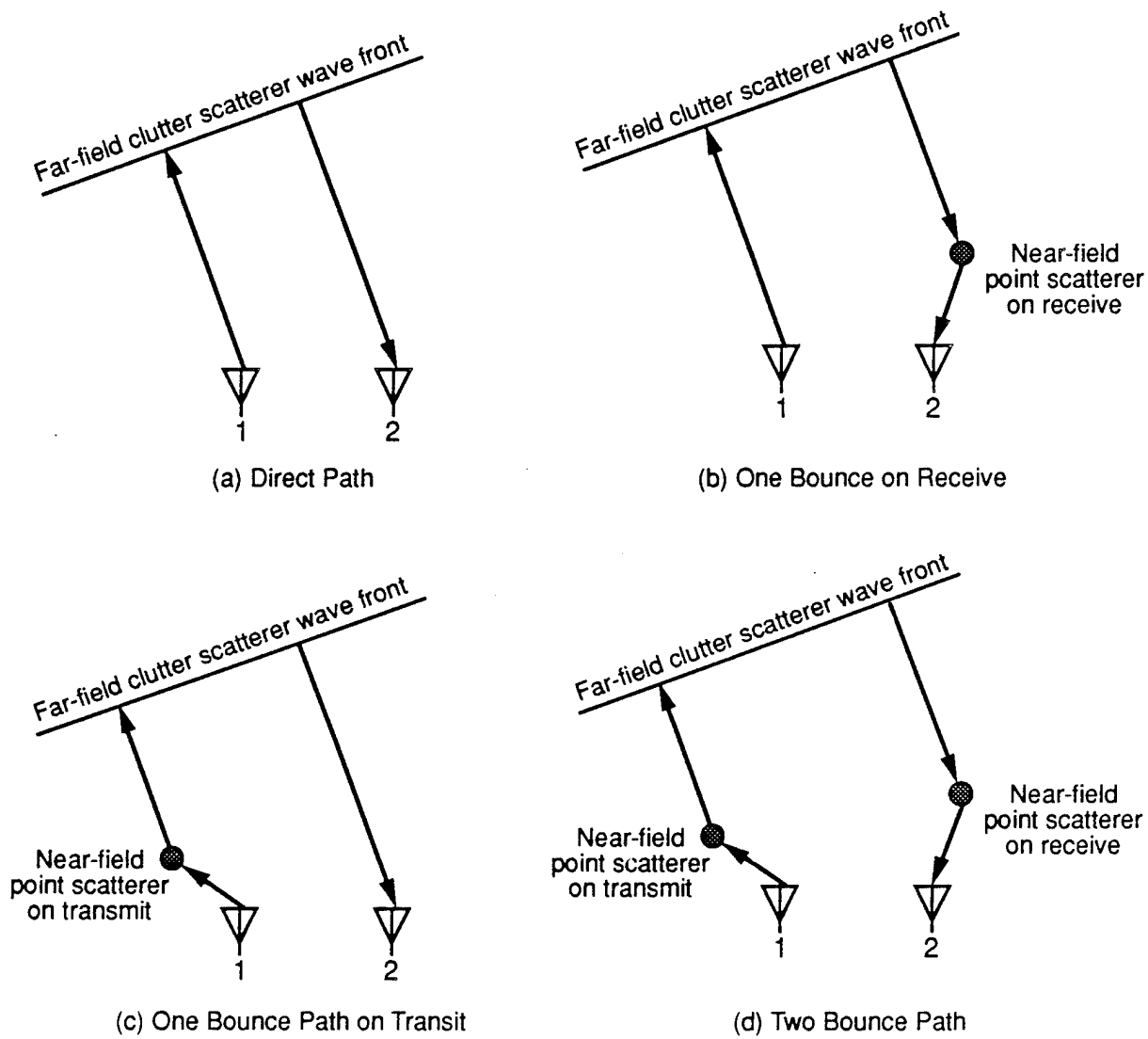


Figure 3. Four Simulated Scattering Paths

provide the complex amplitude and phase information at each far-field point (corresponding to a clutter scatterer location) due to each transmit antenna element in the presence of the aircraft structure. The modified simulation constructs the clutter steady-state covariance matrix using the GTD information [7,8]. This covariance matrix can be used to evaluate the impact of near-field scattering on the STP performance.

### **1.2.3 Additional Elemental Tapering**

The modification allows the capability to read additional complex elemental taper weights (i.e., amplitude and phase) that are applied on both transmit and receive. This capability allows modeling of non-dispersive antenna errors, beam spoiling techniques, predictive-nulling and alternative non-adaptive aperture weighting, and any antenna aperture configurable within a planar grid.

## **1.3 OVERVIEW**

Section 2 presents simulation results for different scenarios showing users how to run different options in the program for their system applications. An illustrative example is provided to show how the program can be used to create performance benchmarks for Rome Laboratory's MCARM program. Section 3 describes the input parameters required to run the program and its outputs. Section 4 presents a step-by-step procedure for running the software either on the VMS- or UNIX-based machines, and run time comparisons for some typical scenarios. Appendix A describes the mathematical details of the program modifications. Appendix B provides an overview of the changes to the software subroutines. Appendix C contains the inputs and outputs from the simulation for the examples described in Section 2.

## **1.4 SUMMARY**

The enhanced capabilities of the Advanced Airborne Radar Simulation described in this report allow system engineers to evaluate the performance of STP techniques for medium- and high-PRF waveforms wherein the system may require elevation degrees of freedom to

reduce the contribution of short-range clutter and, jamming located in the azimuth mainlobe. One of the factors that can limit the performance of STP is the near-field scattering effects from the antenna-aircraft interactions. The point scattering model feature of the simulation provides parametric performance predictions. In addition, the option to integrate the GTD outputs into the simulation allows a more accurate evaluation of the effects of antenna-platform interactions on STP performance. The capability of the simulation to read desired additional elemental taper weights allows the evaluation of STP performance with different antenna apertures. This upgrade was used in the Joint Services Space-Time Adaptive Processing Requirements Study to evaluate the feasibility and potential benefits of applying STP to an airborne platform using an elliptical aperture. The mathematical details of the modifications are presented to enable users to understand the changes in the software. The examples described in this paper illustrate the key features of the enhanced simulation. In addition, an illustrative example is provided to show how the program can be used to create performance benchmark's for Rome Laboratory's MCARM program.

## SECTION 2

### ILLUSTRATIVE EXAMPLES

The illustrative examples presented in this section show the salient features of the enhanced simulation. This should aid users in adapting this program to their system applications.

#### 2.1 ELEVATION DEGREES OF FREEDOM

Two examples illustrate the elevation degrees of freedom (DOF) feature of the simulation. First, we validate the program with jammer nulling using a 20-element horizontal linear array in a clutter-free environment, where a single jammer is located in azimuth at -32 degrees (relative to broadside). We then rotated the array by ninety degrees and placed a single jammer 32 degrees in elevation. The jammer-plus-noise-to-noise ratio (JNR) results from the two programs were identical when using the modified simulation. Second, we illustrate how elevation DOF can be used to mitigate short- and long-range clutter competing with a long-range target. Although the spatial elevation DOF alone can mitigate short-range clutter, additional temporal DOF are required to cancel long-range clutter while maintaining the mainbeam and not cancelling the target, as illustrated in Section 2.1.2.

##### 2.1.1 Sidelobe Jammer Nulling

In this example, we chose a horizontal 20-element linear array electronically scanned in azimuth to -10.0 degrees (relative to broadside) and a sidelobe jammer located in azimuth at -32.0 degrees (relative to broadside). Using the previous version of the simulation, the quiescent jammer-plus-noise-to-noise ratio (JNR) was 44.0 dB, and the adapted JNR using element space processing (i.e., 20 elevation DOF) was 8.2 dB. Note that the jammer was not completely cancelled due to a specified cancellation ratio of 55.0 dB. Next, a vertical 20-element linear array (i.e., 20 elevation degrees of freedom) electronically scanned in elevation to 10.0 degrees was used to cancel a sidelobe jammer located in elevation at 32.0 degrees. Figure 4 shows the quiescent and adapted JNR using the modified simulation. These performance measures are identical to those of the horizontal array case. Figure 5 shows the quiescent and adapted elevation receive antenna gain patterns, illustrating that

<u>Performance *</u> <u>Measures (in dB)</u>	<u>Adaptive</u>	<u>Quiescent</u>
$\left(\frac{J+N}{N}\right)$	8.21	44.02
$\left(\frac{S}{I}\right)$	28.87	-6.91
$\left(\frac{S}{N}\right)$	37.09	37.11

---

\*  $\left(\frac{J+N}{N}\right)$  = jammer-plus-noise-to-noise ratio

$\left(\frac{S}{I}\right)$  = signal-to-interference ratio

$\left(\frac{S}{N}\right)$  = signal-to-noise ratio

Figure 4. Performance Measures for Cancelling a Sidelobe Jammer With Twenty Elevation Degrees of Freedom

Number of Antenna Columns = 1	Radar Bandwidth = 1.0E06 Hz
Number of Antenna Rows = 20	Jammer Model = Wideband
Frequency = L-Band	Jammer Elevation Angle = 32 Degrees
Elevation Weighting = 30 dB Taylor, $\bar{N} = 5$	Cancellation Ratio = 55 dB
Elevation Electronic Scan Angle = 10 Degrees	Number of Pulses Processed = 1

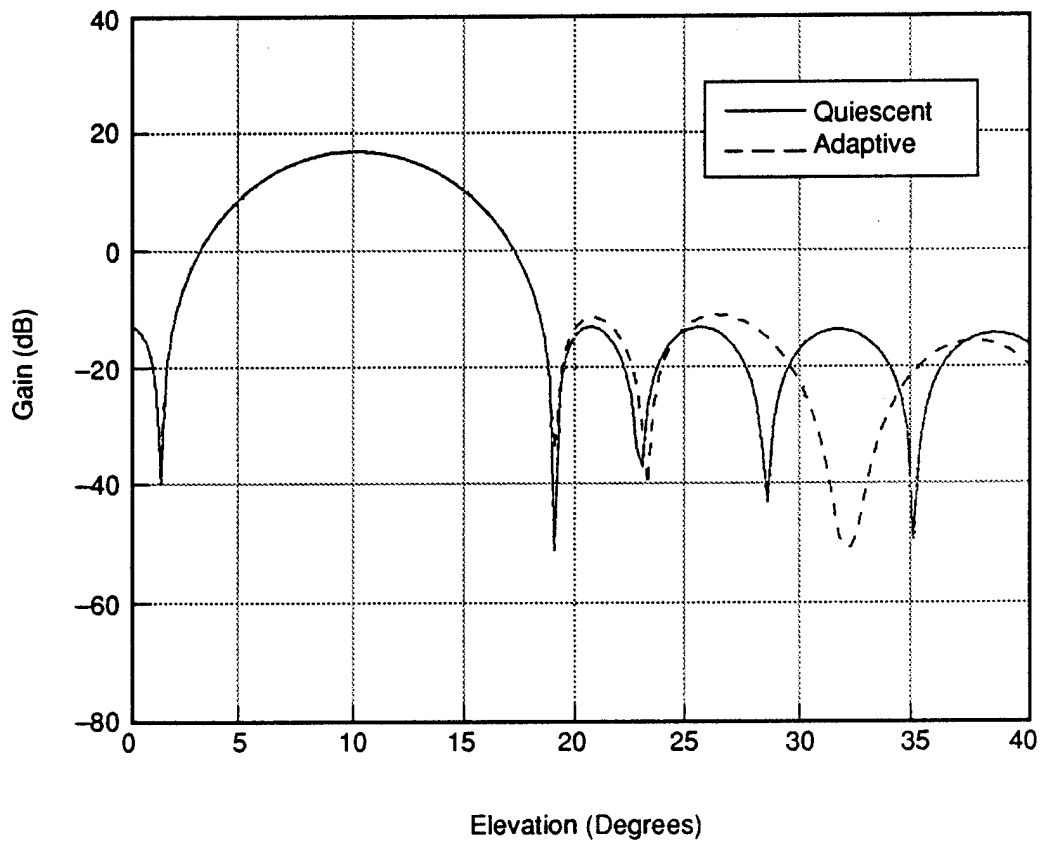


Figure 5. Elevation Receive Antenna Gain Patterns for Cancelling a Sidelobe Jammer With Twenty Elevation Degrees of Freedom

there is an adapted null at 32.0 degrees used to cancel the sidelobe jammer. The performance measures and patterns were identical for the horizontal and vertical array configurations, demonstrating the successful implementation of spatial degrees of freedom in the simulation.

### **2.1.2 Clutter Cancellation**

This example illustrates how elevation DOF can adaptively cancel short- and long-range clutter competing with a long-range target. For this example, we use a 30 x 8 planar array electronically scanned in elevation to 2.8 degrees. The pulse repetition frequency of the radar waveform is 1400 Hz, which causes an additional three range ambiguities at elevations of 3.1, 4.9, and 75.4 degrees, respectively. Figure 6 shows the performance measures when eight elevation DOF are used to adaptively cancel the clutter. The CNR is reduced from 60.0 to 0.3 dB. However, there is also target cancellation, as indicated by the significant loss in signal-to-noise ratio (SNR) and small improvement in signal-to-interference ratio (SIR). The cancellation of both the target and clutter is further illustrated by the quiescent and adapted elevation receive antenna gain patterns. Figure 7 illustrates that an adaptive null in the elevation gain pattern at 75.4 degrees cancels the short-range clutter. However, there are adaptive nulls in the mainlobe corresponding to the elevation locations of the long-range clutter (which includes the elevation location of the target). Temporal DOF (i.e., pulses) can be used to adaptively discriminate a moving target from the long-range clutter. Figure 8 shows the performance measures with 32 degrees of freedom when four temporal and eight elevation DOF are simultaneously used to adaptively cancel the clutter. Eigenvalue compensation was used to minimize the antenna pattern distortion [3,4]. The CNR is reduced from 60.0 to 6.5 dB, while the SNR is increased from 5.7 to 10.7 dB, resulting in a significant improvement in SIR from -54.4 to 4.1 dB. Figure 9 illustrates the elevation receive antenna gain pattern evaluated at the target Doppler (i.e., half the blind speed).

## **2.2 NEAR-FIELD POINT SCATTERING**

The two examples are presented to illustrate the near-field point scattering feature of the simulation. First, the effects of near-field point scatterers on the cancellation of a single



<u>Performance *</u> <u>Measures (in dB)</u>	<u>Adaptive</u>	<u>Quiescent</u>
$\left(\frac{C+N}{N}\right)$	0.34	60.10
$\left(\frac{S}{I}\right)$	-40.46	-54.37
$\left(\frac{S}{N}\right)$	-40.12	5.74

---

\*  $\left(\frac{C+N}{N}\right)$  = clutter-plus-noise-to-noise ratio

$\left(\frac{S}{I}\right)$  = signal-to-interference ratio

$\left(\frac{S}{N}\right)$  = signal-to-noise ratio

Figure 6. Performance Measures for Clutter Cancellation  
With Eight Elevation Degrees of Freedom

Number of Antenna Columns = 30  
 Number of Antenna Rows = 8  
 Frequency = L-Band  
 PRF = 1400 Hz  
 Azimuth Weighting = 30 dB Taylor,  $\bar{N} = 5$   
 Elevation Weighting = 30 dB Taylor,  $\bar{N} = 5$

Elevation Electronic Scan Angle = 2.8 Degrees  
 Radar Bandwidth = 1.0E06 Hz  
 Clutter Model = Constant Gamma (-9 dB)  
 Number of Range Ambiguities = 3  
 Number of Receive Azimuth Subarrays = 1  
 Number of Pulses Processed = 1

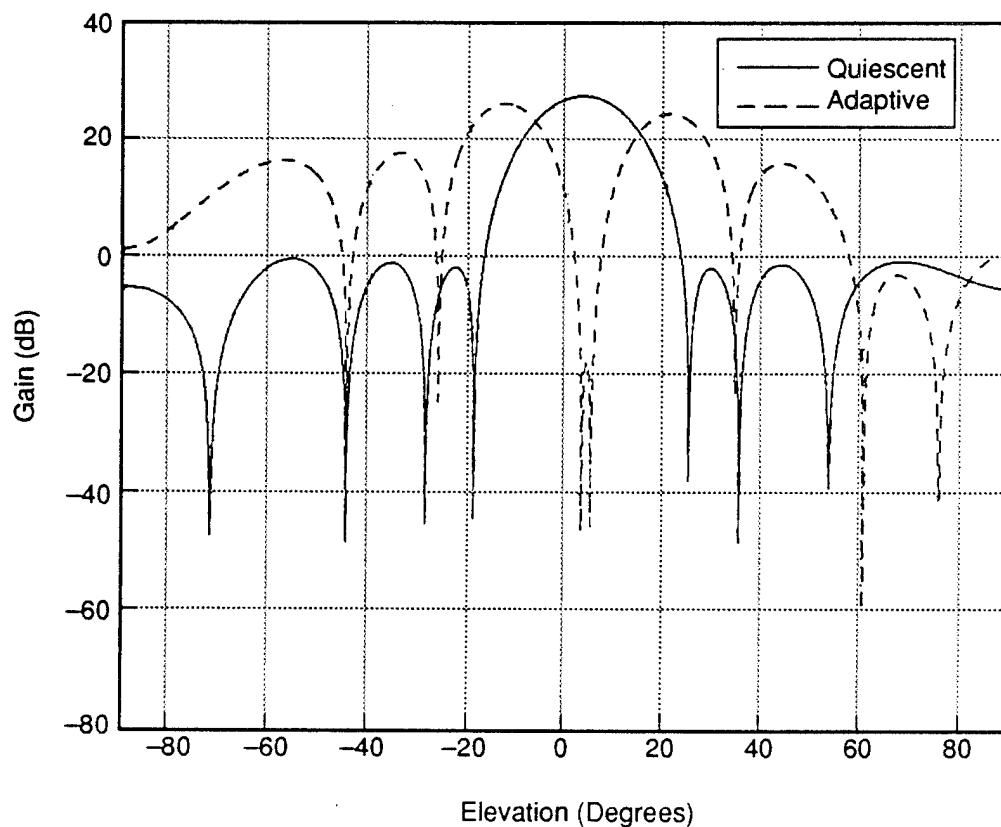


Figure 7. Elevation Receive Antenna Gain Patterns for Clutter Cancellation With Eight Elevation Degrees of Freedom

Performance * <u>Measures (in dB)</u>	<u>Adaptive</u>	<u>Quiescent</u>
$\left( \frac{C+N}{N} \right)$	6.51	60.10
$\left( \frac{S}{I} \right)$	4.14	-54.37
$\left( \frac{S}{N} \right)$	10.65	5.74

---

\*  $\left( \frac{C+N}{N} \right)$  = clutter-plus-noise-to-noise ratio

$\left( \frac{S}{I} \right)$  = signal-to-interference ratio

$\left( \frac{S}{N} \right)$  = signal-to-noise ratio

Figure 8. Performance Measures for Clutter Cancellation  
With Eight Elevation Degrees of Freedom and Four Pulses

Number of Antenna Columns = 30	Elevation Electronic Scan Angle = 2.8 Degrees
Number of Antenna Rows = 8	Radar Bandwidth = 1.0E06 Hz
Frequency = L-Band	Clutter Model = Constant Gamma (-9 dB)
PRF = 1400 Hz	Number of Range Ambiguities = 3
Azimuth Weighting = 30 dB Taylor, $\bar{N} = 5$	Number of Receive Azimuth Subarrays = 1
Elevation Weighting = 30 dB Taylor, $\bar{N} = 5$	Number of Pulses Processed = 4

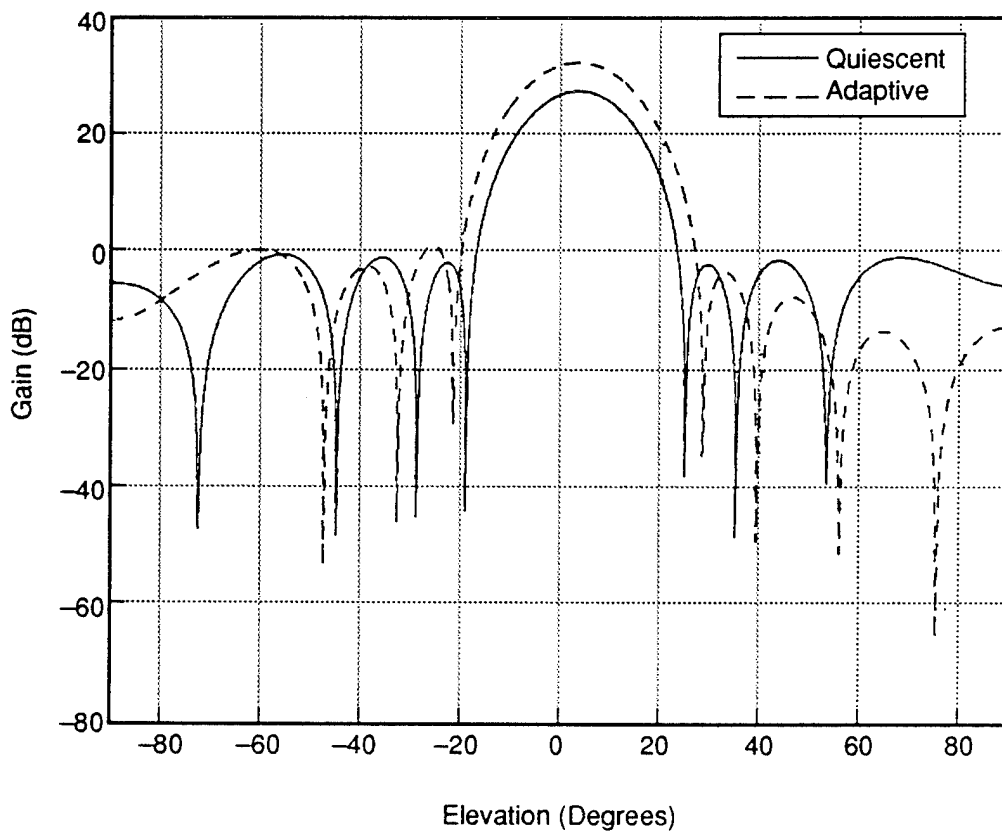


Figure 9. Elevation Receive Antenna Gain Patterns for Clutter Cancellation With Eight Elevation Degrees of Freedom and Four Pulses

sidelobe jammer are illustrated. The second example illustrates the effects of near-field point scatterers on clutter cancellation.

### **2.2.1 Sidelobe Jammer Nulling**

A 16-element horizontal linear array was simulated, with the antenna-platform interactions represented by a line of eleven closely spaced point scatterers (each with a bistatic cross-section of  $2 \text{ m}^2$ ), as shown in Figure 10. The array is colinear with the x-axis and centered about the origin, and the platform heading is in the positive x-direction. The single sidelobe jammer is located a -43 degrees in azimuth. Figure 11 shows the quiescent and adapted azimuth receive antenna gain patterns without near-field scattering. As can be seen from Figure 11, an adapted null at -43 degrees is used to cancel the jammer. Figure 12 shows the quiescent and adapted performance measures in the absence of near-field scattering. Note that the jammer was not completely canceled (i.e., adapted jammer-plus-noise-to-noise ratio (JNR) equals 2.9 dB) due to the cancellation ratio of 50 dB. Figure 13 shows the quiescent and adapted patterns in the presence of the near-field point scatterers. The quiescent gain in the azimuth direction of the jammer increased the JNR by nearly 13 dB, as shown in Figure 14. The near-field scattering and channel mismatch effects increased the adapted JNR from 2.9 to 6.3 dB. However, reducing the bistatic cross-section of the near-field point scatterers to  $0.5 \text{ m}^2$  results in no increase of the adapted JNR from 2.9 dB.

### **2.2.2 Clutter Cancellation**

Figure 15 illustrates the adapted signal-to-interference ratio (SIR) without near-field scattering for a varying number of spatial (i.e., antenna columns) degrees of freedom (DOF) and temporal (i.e., pulses) DOF. The adapted SIR is normalized by the adapted SIR obtained in the noise-only case resulting in a maximum achievable value of 0 dB. From Figure 15 it is clear that to cancel the clutter with an internal motion of 0.1 m/s and achieve an adapted SIR of at least -3 dB requires eight elements and three pulses. However, to achieve an adapted SIR of at least -7 dB with only four elements would require six pulses. Figure 16 illustrates the adapted SIR when there are eleven near-field point scatterers. In order to achieve an adapted SIR of less than 3 dB with eight or twelve elements now requires four pulses. Finally, using four elements and six pulses achieves an adapted SIR of only -19 dB.

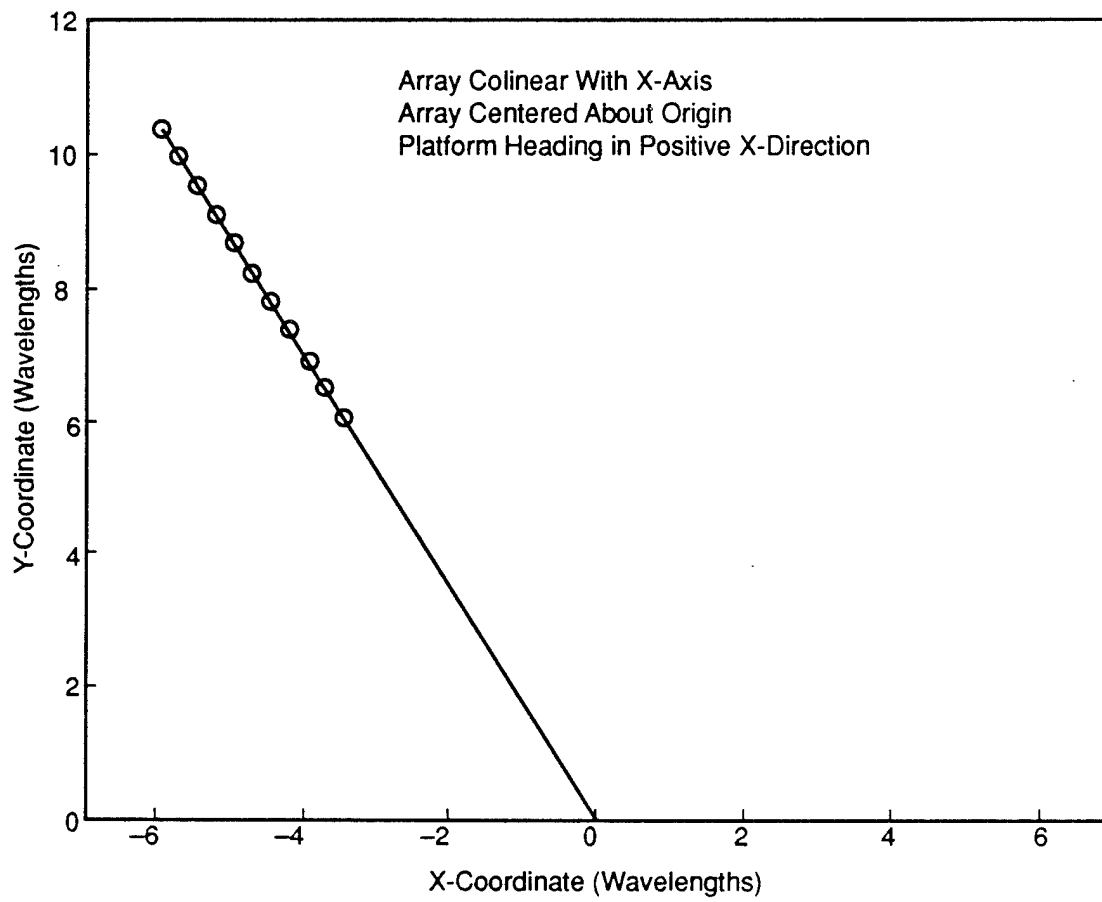


Figure 10. Location of Eleven Near-Field Point Scatterers

Number of Antenna Columns = 16	Jammer Model = Wideband
Number of Antenna Rows = 1	Jammer Azimuth Angle = - 43 Degrees
Frequency = L-Band	Cancellation Ratio = 50 dB
Azimuth Weighting = Uniform	Number of Pulses Processed = 1
Azimuth Electronic Scan Angle = 0 Degrees	Number of Near-Field Point Scatterers = 0
Radar Bandwidth = 1.0E06 Hz	

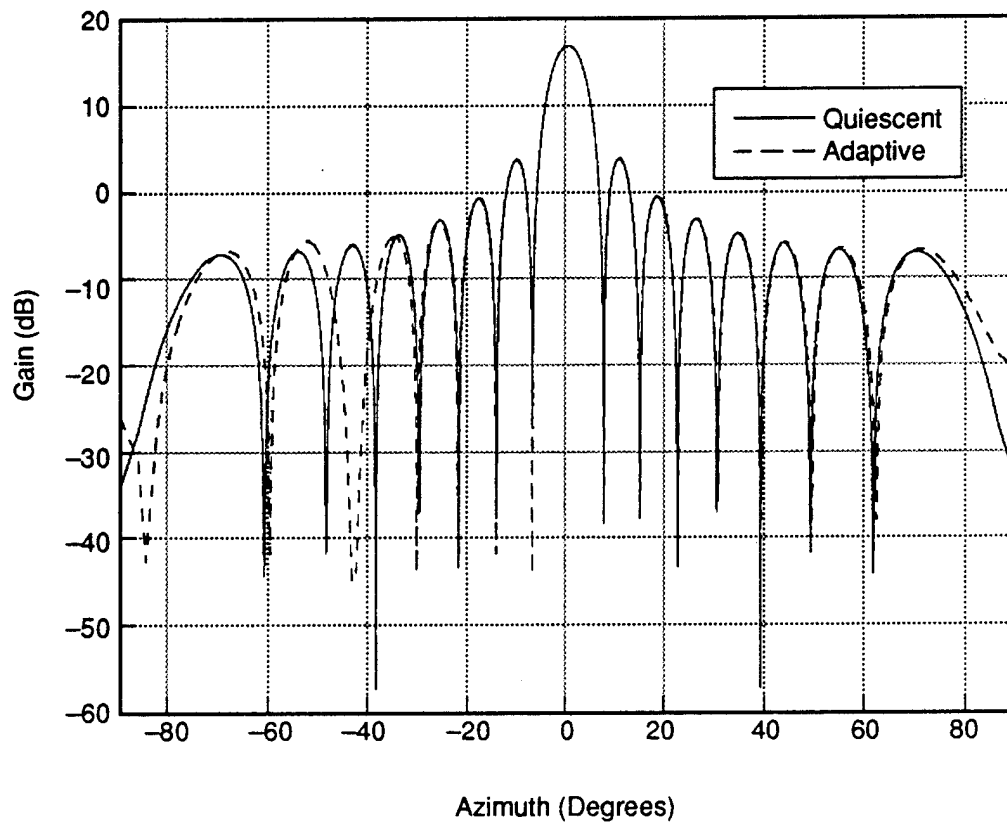


Figure 11. Azimuth Receive Antenna Gain Patterns for Cancelling a Sidelobe Jammer, Without Near-Field Scattering

Performance * Measures (in dB)	<u>Adaptive</u>	<u>Quiescent</u>
$\left(\frac{J+N}{N}\right)$	2.92	38.80
$\left(\frac{S}{I}\right)$	21.58	-14.28
$\left(\frac{S}{N}\right)$	24.50	24.52

---

\*  $\left(\frac{J+N}{N}\right)$  = jammer-plus-noise-to-noise ratio

$\left(\frac{S}{I}\right)$  = signal-to-interference ratio

$\left(\frac{S}{N}\right)$  = signal-to-noise ratio

Figure 12. Performance Measures for Cancelling a Sidelobe Jammer, Without Near-Field Scattering



Number of Antenna Columns = 16	Jammer Model = Wideband
Number of Antenna Rows = 1	Jammer Azimuth Angle = -43 Degrees
Frequency = L-Band	Cancellation Ratio = 50 dB
Azimuth Weighting = Uniform	Number of Pulses Processed = 1
Azimuth Electronic Scan Angle = 0 Degrees	Number of Near-Field Point Scatterers = 11
Radar Bandwidth = 1.0E06 Hz	Bistatic Cross-Section = 2.0 m <sup>2</sup>

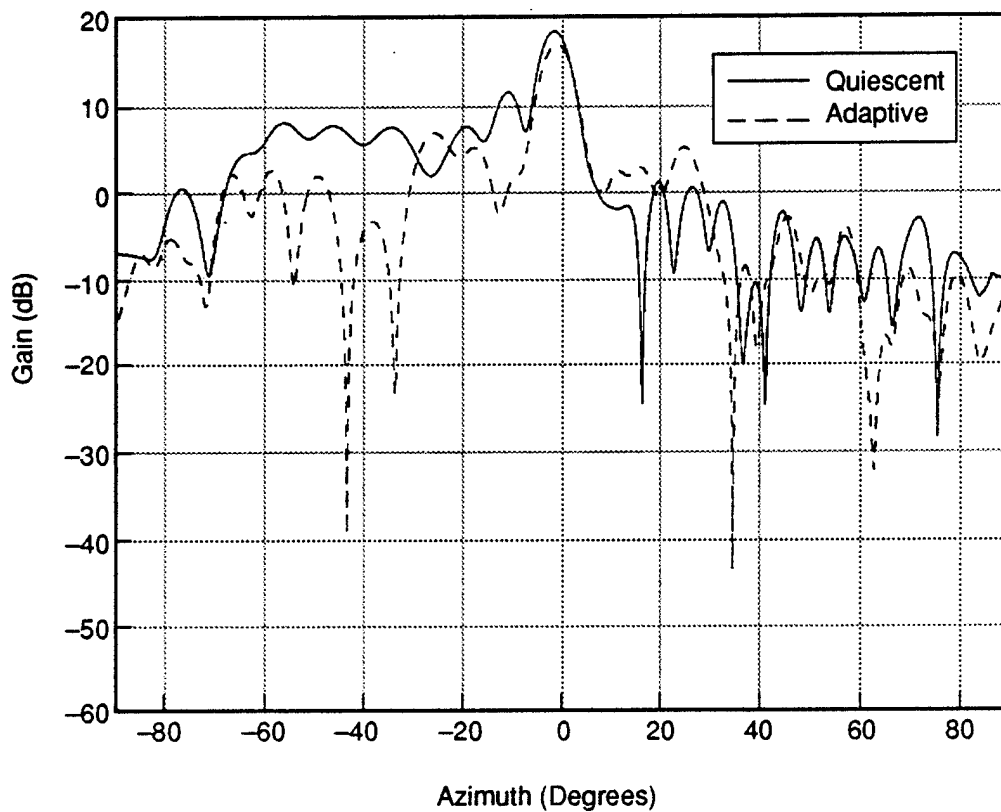


Figure 13. Azimuth Receive Antenna Gain Patterns for Cancelling a Sidelobe Jammer, With Near-Field Scattering

Performance * <u>Measures (in dB)</u>	<u>Adaptive</u>	<u>Quiescent</u>
$\left(\frac{J+N}{N}\right)$	6.35	51.61
$\left(\frac{S}{I}\right)$	16.97	-27.09
$\left(\frac{S}{N}\right)$	23.31	24.52
<hr/>		
* $\left(\frac{J+N}{N}\right)$ = jammer-plus-noise-to-noise ratio		
$\left(\frac{S}{I}\right)$ = signal-to-interference ratio		
$\left(\frac{S}{N}\right)$ = signal-to-noise ratio		

Figure 14. Performance Measures for Cancelling a Sidelobe Jammer, With Near-Field Scattering

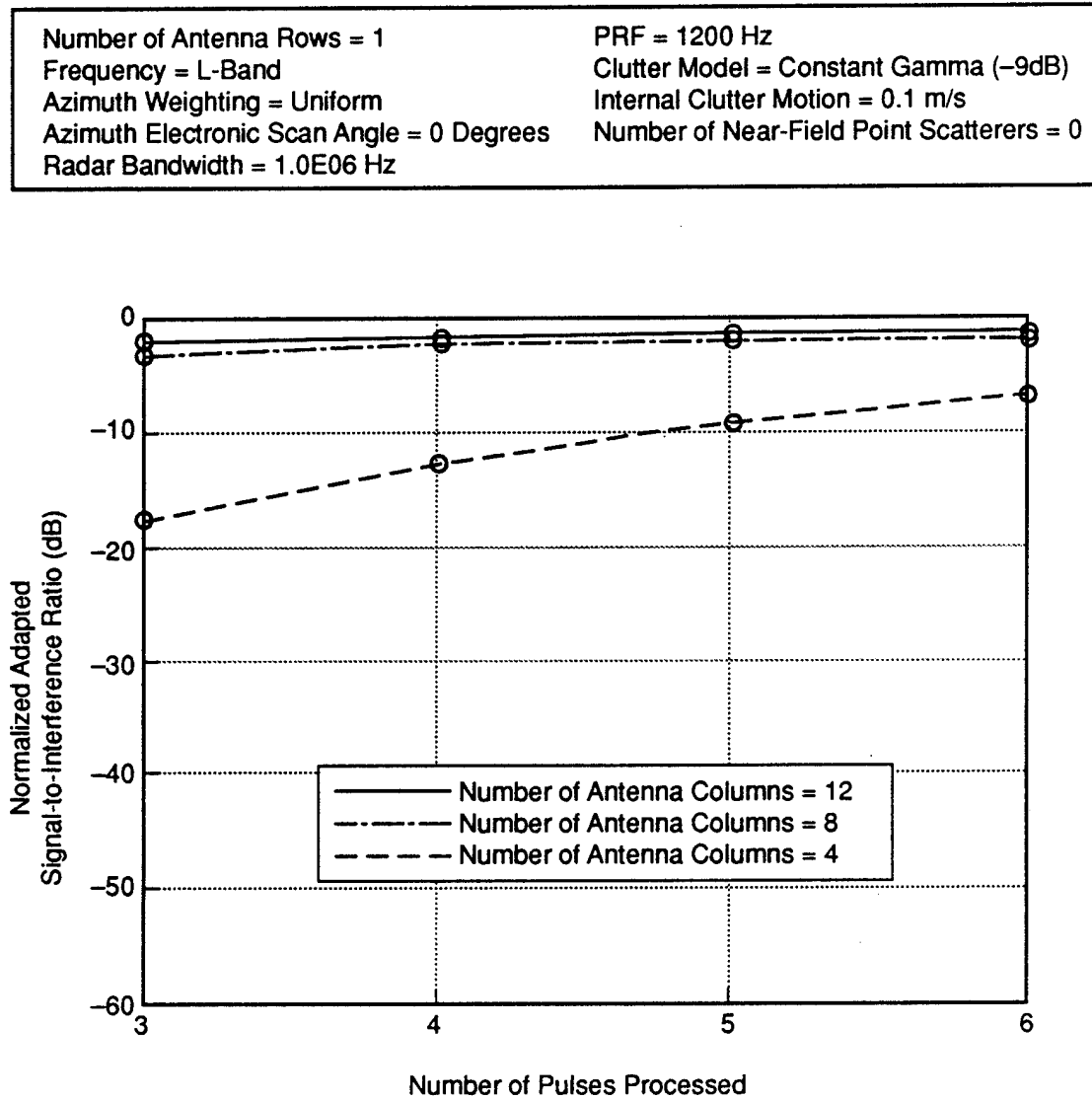


Figure 15. Performance Measures for Cancelling Clutter, Without Near-Field Scattering

Number of Antenna Rows = 1	PRF = 1200 Hz
Frequency = L-Band	Clutter Model = Constant Gamma (-9 dB)
Azimuth Weighting = Uniform	Internal Clutter Motion = 0.1 m/s
Azimuth Electronic Scan Angle = 0 Degrees	Number of Near-Field Point Scatterers = 11
Radar Bandwidth = 1.0E06 Hz	Bistatic Cross-Section = 2.0 m <sup>2</sup>

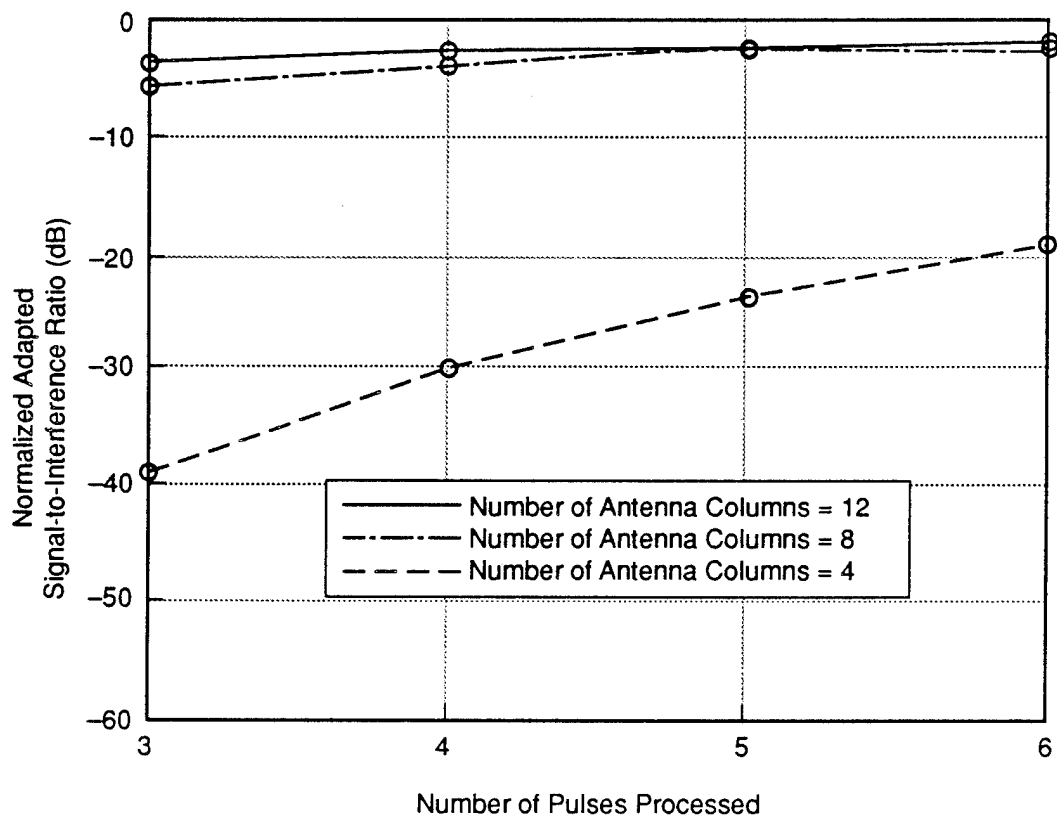


Figure 16. Performance Measures for Cancelling Clutter, With Near-Field Scattering

### **2.3 ADDITIONAL ELEMENTAL TAPERING**

This example illustrates how an elliptical array can be modeled by reading additional elemental taper weights from a user-specified file. Figure 17 shows the amplitude of the aperture weighting for an elliptical array consisting of 26 antenna rows and 168 antenna columns. Note that the amplitude of the weights outside of the elliptical aperture boundary are specified as zero. Figure 18 illustrates the quiescent clutter-plus-noise-to-noise ratio (CNR) versus Doppler for a set of unambiguous ranges. This example illustrates some of the work done for the Joint Services Space-Time Adaptive Processing Requirements Study.

### **2.4 ILLUSTRATIVE MCARM EXAMPLE**

This example shows how the simulation can be used to create performance benchmarks for Rome Laboratory's MCARM program. Table 1 lists the input parameter values for the MCARM example. Figures 19 and 20 illustrate the non-adapted CNR versus Doppler for a set of unambiguous ranges. Figures 21 and 22 illustrate the non-adapted signal-to-clutter-plus-noise ratio (SCR) versus Doppler and range. Figures 23 to 26 show the performance of two-pulse STP by illustrating a significant reduction in CNR and improvement in SCR.

Number of Antenna Rows = 26	Number of Range Ambiguities = 62
Number of Antenna Columns = 168	Radar Bandwidth = $3.5 \times 10^6$ Hz
Frequency = S-Band	Number of Unambiguous Ranges = 140
Aperture Weighting = File Specified	Number of Coherently Integrated Outputs = 256
PRF = 25000 Hz	Number of Doppler Filters = 256
Azimuth Electronic Scan Angle = 22.5 Degrees	Doppler Weighting = 90 dB Dolph-Chebyshev
Elevation Electronic Scan Angle = 1.4 Degrees	Clutter Model = Constant Gamma (-9 dB)
Azimuth Crab Angle = 90.0 Degrees	

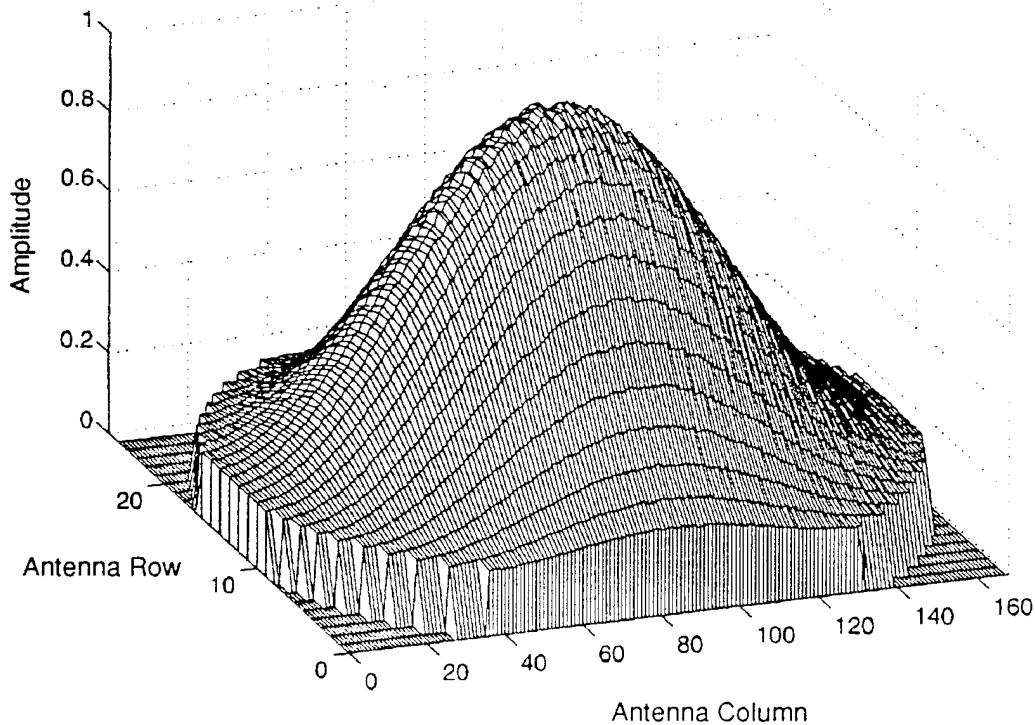


Figure 17. Amplitude of Elemental Taper Weights for the Elliptical Array Example

Number of Antenna Rows = 26	Number of Range Ambiguities = 62
Number of Antenna Columns = 168	Radar Bandwidth = 3.5E06 Hz
Frequency = S-Band	Number of Unambiguous Ranges = 140
Aperture Weighting = File Specified	Number of Coherently Integrated Outputs = 256
PRF = 25000 Hz	Number of Doppler Filters = 256
Azimuth Electronic Scan Angle = 22.5 Degrees	Doppler Weighting = 90 dB Dolph-Chebyshev
Elevation Electronic Scan Angle = 1.4 Degrees	Clutter Model = Constant Gamma (-9 dB)
Azimuth Crab Angle = 90.0 Degrees	

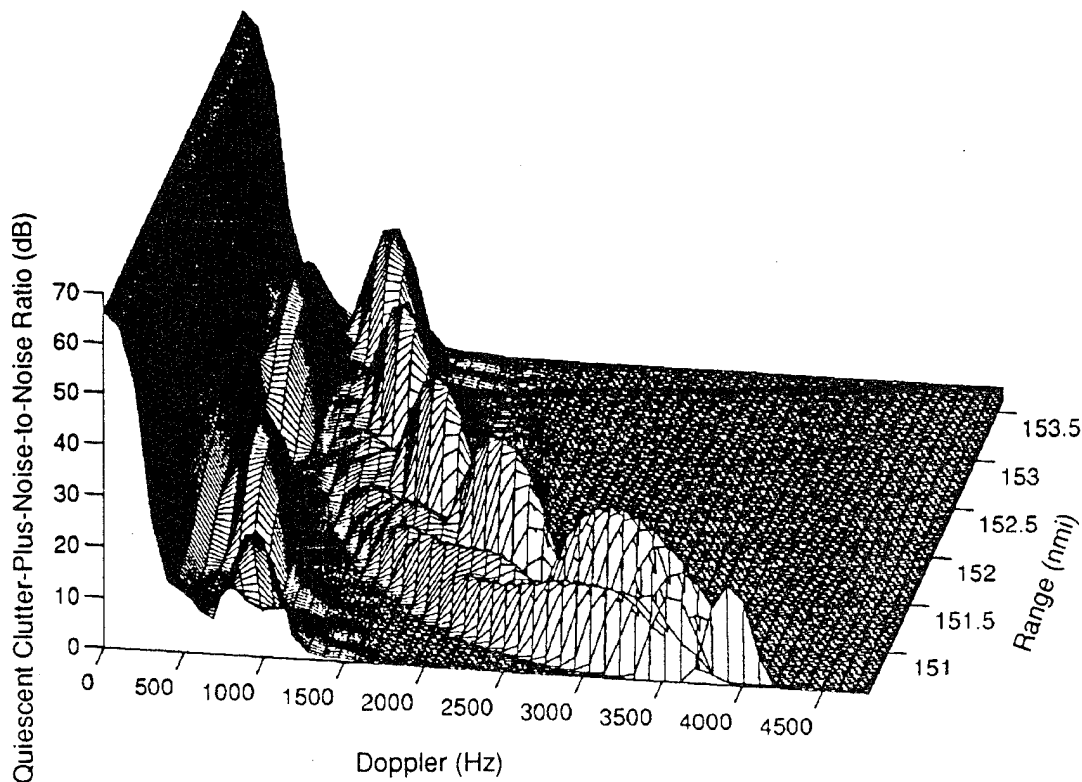


Figure 18. Quiescent Clutter-Plus-Noise-to-Noise Ratio versus Doppler and Range for the Elliptical Array Example

Table 1. Input Parameters for the MCARM Example

Transmit Power (kw)	14.4
Number of Antenna Columns	12
Number of Antenna Rows	8
Frequency	L-Band
Pulse Repetition Frequency (Hz)	2000.0
Radar Bandwidth (MHz)	1.0
Azimuth Scan Angle (Degrees)	14.5
Elevation Scan Angle (Degrees)	2.5
Platform Altitude (Feet)	4921.5
Platform Velocity (nmi/sec)	219.7
Platform Crabbing	None
Uncompressed Pulsewidth ( $\mu$ sec)	100.0
Fractional Wavelength Spacing—Columns	0.454
Fractional Wavelength Spacing—Rows	0.588
Noise Figure (dB)	2.5
System Losses	None
Additional Losses on Target Only (dB)	4.5
Atmospheric and Lens Losses	Included



Table 1. Input Parameters for the MCARM Example (Concluded)

Cancellation Ratio (dB)	60.0
Clutter Model	Constant Sigma
Mean Clutter Level, Gamma (dB)	-9.0
Internal Clutter Motion	None
Number of Near-Field Scatterers	None
Number of Coherently Integrated Outputs	200
Number of Doppler Filters	200
Doppler Weighting	100 dB Dolph-Chebyshev
Azimuth Transmit Weighting	Uniform
Elevation Transmit Weighting	Uniform
Azimuth Receive Weighting	35 dB Taylor, $\bar{N} = 4$
Elevation Receive Weighting	Uniform
Number of Receive Elevation Subarrays	2
Number of Elements Per Receive Elevation Subarray	4
Target Radar Cross-Section (m <sup>2</sup> )	2.0
Number of Non-Adaptive Pulses Processed	1
Number of Adaptive Pulses Processed	2
Steering Vector Doppler	Half Blind Speed

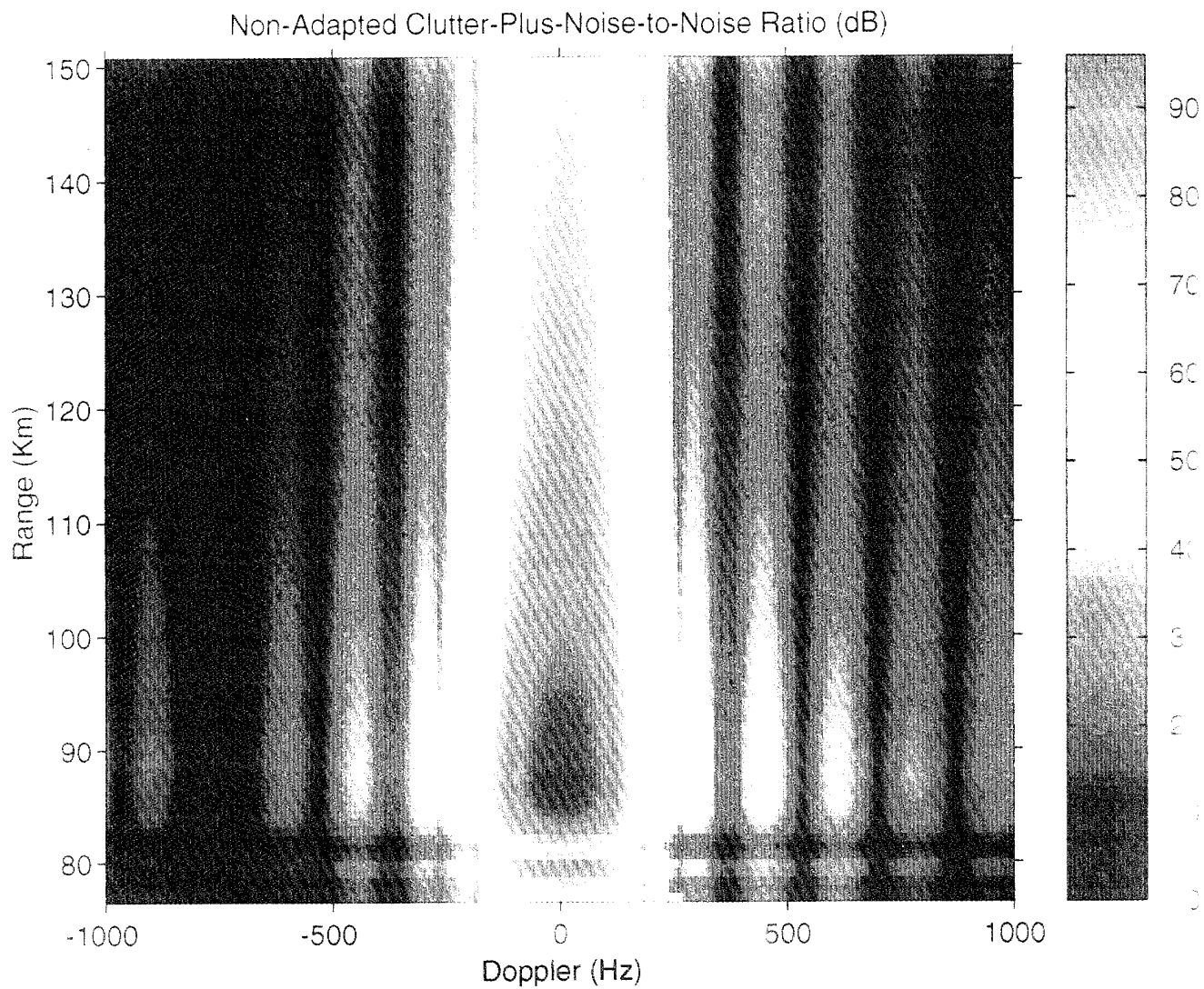


Figure 19. Non-Adapted Clutter-Plus-Noise-to-Noise Ratio Versus Doppler and Range for the MCARM Example—View 1



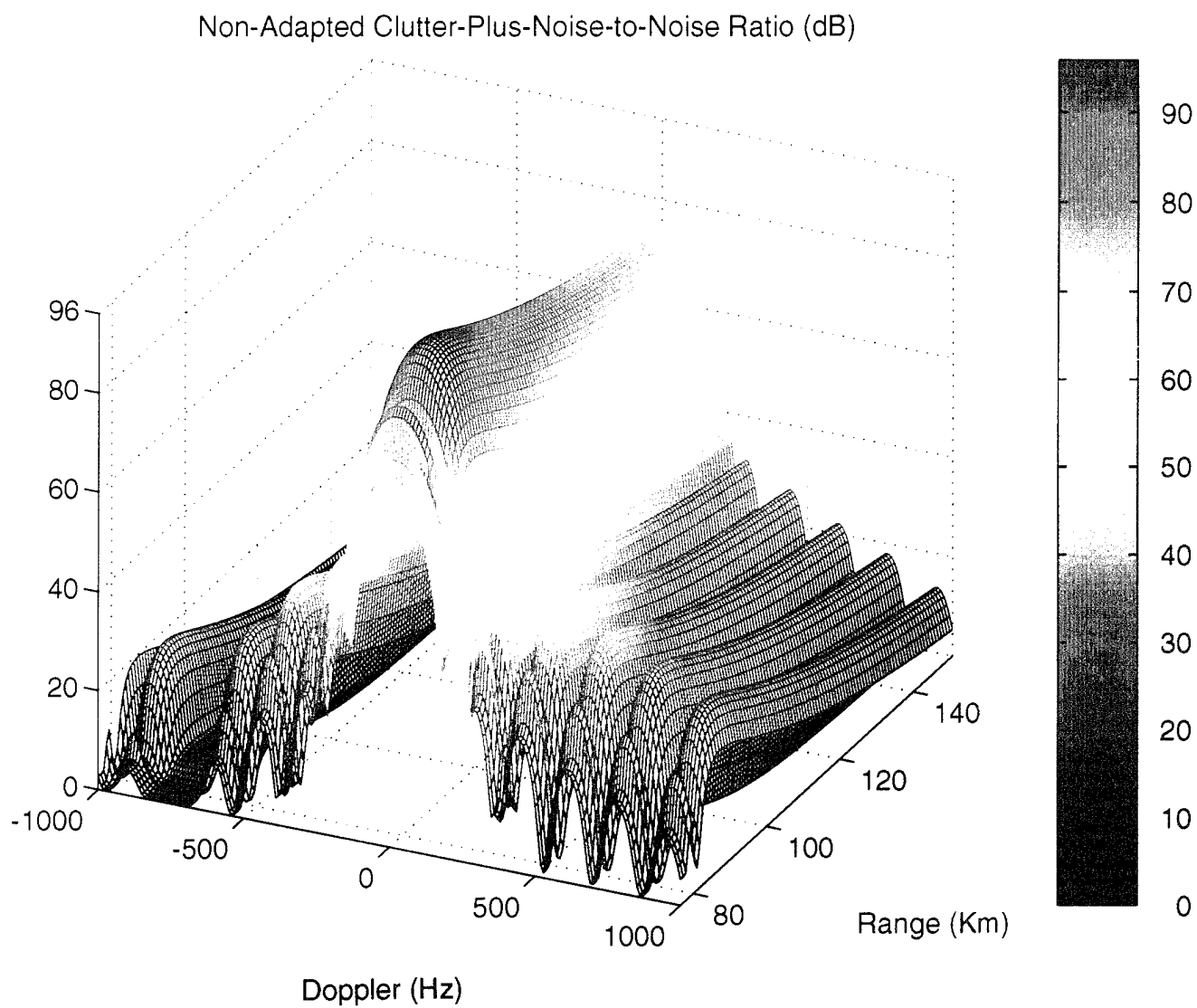


Figure 20. Non-Adapted Clutter-Plus-Noise-to-Noise Ratio Versus Doppler and Range for the MCARM Example—View 2

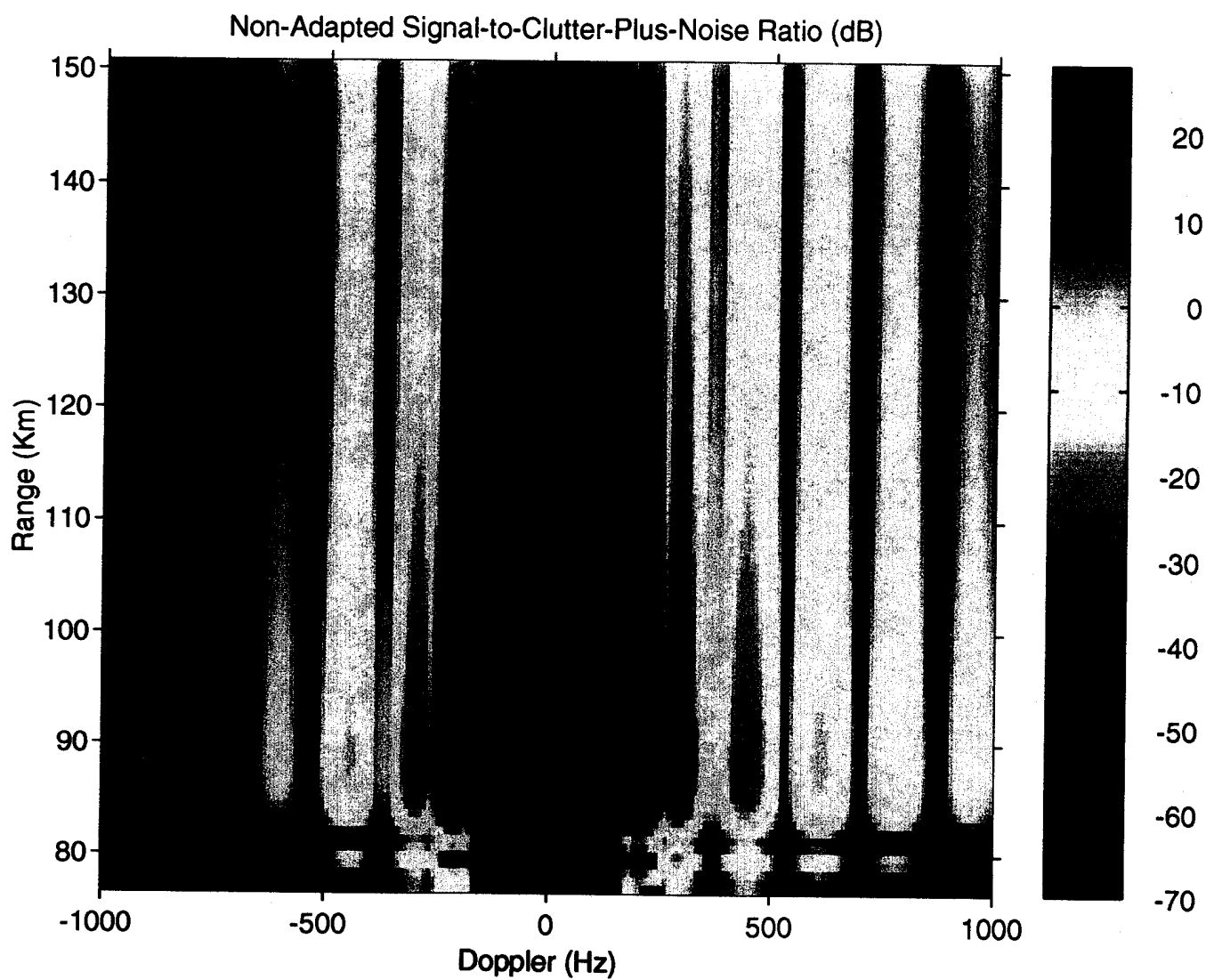


Figure 21. Non-Adapted Signal-to-Clutter-Plus-Noise Ratio Versus Doppler and Range for the MCARM Example—View 1

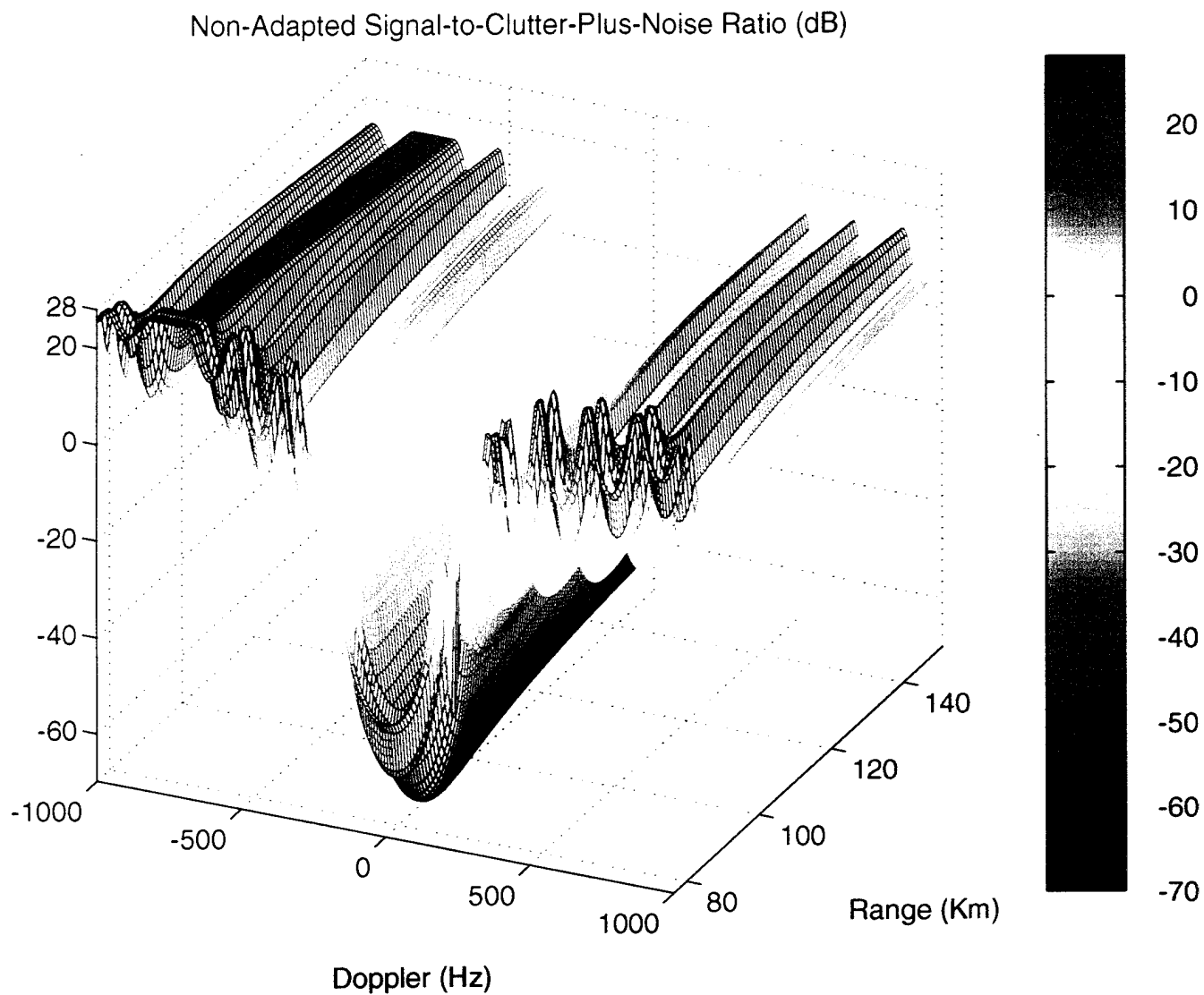


Figure 22. Non-Adapted Signal-to-Clutter-Plus-Noise Ratio Versus Doppler and Range for the MCARM Example—View 2

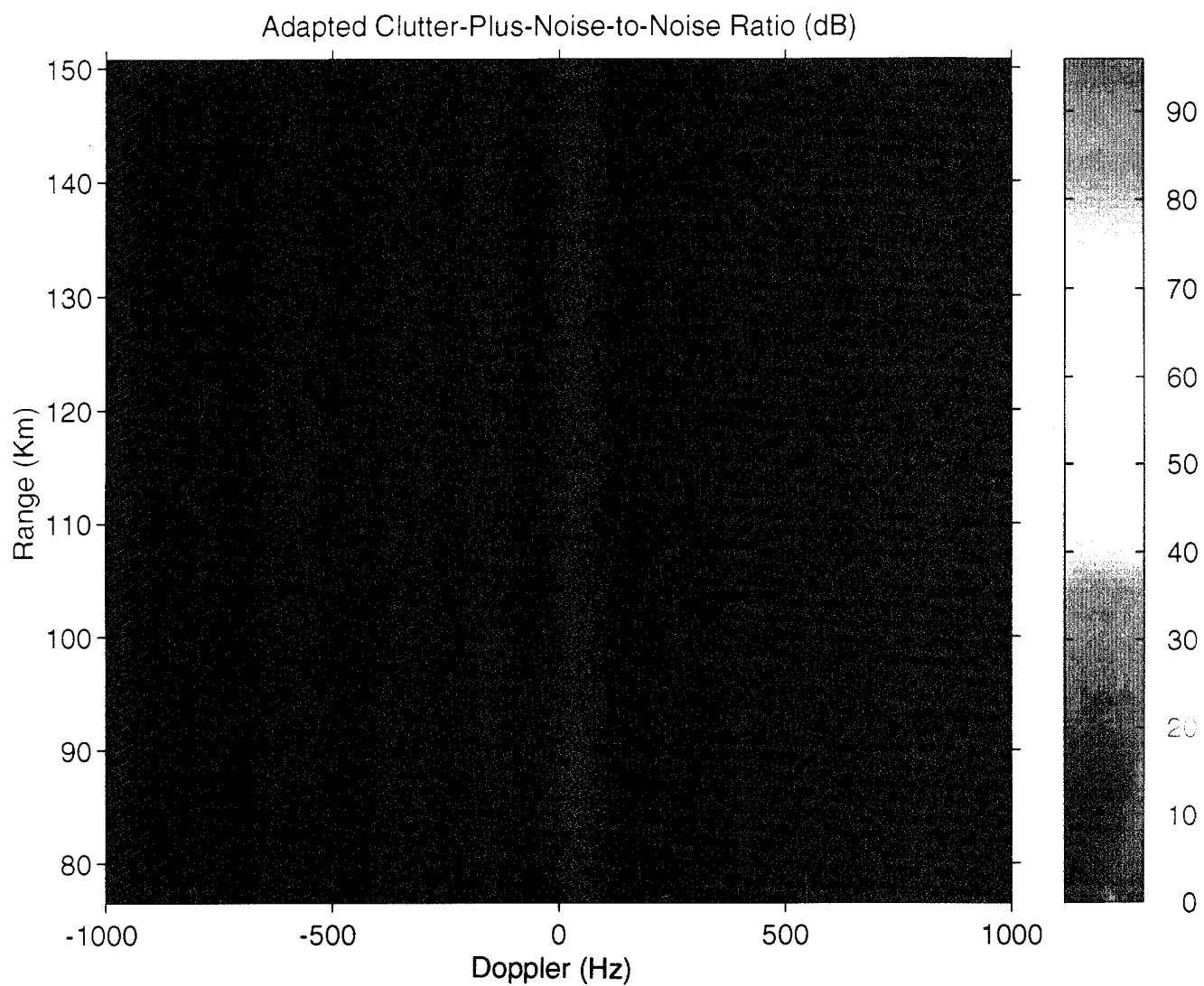


Figure 23. Adapted Clutter-Plus-Noise-to-Noise Ratio Versus Doppler and Range for the MCARM Example—View 1

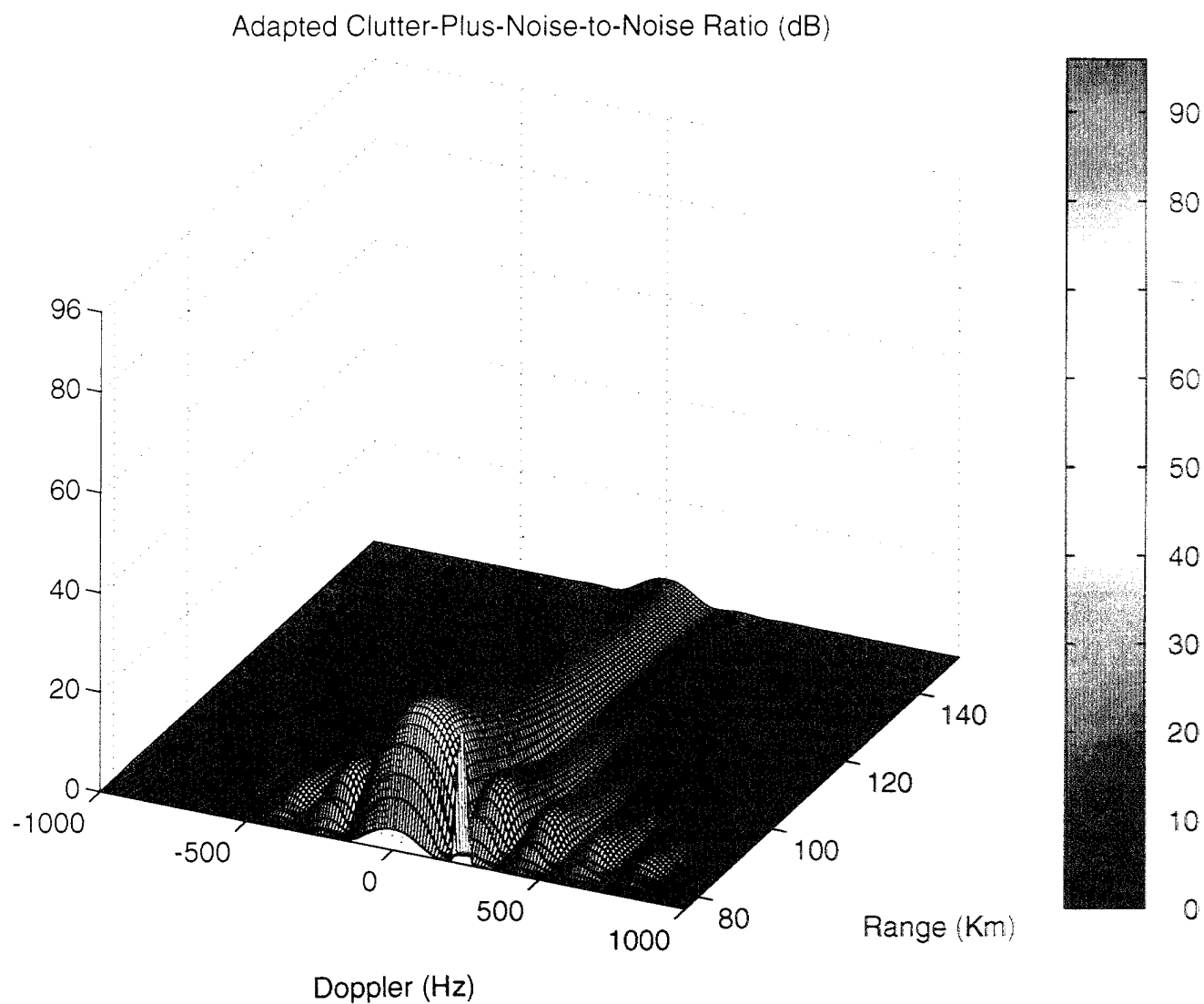


Figure 24. Adapted Clutter-Plus-Noise-to-Noise Ratio Versus Doppler and Range for the MCARM Example—View 2



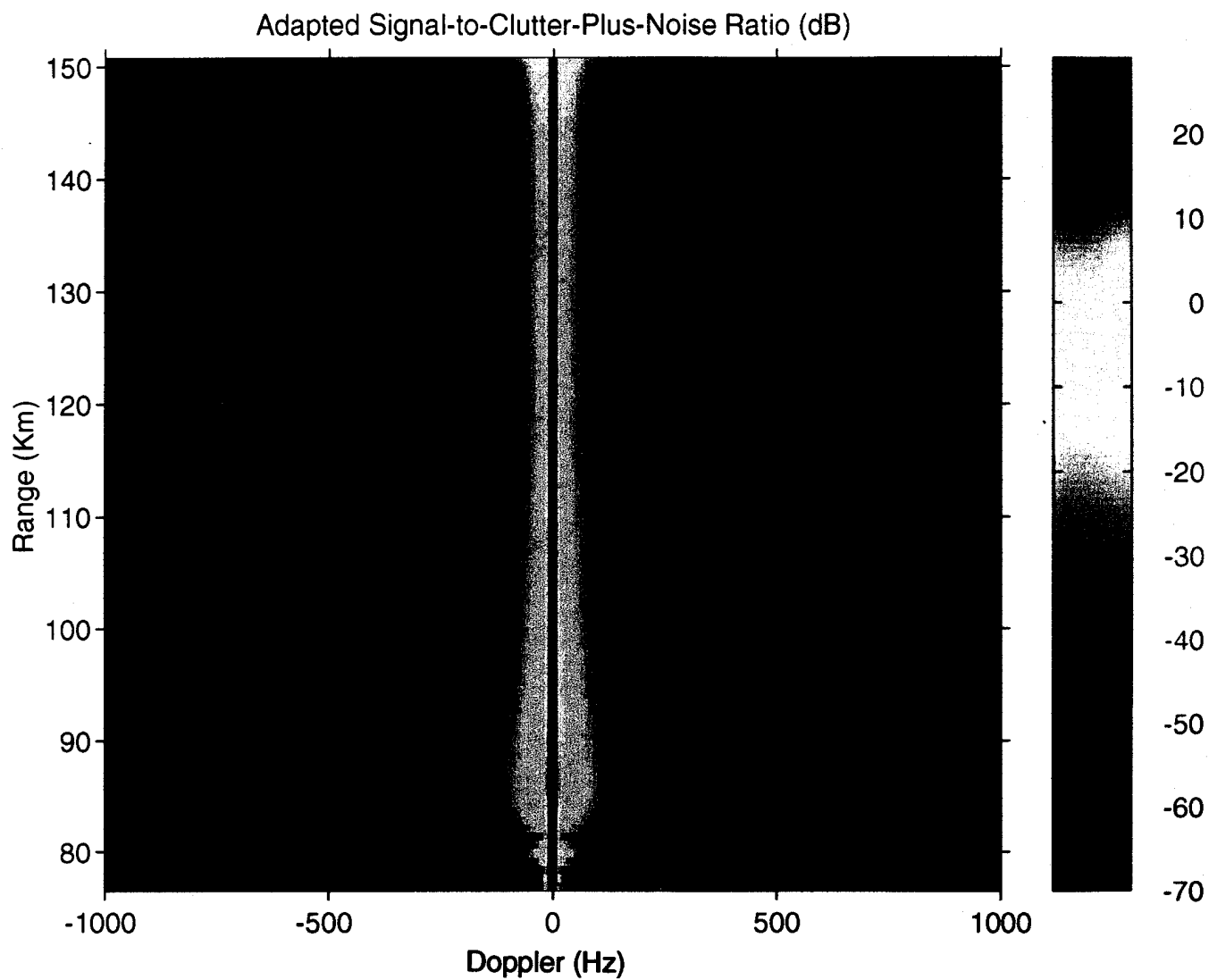


Figure 25. Adapted Signal-to-Clutter-Plus-Noise Ratio Versus Doppler and Range for the MCARM Example—View 1

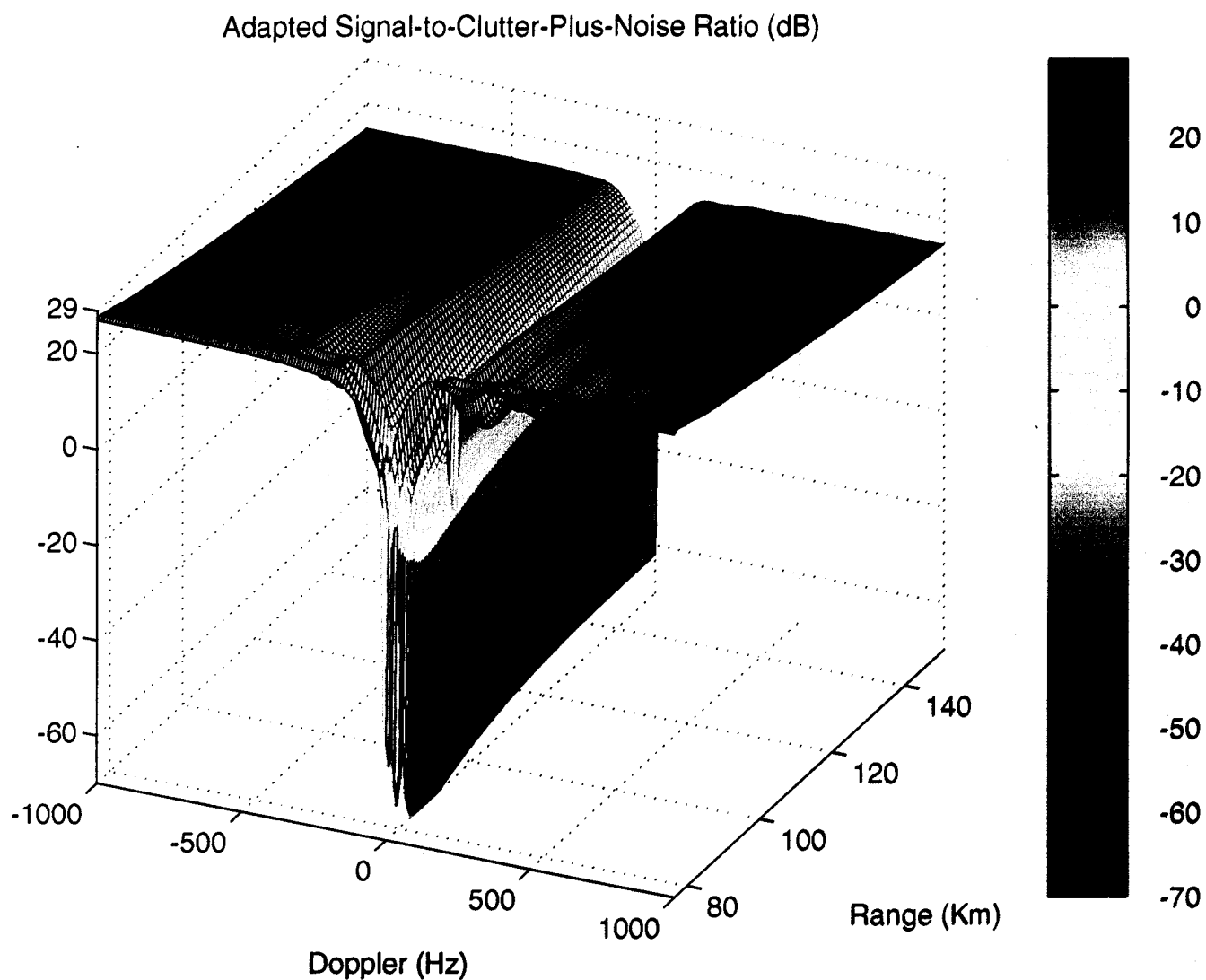


Figure 26. Adapted Signal-to-Clutter-Plus-Noise Ratio Versus Doppler and Range for the MCARM Example—View 2

## SECTION 3

### DESCRIPTION OF SIMULATION INPUTS AND OUTPUTS

This section describes the inputs and outputs of the Advanced Airborne Radar Simulation. The outputs are written to eight different output files. For clarity, the inputs are categorized into four types of parameters: radar, antenna, environmental, and processing.

#### 3.1 SIMULATION INPUTS

##### 3.1.1 Radar Parameters

The radar parameters consist of the radar center frequency, transmit power, PRF, platform altitude, aircraft velocity, number of narrowband frequency returns for the clutter and target, bandwidth of each frequency return, and time-bandwidth product of the transmitted signal. The input names for the radar parameters used in the simulation are

<i>DEFR</i>	=	Bandwidth of each narrowband frequency return for clutter and target within the band of the compressed transmitted signal (in hertz).
<i>FC</i>	=	Carrier or radar center frequency (in hertz).
<i>FREP</i>	=	Pulse repetition frequency (in hertz).
<i>NFR</i>	=	Number of narrowband frequency returns for clutter and target within the band of the compressed transmitted signal.
<i>PLATALT</i>	=	Platform altitude (in feet).
<i>TIME_BW</i>	=	Ratio of uncompressed to compressed pulsewidths (i.e., time-bandwidth product).
<i>VELNM</i>	=	Aircraft velocity (in nautical miles per hour).
<i>XMT_PWR</i>	=	Transmitted power (in watts).

### 3.1.2 Antenna Parameters

The planar-array antenna parameters consist of the number of antenna rows and columns, spacing between antenna rows and columns in wavelengths, transmit and receive weighting, 3 dB beamwidths, electronic scan angles where the beam is pointed, array orientation relative to the aircraft heading, and the element-to-element cancellation ratio. Note that additional complex elemental taper weights can be read from a file. Appendix A discusses the order that the weights are read from the file. The input names for the antenna parameters used in the simulation are

<i>CANRATDB</i>	=	Element-to-element cancellation ratio (in dB).
<i>DEWL</i>	=	Spacing between array columns in wavelengths.
<i>DEWLELEV</i>	=	Spacing between array rows in wavelengths.
<i>IELPG</i>	=	Control on type of elemental pattern (0 = isotropic, 1 = GE cosine model, 2 = half-wavelength dipole).
<i>ISUBTPR</i>	=	Control on type of aperture weighting used to combine azimuth subarrays on receive (0 = uniform, 1 = Taylor).
<i>ISUBTPR2</i>	=	Control on type of aperture weighting in each elevation subarray on receive (0 = uniform, 1 = Taylor).
<i>ITAPER</i>	=	Control on type of aperture weighting on transmit (0 = uniform, 1 = Taylor).
<i>ITPRFILE</i>	=	Control on whether additional complex elemental taper weights are read from a file (0 = no, 1 = yes).
<i>ITPRSUB</i>	=	Control on type of aperture weighting in each azimuth subarray on receive (0 = uniform, 1 = Taylor).
<i>ITPRSUB2</i>	=	Control on type of aperture weighting in each elevation subarray on receive (0 = uniform, 1 = Taylor).
<i>NBAR</i>	=	Azimuth Taylor weighting design parameter on transmit.
<i>NBARELEV</i>	=	Elevation Taylor weighting design parameter on both transmit and receive.
<i>NBARSUB</i>	=	Azimuth Taylor weighting design parameter in each azimuth subarray on receive.

<i>NBARSUB2</i>	=	Elevation Taylor weighting design parameter in each elevation subarray on receive.
<i>NSUBBAR</i>	=	Azimuth Taylor weighting design parameter used to combine azimuth subarrays on receive.
<i>NSUBBAR2</i>	=	Elevation Taylor weighting design parameter used to combine elevation subarrays on receive.
<i>NUMAZIM</i>	=	Number of antenna columns.
<i>NUMELEV</i>	=	Number of antenna rows.
<i>SLDBELEV</i>	=	Quiescent transmit and receive antenna sidelobe level in elevation, if Taylor weighting is selected (in dB).
<i>SLDBSUB</i>	=	Quiescent azimuth antenna sidelobe level in each azimuth subarray on receive, if Taylor weighting is selected (in dB).
<i>SLDBSUB2</i>	=	Quiescent elevation antenna sidelobe level in each elevation subarray on receive, if Taylor weighting is selected (in dB).
<i>SLLDB</i>	=	Quiescent transmit antenna sidelobe level in azimuth, if Taylor weighting is selected (in dB).
<i>SUBSLDB</i>	=	Quiescent azimuth antenna sidelobe level used to combine azimuth subarrays on receive, if Taylor weighting is selected (in dB).
<i>SUBSLDB2</i>	=	Quiescent elevation antenna sidelobe level used to combine elevation subarrays on receiving, if Taylor weighting is selected (in dB).
<i>THS</i>	=	Electronic scan angle in azimuth relative to the array broadside (in degrees).
<i>THSCN1</i>	=	Array broadside relative to the aircraft heading (in degrees).
<i>THS_EL</i>	=	Electronic scan angle in elevation (in degrees).
<i>TH_AZ3DB</i>	=	Azimuth 3 dB beamwidth (in degrees).
<i>TH_EL3DB</i>	=	Elevation 3 dB beamwidth (in degrees).

### 3.1.3 Environmental Parameters

The input environmental parameters are divided into five subcategories: clutter, jamming, target, noise, and losses. Note that the bandwidths of the clutter, target, and noise signal

components are equal to the bandwidth of the compressed transmitted signal (see *DEFR* and *NFR*).

#### 3.1.3.1 Clutter

The clutter parameters consist of the number of scatterers in a clutter range ring, the azimuth spacing between the scatterers, the RMS value of the ICM, and the gamma parameter for the clutter model. The input names for the parameters used in the simulation are

<i>DTTHC</i>	=	Azimuth spacing between scatterers in a range ring (in degrees).
<i>GAMMA</i>	=	Constant gamma used to model the clutter backscatter RCS (in dB meters squared per meters squared).
<i>ICLUT</i>	=	Control on type of clutter model (0 = constant gamma, 1 = constant sigma).
<i>NCL</i>	=	Number of scatterers in a range ring.
<i>SIGMA_V</i>	=	Standard deviation of ICM (in meters per second).

#### 3.1.3.2 Jamming

The jamming parameters consist of the radiated jammer powers, jammer ranges and locations in azimuth and elevation, and the number of jammers. The input names for the parameters used in the simulation are

<i>DEFR_J</i>	=	Bandwidth of each narrowband component of the jammers (in hertz).
<i>FC_J</i>	=	Jammer center frequencies (in hertz).
<i>IDCORR_J</i>	=	Control on whether element-to-element delay is included in the limits of integration when calculating a wideband jammer signal (0 = no, 1 = yes).
<i>NEJI</i>	=	Number of jammers.
<i>NFR_J</i>	=	Number of narrowband frequency components of the jammers.
<i>P</i>	=	Radiated jammer output powers over the jammer bandwidths.
<i>PHIPLS_J</i>	=	Doppler of jammers normalized by the radar ambiguous Doppler.

*RNG\_JAM* = Range of jammers (in nautical miles).  
*THJ\_EL* = Location of jammers in elevation (in degrees).  
*TTHJ* = Location of jammers in azimuth relative to the array broadside (in degrees).

### 3.1.3.3 Target

The target parameters consist of the target range, altitude, cross-section, and Doppler. Note that the target location in azimuth corresponds to the azimuth scan angle *THS*. The input names for the parameters used in the simulation are

*PHIPLSE* = Doppler of target normalized by the radar ambiguous Doppler.  
*SIGMA\_T* = Target RCS (in meters squared).  
*TARGALT* = Target altitude (in feet).  
*TARGRNG* = Target range (in nautical miles).

### 3.1.3.4 Noise

The only input noise parameter is the system noise figure:

*F\_N* = System noise figure (in dB).

### 3.1.3.5 Losses

The loss parameters are divided into three types: range-independent system losses, range-dependent atmospheric and lens losses, and additional losses on target-only. The input names for the parameters used in the simulation are

*ILOSS* = Control on whether range-dependent atmospheric and lens losses are calculated (0 = no, 1 = yes).  
*L\_S* = Range-independent system losses (in dB).  
*L\_T* = Additional losses on target-only (in dB).

### 3.1.3.6 Near-Field Scattering Effects

The parameters for specifying the near-field point scattering effects consist of the number of point scatterers, and their associated locations and bistatic cross-sections. Note that if the number of scatterers equals -1, then the complex elemental voltages for the clutter are read from a file provided by the GTD simulation. The order that the voltages are read from the GTD file is discussed in Appendix A and illustrated in Figure A-1. The input names for the parameters used in the simulation are

- BCSQ* = Bistatic cross-section of near-field point scatterers (in meters squared).
- ITARGQ* = Control on whether near-field point scattering effects are included in the target signal calculation (0 = no, 1 = yes).
- NUMQ* = Number of near-field point scatterers. If equal to -1, then a GTD file is read.
- XQ* = Near-field point scatterer location in x-direction (in wavelengths).
- YQ* = Near-field point scatterer location in y-direction (in wavelengths).
- ZQ* = Near-field point scatterer location in z-direction (in wavelengths).

### 3.1.4 Processing Parameters

The architecture parameters in both modes are divided into six categories: general parameters applicable to all architectures, subarray, element space, beam space, receive antenna pattern, and Doppler.

#### 3.1.4.1 General

The general processing parameters described in this section are common to all the three processing architectures (i.e., element space, beam space, and subarray) in both modes. Note that the user has the option (*IREADQC* = 1) to read the interference covariance matrix from an input file (input unit 35 renamed with extension .cov2). The input names for the parameters used in the simulation are

- DTDL* = Time delay between sampling interval taps (in seconds).



<i>IADAPT</i>	=	Control on whether adaptive processing is performed (0 = no, 1 = yes).
<i>ICORR</i>	=	Control on whether eigenvalue compensation is performed. Applicable only if the adaptive mode is selected (0 = no, 1 = yes).
<i>IELEM</i>	=	Control on type of processing architecture (0 = beam space, 1 = element space or subarray).
<i>IPRINTQC</i>	=	Control on whether the interference covariance matrix is written to an output unit. Applicable only if the adaptive mode is selected (0 = no, 1 = yes).
<i>IPRNTEIG</i>	=	Control on whether the eigenvalues of the interference covariance matrix are calculated and written to an output unit. Applicable only if the adaptive mode is selected (0 = no, 1 = yes).
<i>IREADQC</i>	=	Control on whether the interference covariance matrix (not including thermal noise) is read from a file (0 = no, 1 = yes).
<i>ITAC</i>	=	Control on type of TACCAR calculation used to center the mainbeam clutter spectrum about zero-Doppler (1 = phase shift, 2 = time shift approximated by phase shifts).
<i>IUSMTI</i>	=	Number of delays used with MTI preprocessing, where 0 implies no preprocessing.
<i>NP</i>	=	Number of pulses to be processed (processing order).
<i>NTAP</i>	=	Number of sampling interval taps.

Note that in the non-adaptive mode (*IADAPT* = 0), N-pulse MTI processing can be simulated by either setting *IUSMTI* equal to N-1 and *NP* equal to one, or by setting *IUSMTI* equal to zero and *NP* equal to N.

#### 3.1.4.2 Subarray

When subarray processing is selected (i.e., *IELEM* = 1), the processing parameters, in addition to the general processing inputs, consist of the number of azimuth subarrays, the number of antenna columns per azimuth subarray, the number of antenna columns in the overlap of adjacent azimuth subarrays, the number of elevation subarrays, the number of

antenna rows per elevation subarray, and the number of antenna rows in the overlap of adjacent elevation subarrays. The input names for the parameters used in the simulation are

<i>NEL_SUB</i>	=	Number of antenna columns per azimuth subarray.
<i>NEL_SUB2</i>	=	Number of antenna rows per elevation subarray.
<i>NOVRLAP</i>	=	Number of antenna columns in the overlap of adjacent azimuth subarrays.
<i>NOVRLAP2</i>	=	Number of antenna rows in the overlap of adjacent elevation subarrays.
<i>NSUB_AZ</i>	=	Number of azimuth subarrays.
<i>NSUB_EL</i>	=	Number of elevation subarrays.

#### **3.1.4.3 Element Space**

When element space processing is selected (i.e., *IELEM* = 1), the processing inputs are the general parameters described in Section 3.1.4.1. However, the subarray processing inputs must be appropriately selected to reflect subarrays consisting of a single antenna element (i.e., *NEL\_SUB* = 1, *NOVRLAP* = 0, *NSUB\_AZ* = *NUMAZIM*, *NEL\_SUB2* = 1, *NOVRLAP2* = 0, and *NSUB\_EL* = *NUMELEV*).

#### **3.1.4.4 Beam Space**

When beam space processing is selected (i.e., *IELEM* = 0), several input parameters in addition to the general parameters described earlier are required. The first input (i.e., *NDFT*) is the total number of azimuth beams formed, where the beams are uniformly distributed in sine of azimuth space and centered around the electronic scan angle in azimuth. The second input (i.e., *NBEAM*) is the number of azimuth beams to be processed. The third input parameter (i.e., *NLKB*) is the number of azimuth beams to be processed that are clustered around the center azimuth beam. The remaining azimuth beams to be processed (i.e., *NBEAM* - *NLKB*) are selected based on the maximum received quiescent jamming power. The input names for the parameters used in the simulation are

- NBEAM* = Number of azimuth beams to be processed, which is a subset of the total number of azimuth beams formed.
- NDFT* = Total number of azimuth beams formed.
- NLKB* = Number of processed azimuth beams clustered around the center azimuth beam.

### 3.1.4.5 Receive Antenna Pattern

The receive antenna gain pattern calculation has two options. The first option (i.e., *IPLOTP* = 1) calculates the azimuth-elevation antenna pattern for a Doppler cut corresponding to the target normalized Doppler. The second option (i.e., *IPLOTP* = 2) calculates the antenna pattern in azimuth-elevation and Doppler by reading the weights from a file (input unit 22 renamed with extension .wght). Note that no other calculations are performed by the simulation when this option is selected. The input parameters used in this calculation consist of the azimuth-elevation angles and normalized Doppler frequencies where the pattern is evaluated. The antenna gain patterns are calculated using the quiescent and adapted (or non-adapted) weights. The input names for the parameters used in the simulation are

- DPASCN* = Increment between sine of azimuth angles at which the azimuth-elevation or azimuth-elevation-Doppler receive antenna patterns are evaluated.
- DPASCN2* = Increment between normalized Dopplers at which the azimuth-elevation-Doppler receive antenna patterns are evaluated.
- DPASCN3* = Increment between sine of elevation angles at which the azimuth-elevation or azimuth-elevation-Doppler receive patterns are evaluated.
- IPLOTP* = Control on whether the azimuth-elevation or azimuth-elevation-Doppler receive antenna patterns are calculated and written to output files (0 = no, 1 = azimuth-elevation, 2 = azimuth-elevation-Doppler).

<i>NPTS</i>	=	Number of sine of azimuth angles at which the receive azimuth-elevation or azimuth-elevation-Doppler antenna patterns are evaluated.
<i>NPTS2</i>	=	Number of normalized Dopplers at which the receive azimuth-elevation-Doppler antenna patterns are evaluated.
<i>NPTS3</i>	=	Number of sine of elevation angles at which azimuth-elevation or azimuth-elevation-Doppler antenna patterns are evaluated.
<i>PASCN1</i>	=	Initial sine of azimuth angle for evaluating the receive azimuth-elevation or azimuth-elevation-Doppler antenna patterns.
<i>PASCN2</i>	=	Initial normalized Doppler for evaluating the azimuth-elevation-Doppler receive antenna patterns.
<i>PASCN3</i>	=	Initial sine of elevation angle for evaluating the receive azimuth-elevation or azimuth-elevation-Doppler receive antenna patterns.

#### 3.1.4.6 Doppler

The Doppler processing parameters consist of the number of outputs to be coherently integrated (i.e., Doppler processed), the type of Doppler weighting, and the number of Doppler frequencies to be evaluated (i.e., Doppler filters). The input names for the parameters used in the simulation are

<i>IDWT</i>	=	Control on type of Doppler weighting (0 = uniform, 1 = Hamming, 2 = Blackman, 3 = Dolph-Chebyshev).
<i>NCI</i>	=	Number of outputs to be coherently integrated (i.e., Doppler processed).
<i>NDOP</i>	=	Number of Doppler filters.
<i>SLDBDOP</i>	=	Sidelobe level of Dolph-Chebyshev Doppler weighting, if selected.

### **3.1.5 Miscellaneous Input Files**

#### **3.1.5.1 File 22**

This file is used as an input when the adapted azimuth-elevation-Doppler antenna pattern is calculated by reading the adaptive weights ( $IPLOTP = 2$ ).

#### **3.1.5.2 File 35**

This file is used as an input when the interference covariance matrix (not including thermal noise) is read from a file ( $IREADQC = 1$ ).

#### **3.1.5.3 File 150**

This file is used as an input when additional complex elemental taper weights are read from a file ( $ITPRFILE = 1$ ). See Appendix A to understand the format for reading the file.

#### **3.1.5.4 File 175**

This file is used as an input when the elemental voltages due to far-field clutter scatterers are read from a file ( $NUMQ = -1$ ). See Figure A-1 to understand the format for reading the file.

## **3.2 SIMULATION OUTPUTS**

This section briefly describes the output files created by the software.

### **3.2.1 Output File 10**

This output file contains the following:

- user input parameters;
- ranges, grazing and depression angles, and losses for the clutter and target;
- steering vector, if any;

- quiescent and adapted (or non-adapted) weights;
- beams selected for processing, if any;
- quiescent and adapted (or non-adapted) performance measures for a single processing output; and
- jammer and clutter scatterer azimuth angle locations.

### **3.2.2 Output File 11**

This output file contains the table of quiescent and adapted (or non-adapted) performance measures for a single processing output.

### **3.2.3 Output File 13**

This output file lists the quiescent and adapted (or non-adapted) azimuth-elevation receive antenna patterns evaluated at the hypothesized normalized target Doppler and at various sine of azimuth and elevation angles.

### **3.2.4 Output Files 14 and 16**

These output files list the quiescent and adapted (or non-adapted) performance measures for each Doppler frequency. Output file 16 does not contain any headings, allowing easy access for plotting.

### **3.2.5 Output File 22**

This output file lists the quiescent and adapted (or non-adapted) weights in the element space.

### **3.2.6 Output File 25**

This output file lists the entries of the consecutive rows of the interference covariance matrix, (if the adaptive mode option is selected). The entries include eigenvalue compensation if the option is selected.

### **3.2.7 Output File 30**

This output file lists the normalized eigenvalues of the interference covariance matrix (if the adaptive mode option is selected). The entries include eigenvalue compensation if the option is selected.

### **3.2.8 Output File 31**

This output file lists the quiescent and adapted (or non-adapted) azimuth-elevation-Doppler receive antenna patterns evaluated at the various sine of azimuth and elevation angles and normalized Dopplers. These patterns are calculated using the appropriate adapted or non-adapted weights in the element space that are read from input file 22 (*IPLOTP* = 2).

## SECTION 4

### RUNNING THE ADVANCED AIRBORNE RADAR SIMULATION

This section presents a step-by-step procedure for running the Advanced Airborne Radar Simulation either on the Research Computer Facility (RCF) UNIX-based machines or the VMS-based Sensor Center VAX, and discusses the minimum and maximum bounds on the program's inputs. Some typical CPU run times on the UNIX-based machine BAUHAUS are provided to illustrate the enhancements in run time, as compared to the original version of the simulation [1].

#### 4.1 RCF UNIX-BASED MACHINES

The source code for the RCF UNIX-based machines is located in the directory /vb/torres/STP\_FATIMA2. The steps needed to run the software are given below.

STEP 1. Create an alias defining the path to the executable file by including the following command in the .cshrc file found in the user's root (or home) directory:

```
alias RUN_STP /home/vb/torres/STP_FATIMA2/RUN_STP
```

STEP 2. Create a work directory with any arbitrary path (defined by *directory\_path*), and change directory to the work directory, with the following commands:

```
mkdir directory_path  
cd directory_path
```

STEP 3. Copy the input file template to the work directory with the following command:

```
cp /home/vb/torres/STP_FATIMA2/template.input template.input
```



STEP 4. Make a copy of the input file template to create an input file (denoted by *filename*) with the user's desired input parameters. Note that the new input file must include the .input extension. Type the following command:

**cp template.input *filename*.input**

STEP 5. Use an editor to change any desired parameters in *filename*.input.

STEP 6. To run the software using *filename*.input, type the following command (note that the extension .input is not included):

**RUN\_STP *filename***

The files described in Section 3 are renamed based on the name of the input file used (*filename*), as follows:

Output File 10  $\Rightarrow$  *filename*.output  
Output File 11  $\Rightarrow$  *filename*.perf  
Output File 13  $\Rightarrow$  *filename*.antpat  
Output File 14  $\Rightarrow$  *filename*.cperf  
Output File 16  $\Rightarrow$  *filename*.cperf2  
Output File 22  $\Rightarrow$  *filename*.wght  
Output File 25  $\Rightarrow$  *filename*.cov  
Output File 30  $\Rightarrow$  *filename*.eig  
Output File 31  $\Rightarrow$  *filename*.spctrm  
*filename*.wght  $\Rightarrow$  Output File 22  
*filename*.cov2  $\Rightarrow$  Output File 35  
*filename*.tprfile  $\Rightarrow$  Output File 150  
*filename*.gtd  $\Rightarrow$  Output File 175

## 4.2 VMS-BASED SENSOR CENTER VAX

The source code for the VMS-based Sensor-Center VAX is located in the directory PUBLIC1:[M18105.SPTIME.SOURCE]. The steps needed to run the software on the Sensor Center VAX are given below.

- STEP 1. Create an alias defining the path to the executable file by including the following command in the LOGIN.COM file found in the user's root (or home) directory:

```
$ RUN_STP:= = @PUBLIC1:[M18105.COM]RUN_STP
```

- STEP 2. Create a work directory with any arbitrary name (path defined by *directory\_path*), and change directory to the work directory with the following commands:

```
CREATE/DIRECTORY directory_path  
SET DEFAULT = directory_path
```

- STEP 3. Copy the template of the software input file to the work directory. Type the following command:

```
COPY PUBLIC1:[M18105.SPTIME]TEMPLATE.INPUT  
TEMPLATE.INPUT
```

- STEP 4. Make a copy of the input file template to create an input file (denoted by *filename.INPUT*) with the user's input parameters. Note that the new input file must include the .INPUT extension. Type the following command:

```
COPY TEMPLATE.INPUT filename.INPUT
```

- STEP 5. Use an editor to change any desired parameters in *filename.INPUT*.

STEP 6. To run the software on the VAX using *filename.INPUT*, type the following command (note the extension *.INPUT* is not included):

**RUN\_STP** *filename*

The output files described in Section 3 are renamed based on the name of the input file used (*filename*), as follows:

Output File 10  $\Rightarrow$  *filename.OUTPUT*  
Output File 11  $\Rightarrow$  *filename.PERF*  
Output File 13  $\Rightarrow$  *filename.ANTPAT*  
Output File 14  $\Rightarrow$  *filename.CPERF*  
Output File 16  $\Rightarrow$  *filename.CPERF2*  
Output File 22  $\Rightarrow$  *filename.WGHT*  
Output File 25  $\Rightarrow$  *filename.COV*  
Output File 30  $\Rightarrow$  *filename.EIG*  
Output File 31  $\Rightarrow$  *filename.SPCTRM*  
*filename.WGHT*  $\Rightarrow$  Output File 22  
*filename.COV2*  $\Rightarrow$  Output File 35  
*filename.TPRFILE*  $\Rightarrow$  Output File 150  
*filename.GTD*  $\Rightarrow$  Output File 175

### 4.3 CPU RUN TIMES

Figure 27 presents some CPU run times for executing the enhanced simulation on the RCF UNIX-based machine BAUHAUS. The run times are shown only for a baseline scenario in the adaptive mode, using different numbers antenna columns and the parameters listed. Figure 27 illustrates the significant enhancement in run time, as compared to the original version of the simulation.

Number of Antenna Rows (NUMELEV) = 8	Number of Range Rings = 1
Number of Clutter Scatterers (NCL) = 181	No MTI Preprocessing (IUSMTI = 0)
Number of Jammers (NESI) = 4	No Antenna Pattern Calculation (IPLOTP = 0)
Adaptive Processing (IADAPT = 1)	No Eigenvalue Compensation (ICORR = 0)
Subarray Space Architecture (IELEM = 1)	No Eigenvalue Calculation (IPRNTEIG = 0)
Number of Elevation Subarrays (NSUB_EL) = 1	Number of Doppler Filters (NDOP) = 50
Number of Pulses Processed (NP) = 2	Number of Coherently Integrated Outputs (NCI) = 16
Number of Frequency Components (NFR) = 1	

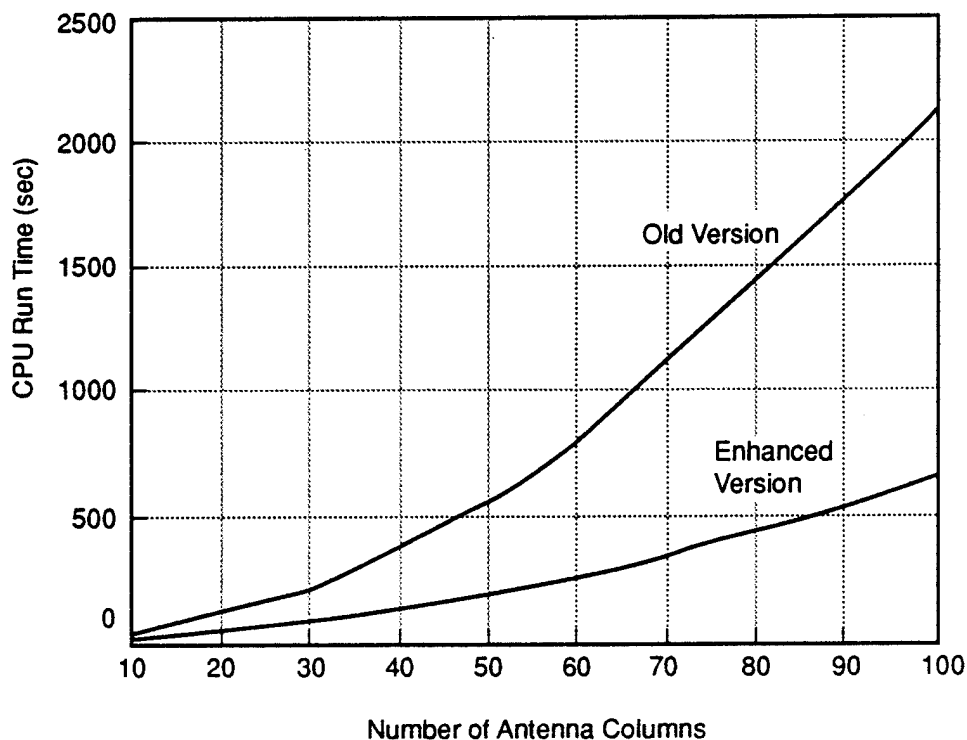


Figure 27. Illustrative CPU Run Times for RCF UNIX-Based Machine BAUHAUS

To give the user additional insight, several additional run times on BAUHAUS are listed below when the baseline parameters are varied. These run times illustrate the effect of varying the baseline scenario parameters such as the number of ambiguous range rings, number of frequency components, number of antenna rows, and the STP architecture. For illustrative purposes, the number of antenna columns is 50 for all the parametric examples. As shown in Figure 27, to execute the baseline scenario the run time is 189 seconds for BAUHAUS, as compared to a previous run time of 565 seconds.

- When the number of ambiguous range rings is increased from 1 to 10 (i.e., for a high-PRF radar example), then the run time is 648 seconds, as compared to a previous run time of 1103 seconds.
- When the number of frequency components ( $NFR$ ) is increased from 1 to 5, then the run time is 748 seconds, as compared to a previous run time of 1768 seconds.
- When the number of jammers ( $NESI$ ) is increased from 4 to 8, and the number of antenna rows is increased from 8 to 16, then the run time is 373 seconds, as compared to a previous run time of 684 seconds. Note that this scenario includes calculation of the antenna pattern ( $IPLOTP = 1$ ) and eigenvalues ( $IPRNTEIG = 1$ ).
- With three-pulse MTI preprocessing ( $IUSMTI = 2$ ), the run time is 1197 seconds, as compared to a previous run time of 3825 seconds.
- With the beam space architecture ( $IELEM = 0$ ), the run time is 418 seconds, as compared to a previous run time of 34242 seconds.

It should be noted that the source code was compiled without any optimizations. However, future applications of the simulation can readily apply machine-dependent optimizations by recompiling the source code.

#### **4.4 BOUNDS ON SIMULATION INPUT PARAMETERS**

Table 2 presents the minimum and the maximum bounds on the input parameters, and additional requirements for certain parameters needed to execute the simulation. This will assist users in understanding the parameter bounds required to execute the program successfully for their applications.

**Table 2. Input Parameter Bounds**

	Input Parameter Name	Minimum Bound	Maximum Bound	Remarks
Radar Parameters	<i>DEFR</i>	> 0.0	N/A	None
	<i>FC</i>	> 0.0	N/A	None
	<i>FREP</i>	> 0.0	N/A	Maximum of 350 ambiguous ranges
	<i>NFR</i>	1	7	None
	<i>PLATALT</i>	> 0.0	N/A	See <i>TARGRNG</i>
	<i>TIME_BW</i>	> 0.0	N/A	None
	<i>VELNM</i>	0.0	N/A	None
	<i>XMT_PWR</i>	> 0.0	N/A	None
Antenna Parameters	<i>CANRATDB</i>	0.0	150.0	None
	<i>DEWL</i>	> 0.0	N/A	None
	<i>DEWLELEV</i>	> 0.0	N/A	None
	<i>IELPG</i>	0	2	None
	<i>ISUBTPR</i>	0	1	None
	<i>ISUBTPR2</i>	0	1	None
	<i>ITAPER</i>	0	1	None
	<i>ITPRFILE</i>	0	1	None
	<i>ITPRSUB</i>	0	1	None
	<i>ITPRSUB2</i>	0	1	None
	<i>NBAR</i>	1	N/A	None
	<i>NBARELEV</i>	1	N/A	None
	<i>NBARSUB</i>	1	N/A	None
	<i>NBARSUB2</i>	1	N/A	None
	<i>NSUBBAR</i>	1	N/A	None
	<i>NSUBBAR2</i>	1	N/A	None
	<i>NUMAZIM</i>	1	SZE2*	Note 0
	<i>NUMELEV</i>	1	50	None
	<i>SLDBELEV</i>	0.0	N/A	None
	<i>SLDBSUB2</i>	0.0	N/A	None
	<i>SLDBSUB</i>	0.0	N/A	None
	<i>SLLDB</i>	0.0	N/A	None
	<i>SUBSLDB</i>	0.0	N/A	None
	<i>SUBSLDB2</i>	0.0	N/A	None
	<i>THS</i>	-90.0	90.0	None
	<i>THSCN1</i>	0.0	180.0	None
	<i>THS_EL</i>	0.0	90.0	None
	<i>TH_AZ3DB</i>	0.0	180.0	$\geq DTTHC$ if $NCL > 0$
	<i>TH_EL3DB</i>	0.0	180.0	None

Table 2. (Continued)

		Input Parameter Name	Minimum Bound	Maximum Bound	Remarks
Environmental Parameters	Clutter	<i>DTTHC</i> <i>GAMMA</i> <i>ICLUT</i> <i>NCL</i> <i>SIGMA_V</i>	> 0.0 N/A 0 0 > 0.0	$\leq TH\_AZ3DB$ N/A 1 1001 N/A	$DTTHC \cdot (NCL - 1) \leq 180.0$ None None $DTTHC \cdot (NCL - 1) \leq 180.0$ None
	Jamming	<i>DEFR_J</i> <i>FC_J</i> <i>IDCORRJ</i> <i>NESI</i> <i>NFR_J</i> <i>P</i> <i>PHIPLS_J</i> <i>RNG_JAM</i>  <i>THJ_EL</i> <i>TTHJ</i>	> 0.0 > 0.0 0 0 1 > 0.0 -0.5 > 0.0  0.0 -90.0	N/A N/A 1 20 7 N/A 0.5 N/A  90.0 90.0	Jammer within radar band Jammer within radar band None None Jammer within radar band None None Maximum range depends on jammer depression angle None None
	Target	<i>PHIPLSE</i> <i>SIGMA_T</i> <i>TARGALT</i>  <i>TARGRNG</i>	-0.5 > 0.0 0.0  $\geq \frac{0.3048}{1852.0} (PLATALT)$	0.5 N/A N/A  Range to Horizon	None None None  None
	Noise	<i>F_N</i>	0.0	N/A	None
	Losses	<i>ILOSS</i> <i>L_S</i> <i>L_T</i>	0 0.0 0.0	1 N/A N/A	None None None
	Near-Field Effects	<i>BCSQ</i> <i>ITARGQ</i> <i>NUMQ</i> <i>XQ</i> <i>YQ</i> <i>ZQ</i>	0.0 0 -1 N/A N/A N/A	N/A 1 99 N/A N/A N/A	$NUMQ > 0$ $NUMQ > 0$ None Cannot equal 0.0, $NUMQ > 0$ Cannot equal 0.0, $NUMQ > 0$ Cannot equal 0.0, $NUMQ > 0$



**Table 2. (Concluded)**

		Input Parameter Name	Minimum Bound	Maximum Bound	Remarks
Processing Parameters	General	<i>DTDL</i>	>0.0	$\leq 1 / (NFR \cdot DEFR)$	None
		<i>IADAPT</i>	0	1	None
		<i>ICORR</i>	0	1	None
		<i>IELEM</i>	0	1	Note 1
		<i>IPRINTQC</i>	0	1	None
		<i>IPRNTEIG</i>	0	1	None
		<i>IREADQC</i>	0	1	None
		<i>ITAC</i>	1	2	None
		<i>IUSMTI</i>	0	<i>SZE*</i>	None
		<i>NP</i>	1	N/A	Note 2
		<i>NTAP</i>	1	28	Note 2
	Subarray	<i>NEL_SUB</i>	1	<i>SZE2*</i>	Notes 1 and 3
		<i>NEL_SUB2</i>	1	<i>SZE2*</i>	Notes 1 and 3
		<i>NOVRLAP</i>	0	<i>SZE2*</i>	Notes 1 and 3
		<i>NOVRLAP2</i>	0	<i>SZE2*</i>	Notes 1 and 3
		<i>NSUB_AZ</i>	1	<i>SZE*</i>	Notes 1, 2 and 3
		<i>NSUB_EL</i>	1	<i>SZE*</i>	Notes 1, 2 and 3
	Beam Space	<i>NBEAM</i>	1	<i>SZE*</i>	Note 4
		<i>NDFT</i>	1	<i>SZE*</i>	Note 5
		<i>NLKB</i>	1	<i>SZE*</i>	$NLKB \leq NBEAM$
	Receive Antenna Pattern	<i>DPASCN</i>	> 0.0	2.0	Note 6
		<i>DPASCN2</i>	> 0.0	1.0	Note 7
		<i>DPASCN3</i>	> 0.0	2.0	Note 8
		<i>IPLOTP</i>	0	2.0	None
		<i>NPTS</i>	1	N/A	Note 6
		<i>NPTS2</i>	1	N/A	Note 7
		<i>NPTS3</i>	1	N/A	Note 8
		<i>PASCN1</i>	-1.0	1.0	Note 6
		<i>PASCN2</i>	-0.5	0.5	Note 7
		<i>PASCN3</i>	-1.0	1.0	Note 8
	Doppler	<i>IDWT</i>	0	3	None
		<i>NCI</i>	0	256	$NCI \leq NDOP$
		<i>NDOP</i>	0	N/A	See <i>NCI</i>
		<i>SLDBDOP</i>	0.0	N/A	None

Note 0:  $NP \cdot NTAP \cdot NUMAZIM \cdot NUMELEV \leq SZE2$

Note 1: For element space:  $NEL\_SUB = 1$ ,  $NOVRLAP = 0$ ,  $NSUB\_AZ = NUMAZIM$ ,  
 $NEL\_SUB2 = 1$ ,  $NOVRLAP2 = 0$ ,  $NSUB\_EL = NUMELEV$

Note 2:  $NP \cdot NTAP \cdot NSUB\_AZ \cdot NSUB\_EL \leq SZE$

Note 3:  $NSUB\_AZ \cdot (NEL\_SUB - NOVRLAP) = NUMAZIM - NOVRLAP$ ,  
 $NSUB\_EL \cdot (NEL\_SUB2 - NOVRLAP2) = NUMELEV - NOVRLAP2$

Note 4:  $NP \cdot NTAP \cdot NBEAM \cdot NSUB\_EL \leq SZE$

Note 5:  $NSUB\_AZ \geq NDFT \geq NBEAM$

Note 6:  $(NPTS - 1) \cdot DPASCN + PASCN1 \leq 1.0$

Note 7:  $(NPTS2 - 1) \cdot DPASCN2 + PASCN2 \leq 0.5$

Note 8:  $(NPTS3 - 1) \cdot DPASCN3 + PASCN3 \leq 1.0$

\*The values of *SZE* and *SZE2* depends on the machine used and can change in the future. They are written to output unit 10.

## LIST OF REFERENCES

1. Suresh Babu, B. N., and J. A. Torres, 1992, "Advanced Airborne Radar Simulation with Adaptive Antenna Techniques, Volume 1," MTR92B0000058V1, The MITRE Corporation, Bedford, Massachusetts.
2. Suresh Babu, B. N., and J. A. Torres, 1992, "Advanced Airborne Radar Simulation with Adaptive Antenna Techniques, Volume 2," MTR92B0000058V2, The MITRE Corporation, Bedford, Massachusetts.
3. Suresh Babu, B. N., and J. A. Torres, 1992, "Advanced Airborne Radar Simulation with Adaptive Antenna Techniques," SCS Summer Computer Simulation Conference.
4. Suresh Babu, B. N., and J. A. Torres, 1993, "Adaptive Airborne Radar Simulation with Equalization Filter Taps," SCS Summer Computer Simulation Conference.
5. Suresh Babu, B. N., and J. A. Torres, 1992, "Investigation of Some Critical Issues of Space-Time Processing (STP) Affecting Airborne Radar Performance," MTR-11055, The MITRE Corporation, Bedford, Massachusetts.
6. Suresh Babu, B. N., and J. A. Torres, 1993, "Theory and Implementation of Equalization Filter Taps in the Advanced Airborne Radar Simulation with Adaptive Antenna Techniques," MTR93B0000017, The MITRE Corporation, Bedford, Massachusetts.
7. E. C. Barile, 1992, "Space-Time Methods in Detecting Targets in Clutter," MTR92B0000007, The MITRE Corporation, Bedford, Massachusetts.
8. D. Lamensdorf, 1990, "A Flexible Model for Creating Realistic Inputs to a Space-Time Processing Simulation," D084-M-653, The MITRE Corporation, Bedford, Massachusetts.

## APPENDIX A

### MATHEMATICAL DETAILS OF PROGRAM MODIFICATIONS

The Advanced Airborne Radar Simulation is based on the modeled steady-state covariance matrix of each of the signals received by an airborne pulse-Doppler phased-array radar. In this attachment, we generalize the models of the steady-state covariance matrix developed in references 1 and 6 to include the effects of near-field scattering, spatial degrees of freedom in elevation, and additional complex elemental weighting. We begin by expressing the received clutter signal after matched filtering (pulse compression) and demodulation to baseband. The clutter model consists of far-field scatterers located at discrete angular locations, extending into the sidelobes of the array transmit beam. There are  $M$  clutter scatterers located at  $N$  ambiguous ranges. Following the model development presented in references 1 and 6, it can be shown that the received clutter signal in the presence of near-field scattering (at element  $(e_x, e_z)$  of a planar array in the  $x$ - $z$  plane, pulse  $k$ , and tap  $\ell$ ) is

$$c_{e_x e_z}(\ell, k) = (B\tau_u)^{1/2} \cdot e^{j\pi(\ell-1)B\tau} \cdot \text{sinc}(\pi(\ell-1)B\tau) \cdot D_{e_x e_z} \cdot \sum_{n=1}^N \sum_{m=1}^M e^{-j\alpha_{nm}} \cdot \hat{b}_{nm} \cdot e^{j\omega_c \beta_{nm}(k-1)T} \cdot \sum_{q=0}^Q A_q \cdot e^{j\omega_c T_{nmq}^{e_x e_z}}, \quad (\text{A-1})$$

where

- $e_x$  = receive element index in  $x$ -direction
- $e_z$  = receive element index in  $z$ -direction
- $\ell$  = tap index
- $k$  = pulse index
- $B$  = bandwidth of compressed pulse (radar bandwidth)
- $\tau_u$  = uncompressed transmitted pulsewidth
- $\tau$  = tap spacing  $\leq 1/B$

- $D_{e_x e_z}$  = additional elemental weighting  
 $N$  = number of ambiguous ranges  
 $M$  = number of clutter scatterers  
 $\alpha_{nm}$  = clutter scatterer random phase  
 $\hat{b}_{nm}$  = clutter scatterer complex echo amplitude  
 $\omega_c$  = radar center frequency  
 $\beta_{nm} = 2 V_{nm}/C$   
 $V_{nm}$  = clutter scatterer radial velocity  
 $c$  = speed of light  
 $T$  = pulse repetition interval  
 $Q$  = number of near-field scatterers  
 $q$  = near-field scatterer index on receive  
 $A_q$  = near-field scatterer reflectivity ( $A_0 \equiv 1$ )  
 $T_{nmq}^{e_x e_z}$  = delay across array to element ( $e_x, e_z$ ) for a clutter scatterer signal reflected from  $q^{\text{th}}$  near-field scatterer.

Note that  $q = 0$  corresponds to the direct path scattering case (i.e., with no near-field scatterers present). The clutter scatterer complex echo amplitude  $\hat{b}_{nm}$  is

$$\hat{b}_{nm} = \sqrt{P_{nm}} \cdot \left\{ \sum_{\forall(\hat{e}_x, \hat{e}_z)} W_{\hat{e}_x \hat{e}_z} \cdot D_{\hat{e}_x \hat{e}_z} \cdot \sum_{\hat{q}=0}^Q A_{\hat{q}} \cdot e^{j\omega_c T_{nm\hat{q}}^{\hat{e}_x \hat{e}_z}} \right\}, \quad (\text{A-2})$$

where

- $P_{nm}$  = clutter scatterer reflected power for single element on transmit in free space, including elemental gain patterns on transmit and receive  
 $\hat{q}$  = near-field scatterer index on transmit  
 $\hat{e}_x$  = transmit element index in  $x$ -direction  
 $\hat{e}_z$  = transmit element index in  $z$ -direction

$D_{\hat{e}_x \hat{e}_z}$  = additional elemental weighting

$W_{\hat{e}_x \hat{e}_z}$  = element weighting on transmit, including electronic scanning.

In Equation (A-2), the bracketed expression is the antenna transmit pattern in the presence of the near-field scatterers, and  $P_{nm}$  is a function of the radar cross-section (RCS) of the clutter scatterer based on the radar range Equation [1]. The RCS is for a set of scatterers constituting homogeneous clutter with a constant backscatter coefficient. The delay  $T_{nmq}^{e_x e_z}$  is given by

$$T_{nmq}^{e_x e_z} = \begin{cases} \frac{e_x \Delta_x \sin \theta_m^B \cos \theta_n^D + e_z \Delta_z \sin \theta_n^D}{c}, & q = 0 \\ \frac{R_n - R_{nmq} - R_{qe_x e_z}}{c}, & q \neq 0 \end{cases} \quad (\text{A-3})$$

where

$\theta_m^B$  = clutter scatterer azimuth relative to broadside

$\theta_n^D$  = ambiguous range depression angle

$\Delta_x$  = elemental spacing in  $x$ -direction

$\Delta_z$  = elemental spacing in  $z$ -direction

$R_n$  =  $n^{\text{th}}$  ambiguous range

$R_{nmq}$  = range between clutter scatterer and near-field scatterer

$R_{qe_x e_z}$  = range between near-field scatterer and element  $(e_x, e_z)$ ,

$$R_{qe_x e_z} = \sqrt{(e_x \Delta_x - x_q)^2 + (y_q)^2 + (e_z \Delta_z - z_q)^2}, \quad (\text{A-4})$$

$$R_{nmq} = \sqrt{(R_n \sin \theta_m^B \cos \theta_n^D - x_q)^2 + (R_n \cos \theta_m^B \cos \theta_n^D - y_q)^2 + (R_n \sin \theta_n^D - z_q)^2}, \quad (\text{A-5})$$

and

$$\begin{aligned} x_q &= \text{near-field scatterer location in } x\text{-direction} \\ y_q &= \text{near-field scatterer location in } y\text{-direction} \\ z_q &= \text{near-field scatterer location in } z\text{-direction.} \end{aligned}$$

The near-field scatterer reflectivity is given by

$$A_q = \sqrt{\frac{\sigma_q}{4\pi \cdot R_{qe_x e_z}^2}}, \quad (\text{A-6})$$

where  $\sigma_q$  is the bistatic cross-section of the near-field scatterer.

The entries of the received clutter steady-state covariance matrix are based on the expected cross-covariance of the clutter signal received between antenna elements, taps, and pulses. If we assume the clutter scatterers are spatially uncorrelated, then

$$E\left[e^{-j(\alpha_{n_1 m_1} - \alpha_{n_2 m_2})}\right] = \delta(n_1 - n_2) \cdot \delta(m_1 - m_2), \quad (\text{A-7})$$

where  $\delta$  is the Kronecker delta. This results in

$$\begin{aligned} E\left[c_{e1_x e1_z}(\ell_1, k_1) c_{e2_x e2_z}^*(\ell_2, k_2)\right] &= (B\tau_u) \cdot e^{j\pi(\ell_1 - \ell_2)B\tau} \cdot \text{sinc}(\pi(\ell_1 - 1)B\tau) \cdot D_{e1_x e1_z} \cdot D_{e2_x e2_z}^* \\ &\cdot \text{sinc}(\pi(\ell_2 - 1)B\tau) \cdot \sum_{n=1}^N \sum_{m=1}^M |\hat{b}_{nm}|^2 \cdot e^{j\omega_c \beta_{nm}(k_1 - k_2)T} \\ &\cdot \sum_{q_1=0}^Q \sum_{q_2=0}^Q A_{q_1} \cdot A_{q_2} \cdot e^{j\omega_c (T_{nmq_1}^{e1_x e1_z} - T_{nmq_2}^{e2_x e2_z})}. \end{aligned} \quad (\text{A-8})$$

Note that the received clutter is temporally stationary from pulse-to-pulse since the entries of the steady-state covariance matrix are a function of the difference in pulse indices (i.e.,  $k_1 - k_2$ ). However, it is spatially stationary from element-to-element (i.e., entries are a function of the difference in element indices) only in the absence of near-field scattering (i.e.,  $Q = 0$ ). Note that the steady-state covariance matrix corresponding to the elemental signals transformed into beams or subarrays (i.e., azimuth and elevation) are computed based on the techniques discussed in reference 1.

Finally, let us define the complex voltage at an antenna element due to a far-field clutter scatterer in the presence of near-field scattering by the term

$$V_{nm}^{e_x e_z} = \sum_{q=0}^Q A_q \cdot e^{j\omega_c T_{nmq}^{e_x e_z}}, \quad (\text{A-9})$$

which occurs in Equations (A-1) and (A-2). This term can be explicitly calculated from the model parameters of the  $Q$  near-field point scatterers. Alternatively, this term can be read from the geometric theory of diffraction (GTD) simulation output file [7, 8]. The interfacing of the GTD output files and the simulation requires that the files have the proper format. Figure A-1 illustrates the order that the complex elemental voltages (i.e., amplitude and phase) are read from the file. Note that the additional complex elemental taper weights (i.e., amplitude and phase) are read from a file using the same antenna indexing format illustrated in Figure A-1(e).

$V_{nm}^{e_x e_z}$  = Complex elemental voltages  
 $n$  = Ambiguous range index; 1 to  $N$   
 $m$  = Clutter scatterer index; 1 to  $M$   
 $e_x$  = Antenna column index; 1 to  $Ne_x$   
 $e_z$  = Antenna row index; 1 to  $Ne_z$

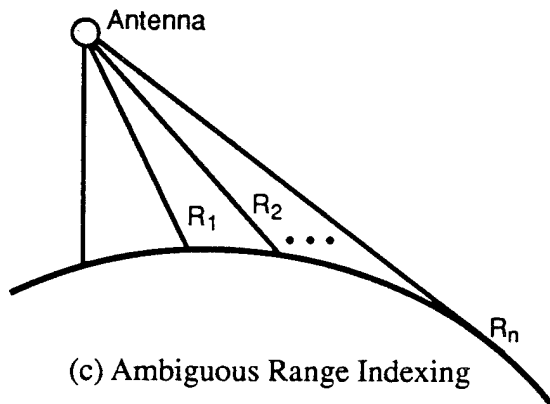
(a) Notation

```

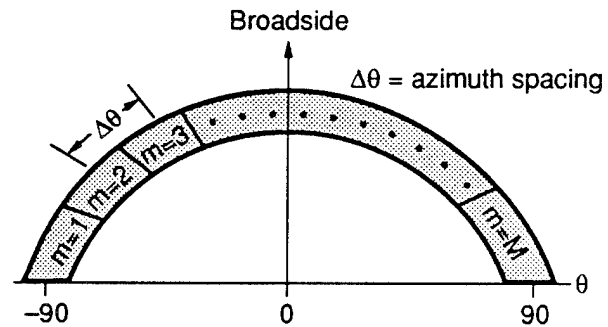
for n = 1 to N
  for m = 1 to M
    for  $e_z$  = 1 to  $Ne_z$ 
      for  $e_x$  = 1 to  $Ne_x$ 
        read  $V_{nm}^{e_x e_z}$  (amplitude and phase)
      end
    end
  end
end

```

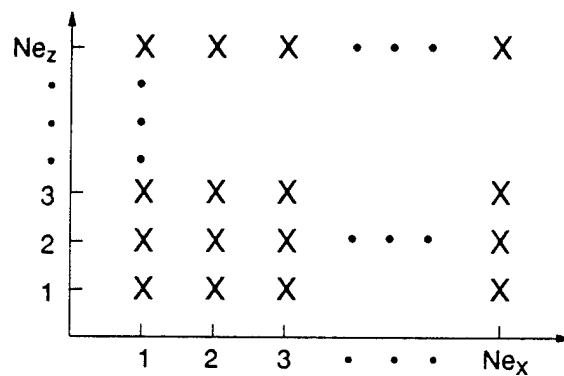
(b) Input Ordering



(c) Ambiguous Range Indexing



(d) Clutter Scatterer Indexing



(e) Antenna Indexing

Figure A-1. Illustrations to Understand How GTD Files are Read



## **APPENDIX B**

### **OVERVIEW OF CHANGES TO SUBROUTINES**

#### **B.1.1 A A N T P S 3**

This new subroutine calculates coordinates of the center of the elevation subarrays relative to the array center, and the coordinates of the array rows relative to the center of their respective elevation subarray. In addition, it calculates the non-adapted moving target indicator (MTI) taper weights for the elevation subarrays on receive.

#### **B.1.2 A Z \_ D O P**

Earlier, this subroutine calculated the two-dimensional quiescent and adapted (or MTI) receive far-field azimuth-Doppler spectrums at the elevation electronic scan angle for a given set of quiescent and adapted (or MTI) weights. The modified subroutine calculates the three-dimensional receive far-field elevation-azimuth-Doppler spectrums for a given set of weights.

#### **B.1.3 B M S P C A N D B M S L C T**

These subroutines calculate the unitary forward and inverse azimuth beam space transformation matrices used to transform between azimuth subarrays and azimuth beams. The new subroutine calculates the azimuth beam space transformation of each receive subarray in elevation.

#### **B.1.4 C O V C A N D C L U T M T I**

These subroutines calculate the received clutter steady-state covariance matrix corresponding to two processing outputs with MTI preprocessing. The entries of the matrix are based upon the expected cross-covariance of the clutter signal received between antenna subarrays, taps,

and pulses. The upgraded subroutines allow the calculation of multiple receive subarrays in elevation.

#### **B.1.5 COVN AND THNSMTI**

These subroutines calculate the received noise steady-state covariance matrix corresponding to two processing outputs with MTI preprocessing. The noise is modeled as uncorrelated pulse-to-pulse, and element-to-element. Tap-to-tap correlation for a given element is based upon the radar bandwidth, and spatial correlation between overlapped subarrays. The modified routines form multiple receive subarrays in elevation.

#### **B.1.6 ELG\_CLUT**

This subroutine calculates the receive gain and phase for a narrowband component of a received clutter scatterer signal from a given ambiguous range at each antenna element, and then at each receive subarray. The transmit antenna pattern is included in this calculation. The new routines form multiple receive subarrays in elevation. The effects of near-field scattering are included in the modified subroutines.

#### **B.1.7 ELG\_RJAM**

This subroutine calculates the gain and phase element for a narrowband component of a received jammer signal at each antenna, and then at each receive subarray. This modified subroutine allows the calculation of multiple receive subarrays in elevation and includes the effects of near-field scattering.

#### **B.1.8 ELPG**

This modified subroutine calculates only the gain of an antenna element for a specified spatial location in azimuth and elevation. This calculation is based upon the specified elemental gain patterns in azimuth and elevation.

### **B.1.9 E L S**

This subroutine calculates the gain and phase for a narrowband component of a received target signal at each antenna, and then at each receive subarray. The transmit antenna pattern is included in this calculation. This modified subroutine allows the calculation of multiple receive subarrays in elevation and includes the effects of near-field scattering.

### **B.1.10 E L S S T E E R**

This subroutine calculates the gain and phase for a narrowband component of a hypothesized received target signal (i.e., steering vector) at each antenna element, and then at each receive subarray. This modified subroutine allows the calculation of multiple receive subarrays in elevation and includes the effects of near-field scattering.

### **B.1.11 E S C A N**

This subroutine calculates the gain and phase at each antenna element, and then at each receive subarray, for a far-field test signal target. This test target is used to evaluate the receive quiescent and adapted (or MTI) elevation-azimuth-Doppler spectrum. To reduce the execution time, the test signal is assumed to consist of a single narrowband component centered about the carrier frequency. This modified subroutine allows the calculation of multiple receive subarrays in elevation and includes the effects of near-field scattering.

### **B.1.12 M A I N**

This modified main program electronically scans the non-adapted MTI elevation weights used for each elevation subarray on receive; calculates adapted (or MTI) weights used to combine both the azimuth and elevation subarrays on receive; and calculates the two-dimensional receive far-field elevation-azimuth spectrum at the target Doppler for a given set of quiescent and adapted (or MTI) weights.

#### **B.1.13 SSGSTEERANDSTEERGEN**

These subroutines calculate the hypothesized received target steady-state covariance matrix corresponding to two processing outputs with MTI preprocessing. This matrix is used to calculate the steering vector. The entries of the matrix are based on the expected cross-covariance of the hypothesized target signal received between antenna subarrays, taps, and pulses. This modified subroutine allows the calculation of multiple receive subarrays in elevation.

#### **B.1.14 SSSGANDSIGNMTI**

These subroutines calculate the received target steady-state covariance matrix corresponding to two processing outputs with MTI preprocessing. The entries of the matrix are based upon the expected cross-covariance of the target signal received between antenna subarrays, taps, and pulses. This modified subroutine forms multiple receive subarrays in elevation and includes the effects of near-field scattering.

## APPENDIX C

### INPUT AND OUTPUT FILES FOR ILLUSTRATIVE EXAMPLES

In this appendix, we present the input and output files for the different illustrative examples discussed earlier in this report. First, for each of the examples, we present the input and output files for a single case. For conciseness, the input and output files for the remaining cases are not presented, and we describe only the changes to the input parameters. The examples should aid users in adapting this program to their applications.

#### C.1 SIDELobe JAMMER NULLING WITH ELEVATION DEGREES OF FREEDOM

In Section 2.1.1, we illustrated how elevation degrees of freedom can be used to cancel a sidelobe jammer. Figure C-1 shows the input file of the simulation. Figure C-2 shows the performance measures from output file 11 used to obtain Figure 4. The "quiescent" and "adaptive" curves of Figure 5 are obtained by plotting the quiescent and adapted elevation receive antenna gains (columns 3 and 4 of output file 13, respectively) versus elevation (arcsine of column 2 of output file 13). Note that for conciseness, output file 13 is not shown.

#### C.2 CLUTTER CANCELLATION WITH ELEVATION DEGREES OF FREEDOM

In Section 2.1.2, we illustrated how elevation degrees of freedom can be used to cancel short- and long-range clutter competing with a long-range target. Figure C-3 shows the input file of the simulation for the case when the number of pulses (i.e.,  $NP$ ) is one. Figure C-4 shows the performance measures from output file 11 used to obtain Figure 6. The "quiescent" and "adaptive" curves of Figure 7 are obtained by plotting the quiescent and adapted elevation receive antenna gains (columns 3 and 4 of output file 13, respectively) versus elevation (arcsine of column 2 of output file 13). Note that for conciseness, output file 13 is not shown. Figures 8 and 9 are similarly obtained by changing the value of  $NP$  from one to four, and including eigenvalue compensation ( $ICORR = 1$ ).

# RADAR PARAMETERS

```

-----
NFR          DEFR          TIME_BW
1            1.00E06       2000.0

FC           FREP          XMT_PWR
1300.0E06    600.0        5.60E06

PLATALT      VELNM
30000.0      350.0

```

# ANTENNA PARAMETERS

```

-----
NUMAZIM      NUMELEV      DEWL          DEWLELEV
1            20           0.50          0.50

NBAR         NBARELEV     SLLDB         SLDLELEV
5            5            30.0          30.0

ITAPER       THS          THS_EL        THSC1
1            00.00        10.00         90.00

ITPRSUB      NBARSUB      SLDBSUB       30.0
1            5            30.0

ISUBTPR      NSUBBAR      SUBSLDB       30.0
1            5            30.0

ITPRSUB2     NBARSUB2     SLDBSUB2      30.0
1            5            30.0

ISUBTPR2     NSUBBAR2     SUBSLDB2      30.0
1            5            30.0

TH_AZ3DB     TH_EL3DB      CANRATDB
80.00        10.00        55.00

IELPG        ITPRFILE
0            0

```

# CLUTTER PARAMETERS

```

-----
NCL          DTTHC        SIGMA_V
0            1.0          4.0E-10

GAMMA        ICLUT
-9.0         0

```

# JAMMING PARAMETERS

```

-----
NESI         IDCORRJ
1            0

TTHJ( 1 - 4 )
00.0E+00     00.0E+00     0.0E+00     0.0E+00

TTHJ( 5 - 8 )
00.0E+00     00.0E+00     0.0E+00     0.0E+00

```

Figure C-1. Input File for Sidelobe Jammer Nulling With Elevation Degrees of Freedom

TTHJ( 9 - 12 )			
00.0E+00	00.0E+00	0.0E+00	0.0E+00
TTHJ( 13 - 16 )			
00.0E+00	00.0E+00	0.0E+00	0.0E+00
TTHJ( 17 - 20 )			
00.0E+00	00.0E+00	0.0E+00	0.0E+00
RNG_JAM( 1 - 4 )			
9.0E+00	60.0E+00	00.0E+00	00.0E+00
RNG_JAM( 5 - 8 )			
00.0E+00	00.0E+00	00.0E+00	00.0E+00
RNG_JAM( 9 - 12 )			
00.0E+00	00.0E+00	00.0E+00	00.0E+00
RNG_JAM( 13 - 16 )			
00.0E+00	00.0E+00	00.0E+00	00.0E+00
RNG_JAM( 17 - 20 )			
00.0E+00	00.0E+00	00.0E+00	00.0E+00
P( 1 - 4 )			
3.00E+04	2.35E+04	0.00E+00	0.00E+00
P( 5 - 8 )			
0.00E+00	0.00E+00	0.00E+00	0.00E+00
P( 9 - 12 )			
0.00E+00	0.00E+00	0.00E+00	0.00E+00
P( 13 - 16 )			
0.00E+00	0.00E+00	0.00E+00	0.00E+00
P( 17 - 20 )			
0.00E+00	0.00E+00	0.00E+00	0.00E+00
THJ_EL( 1 - 4 )			
32.0E+00	00.0E+00	00.0E+00	00.0E+00
THJ_EL( 5 - 8 )			
00.0E+00	00.0E+00	00.0E+00	00.0E+00
THJ_EL( 9 - 12 )			
00.0E+00	00.0E+00	00.0E+00	00.0E+00
THJ_EL( 13 - 16 )			
00.0E+00	00.0E+00	00.0E+00	00.0E+00
THJ_EL( 17 - 20 )			
00.0E+00	00.0E+00	00.0E+00	00.0E+00
NFR_J( 1 - 4 )			
1	1	1	1
NFR_J( 5 - 8 )			
1	1	1	1
NFR_J( 9 - 12 )			
1	1	1	1
NFR_J( 13 - 16 )			
1	1	1	1

Figure C-1. Input File for Sidelobe Jammer Nulling With Elevation Degrees of Freedom  
(Continued)

NFR_J( 17 - 20 )			
1	1	1	1
DEFR_J( 1 - 4 )			
2.00E+06	0.00E+06	0.00E+06	0.00E+06
DEFR_J( 5 - 8 )			
1.00E+06	0.00E+06	0.00E+06	0.00E+06
DEFR_J( 9 - 12 )			
1.00E+06	0.00E+06	0.00E+06	0.00E+06
DEFR_J( 13 - 16 )			
1.00E+06	0.00E+06	0.00E+06	0.00E+06
DEFR_J( 17 - 20 )			
1.00E+06	0.00E+06	0.00E+06	0.00E+06
FC_J( 1 - 4 )			
1300.00E+06	1300.00E+06	1300.00E+06	1300.00E+06
FC_J( 5 - 8 )			
1300.00E+06	1300.00E+06	1300.00E+06	1300.00E+06
FC_J( 9 - 12 )			
1300.00E+06	1300.00E+06	1300.00E+06	1300.00E+06
FC_J( 13 - 16 )			
1300.00E+06	1300.00E+06	1300.00E+06	1300.00E+06
FC_J( 17 - 20 )			
1300.00E+06	1300.00E+06	1300.00E+06	1300.00E+06
PHIPLS_J( 1 - 4 )			
0.00	0.00	0.00	0.00
PHIPLS_J( 5 - 8 )			
0.00	0.00	0.00	0.00
PHIPLS_J( 9 - 12 )			
0.00	0.00	0.00	0.00
PHIPLS_J( 13 - 16 )			
0.00	0.00	0.00	0.00
PHIPLS_J( 17 - 20 )			
0.00	0.00	0.00	0.00
TARGET PARAMETERS			
-----			
TARGRNG	SIGMA_T	PHIPLSE	TARGALT
28.9785116	3.16E00	0.50	0.0
NOISE PARAMETERS			
-----			
F_N			
12.06			
LOSSES PARAMETERS			
-----			

Figure C-1. Input File for Sidelobe Jammer Nulling With Elevation Degrees of Freedom  
(Continued)



L_S	L_T	ILOSS	
0.00	0.00	0	
GENERAL PROCESSING PARAMETERS			
-----			
NP	IUSMTI	IADAPT	IELEM
1	0	1	1
IREADQC	IPRINTQC	IPRNTTEIG	ICORR
0	1	1	0
NTAP	DTDL	ITAC	
1	0.5E-06	2	
SUBARRAY PROCESSING PARAMETERS			
-----			
NSUB_AZ	NEL_SUB	NOVRLAP	
1	1	0	
NSUB_EL	NEL_SUB2	NOVRLAP2	
20	1	0	
BEAM SPACE PROCESSING PARAMETERS			
-----			
NBEAM	NLKB	NDFT	
50	50	50	
RECEIVE ANTENNA PATTERN PARAMETERS			
-----			
NPTS	PASCN1	DPASCN	
1	00.00	0.001	
NPTS2	PASCN2	DPASCN2	IPLOTP
1	-0.50	0.10	1
NPTS3	PASCN3	DPASCN3	
501	-1.00	0.004	
DOPPLER PROCESSING PARAMETERS			
-----			
NCI	IDWT	SLDBDOP	NDOP
0	0	100.0	32
NEAR-FIELD SCATTERING PARAMETERS			
-----			
NUMQ	ITARGQ		
0	0		
XQ	YQ	ZQ	BCSQ
-3.50	6.06	0.01	2.0000
-3.75	6.50	0.01	2.0000
-4.00	6.92	0.01	2.0000
-4.25	7.36	0.01	2.0000
-4.50	7.79	0.01	2.0000

Figure C-1. Input File for Sidelobe Jammer Nulling With Elevation Degrees of Freedom  
(Concluded)

	ADAPTIVE	QUIESCENT
$(J+N) / N$	8.212	44.018
$(C+N) / N$	0.000	0.000
$S / I$	28.874	-6.907
$S / N$	37.086	37.110
$(S/I)/(S/I)$ a q	35.781	
$(S/I)/(S/N)$ a q	-8.24	

Figure C-2. Output File 11 for Sidelobe Jammer Nulling With Elevation Degrees of Freedom

# RADAR PARAMETERS

```

-----
NFR          DEFR          TIME_BW
1            1.00E06        2000.0

FC           FREP           XMT_PWR
1300.0E06    1400.0        5.60E04

PLATALT      VELNM
30000.0      350.0
  
```

# ANTENNA PARAMETERS

```

-----
NUMAZIM      NUMELEV      DEWL      DEWLELEV
30           8            0.50      0.50

NBAR         NBARELEV     SLLDB     SLDBELEV
5            5            30.0      30.0

ITAPER       THS          THS_EL     THSC1
1            00.00        2.772     90.00

ITPRSUB      NBARSUB      SLDBSUB
1            5            30.0

ISUBTPR      NSUBBAR      SUBSLDB
1            5            30.0

ITPRSUB2     NBARSUB2     SLDBSUB2
1            5            30.0

ISUBTPR2     NSUBBAR2     SUBSLDB2
1            5            30.0

TH_AZ3DB     TH_EL3DB     CANRATDB
10.00        7.00        130.00

IELPG        ITPRFILE
0            0
  
```

# CLUTTER PARAMETERS

```

-----
NCL          DTTHC        SIGMA_V
181          1.0          4.0E-10

GAMMA        ICLUT
-9.0         0
  
```

# JAMMING PARAMETERS

```

-----
NESI         IDCORRJ
0            0

TTHJ( 1 - 4 )
20.0E+00     00.0E+00     0.0E+00     0.0E+00

TTHJ( 5 - 8 )
00.0E+00     00.0E+00     0.0E+00     0.0E+00
  
```

Figure C-3. Input File for Clutter Cancellation With Elevation Degrees of Freedom

TTHJ( 9 - 12 )			
00.0E+00	00.0E+00	0.0E+00	0.0E+00
TTHJ( 13 - 16 )			
00.0E+00	00.0E+00	0.0E+00	0.0E+00
TTHJ( 17 - 20 )			
00.0E+00	00.0E+00	0.0E+00	0.0E+00
RNG_JAM( 1 - 4 )			
60.0E+00	60.0E+00	00.0E+00	00.0E+00
RNG_JAM( 5 - 8 )			
00.0E+00	00.0E+00	00.0E+00	00.0E+00
RNG_JAM( 9 - 12 )			
00.0E+00	00.0E+00	00.0E+00	00.0E+00
RNG_JAM( 13 - 16 )			
00.0E+00	00.0E+00	00.0E+00	00.0E+00
RNG_JAM( 17 - 20 )			
00.0E+00	00.0E+00	00.0E+00	00.0E+00
P( 1 - 4 )			
2.87E+06	2.35E+04	0.00E+00	0.00E+00
P( 5 - 8 )			
0.00E+00	0.00E+00	0.00E+00	0.00E+00
P( 9 - 12 )			
0.00E+00	0.00E+00	0.00E+00	0.00E+00
P( 13 - 16 )			
0.00E+00	0.00E+00	0.00E+00	0.00E+00
P( 17 - 20 )			
0.00E+00	0.00E+00	0.00E+00	0.00E+00
THJ_EL( 1 - 4 )			
00.0E+00	00.0E+00	00.0E+00	00.0E+00
THJ_EL( 5 - 8 )			
00.0E+00	00.0E+00	00.0E+00	00.0E+00
THJ_EL( 9 - 12 )			
00.0E+00	00.0E+00	00.0E+00	00.0E+00
THJ_EL( 13 - 16 )			
00.0E+00	00.0E+00	00.0E+00	00.0E+00
THJ_EL( 17 - 20 )			
00.0E+00	00.0E+00	00.0E+00	00.0E+00
NFR_J( 1 - 4 )			
1	1	1	1
NFR_J( 5 - 8 )			
1	1	1	1
NFR_J( 9 - 12 )			
1	1	1	1
NFR_J( 13 - 16 )			
1	1	1	1

Figure C-3. Input File for Clutter Cancellation With Elevation Degrees of Freedom  
(Continued)

NFR_J( 17 - 20 )			
1	1	1	1
DEFR_J( 1 - 4 )			
4.00E+06	0.00E+06	0.00E+06	0.00E+06
DEFR_J( 5 - 8 )			
1.00E+06	0.00E+06	0.00E+06	0.00E+06
DEFR_J( 9 - 12 )			
1.00E+06	0.00E+06	0.00E+06	0.00E+06
DEFR_J( 13 - 16 )			
1.00E+06	0.00E+06	0.00E+06	0.00E+06
DEFR_J( 17 - 20 )			
1.00E+06	0.00E+06	0.00E+06	0.00E+06
FC_J( 1 - 4 )			
1300.00E+06	1300.00E+06	1300.00E+06	1300.00E+06
FC_J( 5 - 8 )			
1300.00E+06	1300.00E+06	1300.00E+06	1300.00E+06
FC_J( 9 - 12 )			
1300.00E+06	1300.00E+06	1300.00E+06	1300.00E+06
FC_J( 13 - 16 )			
1300.00E+06	1300.00E+06	1300.00E+06	1300.00E+06
FC_J( 17 - 20 )			
1300.00E+06	1300.00E+06	1300.00E+06	1300.00E+06
PHIPLS_J( 1 - 4 )			
0.00	0.00	0.00	0.00
PHIPLS_J( 5 - 8 )			
0.00	0.00	0.00	0.00
PHIPLS_J( 9 - 12 )			
0.00	0.00	0.00	0.00
PHIPLS_J( 13 - 16 )			
0.00	0.00	0.00	0.00
PHIPLS_J( 17 - 20 )			
0.00	0.00	0.00	0.00
TARGET PARAMETERS			
-----			
TARGRNG	SIGMA_T	PHIPLSE	TARGALT
178.66	3.16E00	0.50	0.0
NOISE PARAMETERS			
-----			
F_N			
12.06			
LOSSES PARAMETERS			
-----			

Figure C-3. Input File for Clutter Cancellation With Elevation Degrees of Freedom  
(Continued)

L_S	L_T	ILOSS	
0.00	0.00	0	

-----

GENERAL PROCESSING PARAMETERS

-----

NP	IUSMTI	IADAPT	IELEM
1	0	1	1
IREADQC	IPRINTQC	IPRNTEIG	ICORR
0	1	1	0
NTAP	DTDL	ITAC	
1	6.0E-07	2	

-----

SUBARRAY PROCESSING PARAMETERS

-----

NSUB_AZ	NEL_SUB	NOVRLAP
1	30	0
NSUB_EL	NEL_SUB2	NOVRLAP2
8	1	0

-----

BEAM SPACE PROCESSING PARAMETERS

-----

NBEAM	NLKB	NDFT
50	50	50

-----

RECEIVE ANTENNA PATTERN PARAMETERS

-----

NPTS	PASCN1	DPASCN	
1	0.000	0.001	
NPTS2	PASCN2	DPASCN2	IPLOTP
1	-0.50	0.10	1
NPTS3	PASCN3	DPASCN3	
1001	-1.000	0.002	

-----

DOPPLER PROCESSING PARAMETERS

-----

NCI	IDWT	SLDBDOP	NDOP
0	0	100.0	32

-----

NEAR-FIELD SCATTERING PARAMETERS

-----

NUMQ	ITARGQ		
0	0		
XQ	YQ	ZQ	BCSQ
-3.50	6.06	0.01	2.0000
-3.75	6.50	0.01	2.0000
-4.00	6.92	0.01	2.0000
-4.25	7.36	0.01	2.0000
-4.50	7.79	0.01	2.0000

Figure C-3. Input File for Clutter Cancellation With Elevation Degrees of Freedom  
(Concluded)

	ADAPTIVE	QUIESCENT
$(J+N) / N$	0.000	0.000
$(C+N) / N$	0.338	60.102
$S / I$	-40.457	-54.365
$S / N$	-40.119	5.738
$(S/I)/(S/I)$ a q	13.907	
$(S/I)/(S/N)$ a q	-46.20	

Figure C-4. Output File 11 for Clutter Cancellation With Elevation Degrees of Freedom

### **C.3 EFFECTS OF NEAR-FIELD POINT SCATTERERS ON SIDELobe JAMMER NULLING**

In Section 2.2.1, we illustrated how the presence of near-field point scatterers affects the nulling of a sidelobe jammer. Figure C-5 shows the input file of the simulation for the case when eleven near-field point scatterers ( $NUMQ = 11$ ) are modeled. The "quiescent" and "adaptive" curves of Figure 13 are obtained by plotting the quiescent and adapted elevation receive antenna gains (columns 3 and 4 of output file 13, respectively) versus elevation (arcsine of column 2 of output file 13). Note that for conciseness, output file 13 is not shown. Figure C-6 shows the performance measures from output file 11 used to obtain Figure 14. Figures 11 and 12 are similarly obtained by changing the value of  $NUMQ$  from eleven to zero.

### **C.4 EFFECTS OF NEAR-FIELD POINT SCATTERERS ON CLUTTER CANCELLATION**

In Section 2.2.2, we illustrated how the presence of near-field point scatterers affects the cancellation of clutter. Figure C-7 shows the input file of the simulation for the case when eleven near-field point scatterers ( $NUMQ = 11$ ), four antenna columns ( $NUMAZIM = 4$ ,  $NSUB\_AZ = 4$ ), and three pulses ( $NP = 3$ ) are modeled. Figure C-8 shows the performance measures from output file 11. The parametric curves of Figure 16 are obtained by plotting the adapted SIR, changing the number of antenna columns from four to eight or twelve, and varying the number of pulses from three to six. Note that the adapted SIR are normalized by the achieved adapted SIR in the noise-only case ( $NCL = 0$ ). Figure 15 is similarly obtained by changing the value of  $NUMQ$  from eleven to zero.

### **C.5 ELLIPTICAL ARRAY EXAMPLE**

In Section 2.3, we illustrated how an elliptical array can be modeled by reading additional elemental taper weights from a file. Figure C-9 shows the input file of the simulation for this example when the target range ( $TARGRNG$ ) is 153.3150 nautical miles. The curve of



# RADAR PARAMETERS

NFR	DEFR	TIME_BW
1	1.00E06	100.0
FC	FREP	XMT_PWR
1300.0E06	1200.0	1.00E06
PLATALT	VELNM	
30000.0	350.0	

# ANTENNA PARAMETERS

NUMAZIM	NUMELEV	DEWL	DEWLELEV
16	1	0.50	0.50
NBAR	NBARELEV	SLLDB	SLDBELEV
5	5	30.0	30.0
ITAPER	THS	THS_EL	THSC1
0	00.00	3.4	90.00
ITPRSUB	NBARSUB	SLDBSUB	
0	5	30.0	
ISUBTPR	NSUBBAR	SUBSLDB	
0	5	30.0	
ITPRSUB2	NBARSUB2	SLDBSUB2	
1	5	30.0	
ISUBTPR2	NSUBBAR2	SUBSLDB2	
1	5	30.0	
TH_AZ3DB	TH_EL3DB	CANRATDB	
10.00	7.00	50.00	
IELPG	ITPRFILE		
0	0		

# CLUTTER PARAMETERS

NCL	DTTHC	SIGMA_V
0	1.0	1.0E-01
GAMMA	ICLUT	
-9.0	0	

# JAMMING PARAMETERS

NESI	IDCORRJ		
1	0		
TTHJ( 1 - 4 )			
-43.0E+00	00.0E+00	0.0E+00	0.0E+00
TTHJ( 5 - 8 )			
00.0E+00	00.0E+00	0.0E+00	0.0E+00

Figure C-5. Input File for Sidelobe Jammer Nulling With Near-Field Scattering

TTHJ( 9 - 12 )			
00.0E+00	00.0E+00	0.0E+00	0.0E+00
TTHJ( 13 - 16 )			
00.0E+00	00.0E+00	0.0E+00	0.0E+00
TTHJ( 17 - 20 )			
00.0E+00	00.0E+00	0.0E+00	0.0E+00
RNG_JAM( 1 - 4 )			
100.0E+00	60.0E+00	00.0E+00	00.0E+00
RNG_JAM( 5 - 8 )			
00.0E+00	00.0E+00	00.0E+00	00.0E+00
RNG_JAM( 9 - 12 )			
00.0E+00	00.0E+00	00.0E+00	00.0E+00
RNG_JAM( 13 - 16 )			
00.0E+00	00.0E+00	00.0E+00	00.0E+00
RNG_JAM( 17 - 20 )			
00.0E+00	00.0E+00	00.0E+00	00.0E+00
P( 1 - 4 )			
2.00E+04	2.35E+04	0.00E+00	0.00E+00
P( 5 - 8 )			
0.00E+00	0.00E+00	0.00E+00	0.00E+00
P( 9 - 12 )			
0.00E+00	0.00E+00	0.00E+00	0.00E+00
P( 13 - 16 )			
0.00E+00	0.00E+00	0.00E+00	0.00E+00
P( 17 - 20 )			
0.00E+00	0.00E+00	0.00E+00	0.00E+00
THJ_EL( 1 - 4 )			
3.4E+00	00.0E+00	00.0E+00	00.0E+00
THJ_EL( 5 - 8 )			
00.0E+00	00.0E+00	00.0E+00	00.0E+00
THJ_EL( 9 - 12 )			
00.0E+00	00.0E+00	00.0E+00	00.0E+00
THJ_EL( 13 - 16 )			
00.0E+00	00.0E+00	00.0E+00	00.0E+00
THJ_EL( 17 - 20 )			
00.0E+00	00.0E+00	00.0E+00	00.0E+00
NFR_J( 1 - 4 )			
1	1	1	1
NFR_J( 5 - 8 )			
1	1	1	1
NFR_J( 9 - 12 )			
1	1	1	1
NFR_J( 13 - 16 )			
1	1	1	1

Figure C-5. Input File for Sidelobe Jammer Nulling With Near-Field Scattering (Continued)

NFR_J( 17 - 20 )			
1	1	1	1
DEFR_J( 1 - 4 )			
1.00E+06	0.00E+06	0.00E+06	0.00E+06
DEFR_J( 5 - 8 )			
1.00E+06	0.00E+06	0.00E+06	0.00E+06
DEFR_J( 9 - 12 )			
1.00E+06	0.00E+06	0.00E+06	0.00E+06
DEFR_J( 13 - 16 )			
1.00E+06	0.00E+06	0.00E+06	0.00E+06
DEFR_J( 17 - 20 )			
1.00E+06	0.00E+06	0.00E+06	0.00E+06
FC_J( 1 - 4 )			
1300.00E+06	1300.00E+06	1300.00E+06	1300.00E+06
FC_J( 5 - 8 )			
1300.00E+06	1300.00E+06	1300.00E+06	1300.00E+06
FC_J( 9 - 12 )			
1300.00E+06	1300.00E+06	1300.00E+06	1300.00E+06
FC_J( 13 - 16 )			
1300.00E+06	1300.00E+06	1300.00E+06	1300.00E+06
FC_J( 17 - 20 )			
1300.00E+06	1300.00E+06	1300.00E+06	1300.00E+06
PHIPLS_J( 1 - 4 )			
0.00	0.00	0.00	0.00
PHIPLS_J( 5 - 8 )			
0.00	0.00	0.00	0.00
PHIPLS_J( 9 - 12 )			
0.00	0.00	0.00	0.00
PHIPLS_J( 13 - 16 )			
0.00	0.00	0.00	0.00
PHIPLS_J( 17 - 20 )			
0.00	0.00	0.00	0.00
TARGET PARAMETERS			
-----			
TARGRNG	SIGMA_T	PHIPLSE	TARGALT
100.0	3.16E02	0.50	0.0
NOISE PARAMETERS			
-----			
F_N			
2.06			
LOSSES PARAMETERS			
-----			

Figure C-5. Input File for Sidelobe Jammer Nulling With Near-Field Scattering (Continued)

L_S	L_T	ILOSS	
0.00	0.00	0	

GENERAL PROCESSING PARAMETERS

---

NP	IUSMTI	IADAPT	IELEM
1	0	1	1
IREADQC	IPRINTQC	IPRNTEIG	ICORR
0	0	0	0
NTAP	DTDLE	ITAC	
1	1.0E-06	2	

SUBARRAY PROCESSING PARAMETERS

---

NSUB_AZ	NEL_SUB	NOVRLAP
16	1	0
NSUB_EL	NEL_SUB2	NOVRLAP2
1	1	0

BEAM SPACE PROCESSING PARAMETERS

---

NBEAM	NLKB	NDFT
50	50	50

RECEIVE ANTENNA PATTERN PARAMETERS

---

NPTS	PASCN1	DPASCN	
1001	-1.000	0.002	
NPTS2	PASCN2	DPASCN2	IPLOTP
1	-0.50	0.10	1
NPTS3	PASCN3	DPASCN3	
1	0.0593063	0.001	

DOPPLER PROCESSING PARAMETERS

---

NCI	IDWT	SLDBDOP	NDOP
0	0	100.0	32

NEAR-FIELD SCATTERING PARAMETERS

---

NUMQ	ITARGQ		
11	0		
XQ	YQ	ZQ	BCSQ
-3.50	6.06	0.01	2.0000
-3.75	6.50	0.01	2.0000
-4.00	6.92	0.01	2.0000
-4.25	7.36	0.01	2.0000
-4.50	7.79	0.01	2.0000

Figure C-5. Input File for Sidelobe Jammer Nulling With Near-Field Scattering (Continued)

-4.75	8.23	0.01	2.0000
-5.00	8.66	0.01	2.0000
-5.25	9.09	0.01	2.0000
-5.50	9.53	0.01	2.0000
-5.75	9.96	0.01	2.0000
-6.00	10.39	0.01	2.0000

Figure C-5. Input File for Sidelobe Jammer Nulling With Near-Field Scattering (Concluded)

	ADAPTIVE	QUIESCENT
$(J+N) / N$	6.345	51.606
$(C+N) / N$	0.000	0.000
$S / I$	16.966	-27.085
$S / N$	23.311	24.521
$(S/I)/(S/I)$ a q	44.051	
$(S/I)/(S/N)$ a q	-7.56	

Figure C-6. Output File 11 for Sidelobe Jammer Nulling With Near-Field Scattering

# RADAR PARAMETERS

NFR	DEFR	TIME_BW
1	1.00E06	100.0
FC	FREP	XMT_PWR
1300.0E06	1200.0	1.00E06
PLATALT	VELNM	
30000.0	350.0	

# ANTENNA PARAMETERS

NUMAZIM	NUMELEV	DEWL	DEWLELEV
4	1	0.50	0.50
NBAR	NBARELEV	SLLDB	SLDBELEV
5	5	30.0	30.0
ITAPER	THS	THS_EL	THSC1
0	00.00	2.772	90.00
ITPRSUB	NBARSUB	SLDBSUB	
0	5	30.0	
ISUBTPR	NSUBBAR	SUBSLDB	
0	5	30.0	
ITPRSUB2	NBARSUB2	SLDBSUB2	
1	5	30.0	
ISUBTPR2	NSUBBAR2	SUBSLDB2	
1	5	30.0	
TH_AZ3DB	TH_EL3DB	CANRATDB	
10.00	7.00	130.00	
IELPG	ITPRFILE		
0	0		

# CLUTTER PARAMETERS

NCL	DTHC	SIGMA_V
181	1.0	1.0E-01
GAMMA	ICLUT	
-9.0	0	

# JAMMING PARAMETERS

NESI	IDCORRJ		
0	0		
TTHJ( 1 - 4 )			
20.0E+00	00.0E+00	0.0E+00	0.0E+00
TTHJ( 5 - 8 )			
00.0E+00	00.0E+00	0.0E+00	0.0E+00

Figure C-7. Input File for Clutter Cancellation With Near-Field Scattering

TTHJ( 9 - 12 )			
00.0E+00	00.0E+00	0.0E+00	0.0E+00
TTHJ( 13 - 16 )			
00.0E+00	00.0E+00	0.0E+00	0.0E+00
TTHJ( 17 - 20 )			
00.0E+00	00.0E+00	0.0E+00	0.0E+00
RNG_JAM( 1 - 4 )			
60.0E+00	60.0E+00	00.0E+00	00.0E+00
RNG_JAM( 5 - 8 )			
00.0E+00	00.0E+00	00.0E+00	00.0E+00
RNG_JAM( 9 - 12 )			
00.0E+00	00.0E+00	00.0E+00	00.0E+00
RNG_JAM( 13 - 16 )			
00.0E+00	00.0E+00	00.0E+00	00.0E+00
RNG_JAM( 17 - 20 )			
00.0E+00	00.0E+00	00.0E+00	00.0E+00
P( 1 - 4 )			
2.87E+06	2.35E+04	0.00E+00	0.00E+00
P( 5 - 8 )			
0.00E+00	0.00E+00	0.00E+00	0.00E+00
P( 9 - 12 )			
0.00E+00	0.00E+00	0.00E+00	0.00E+00
P( 13 - 16 )			
0.00E+00	0.00E+00	0.00E+00	0.00E+00
P( 17 - 20 )			
0.00E+00	0.00E+00	0.00E+00	0.00E+00
THJ_EL( 1 - 4 )			
00.0E+00	00.0E+00	00.0E+00	00.0E+00
THJ_EL( 5 - 8 )			
00.0E+00	00.0E+00	00.0E+00	00.0E+00
THJ_EL( 9 - 12 )			
00.0E+00	00.0E+00	00.0E+00	00.0E+00
THJ_EL( 13 - 16 )			
00.0E+00	00.0E+00	00.0E+00	00.0E+00
THJ_EL( 17 - 20 )			
00.0E+00	00.0E+00	00.0E+00	00.0E+00
NFR_J( 1 - 4 )			
1	1	1	1
NFR_J( 5 - 8 )			
1	1	1	1
NFR_J( 9 - 12 )			
1	1	1	1
NFR_J( 13 - 16 )			
1	1	1	1

Figure C-7. Input File for Clutter Cancellation With Near-Field Scattering (Continued)



NFR_J( 17 - 20 )			
1	1	1	1
DEFR_J( 1 - 4 )			
4.00E+06	0.00E+06	0.00E+06	0.00E+06
DEFR_J( 5 - 8 )			
1.00E+06	0.00E+06	0.00E+06	0.00E+06
DEFR_J( 9 - 12 )			
1.00E+06	0.00E+06	0.00E+06	0.00E+06
DEFR_J( 13 - 16 )			
1.00E+06	0.00E+06	0.00E+06	0.00E+06
DEFR_J( 17 - 20 )			
1.00E+06	0.00E+06	0.00E+06	0.00E+06
FC_J( 1 - 4 )			
1300.00E+06	1300.00E+06	1300.00E+06	1300.00E+06
FC_J( 5 - 8 )			
1300.00E+06	1300.00E+06	1300.00E+06	1300.00E+06
FC_J( 9 - 12 )			
1300.00E+06	1300.00E+06	1300.00E+06	1300.00E+06
FC_J( 13 - 16 )			
1300.00E+06	1300.00E+06	1300.00E+06	1300.00E+06
FC_J( 17 - 20 )			
1300.00E+06	1300.00E+06	1300.00E+06	1300.00E+06
PHIPLS_J( 1 - 4 )			
0.00	0.00	0.00	0.00
PHIPLS_J( 5 - 8 )			
0.00	0.00	0.00	0.00
PHIPLS_J( 9 - 12 )			
0.00	0.00	0.00	0.00
PHIPLS_J( 13 - 16 )			
0.00	0.00	0.00	0.00
PHIPLS_J( 17 - 20 )			
0.00	0.00	0.00	0.00
TARGET PARAMETERS			
-----			
TARGRNG	SIGMA_T	PHIPLSE	TARGALT
100.0	3.16E02	0.50	0.0
NOISE PARAMETERS			
-----			
F_N			
2.06			
LOSSES PARAMETERS			
-----			

Figure C-7. Input File for Clutter Cancellation With Near-Field Scattering (Continued)

L_S	L_T	ILOSS	
0.00	0.00	0	

GENERAL PROCESSING PARAMETERS

---

NP	IUSMTI	IADAPT	IELEM
3	0	1	1
IREADQC	IPRINTQC	IPRNTEIG	ICORR
0	0	0	0
NTAP	DTDLE	ITAC	
1	5.0E-07	2	

SUBARRAY PROCESSING PARAMETERS

---

NSUB_AZ	NEL_SUB	NOVRLAP
4	1	0
NSUB_EL	NEL_SUB2	NOVRLAP2
1	1	0

BEAM SPACE PROCESSING PARAMETERS

---

NBEAM	NLKB	NDFT
50	50	50

RECEIVE ANTENNA PATTERN PARAMETERS

---

NPTS	PASCN1	DPASCN	
1001	-1.00	0.002	
NPTS2	PASCN2	DPASCN2	IPLOTP
1	-0.50	0.10	1
NPTS3	PASCN3	DPASCN3	
1	0.0483616	0.001	

DOPPLER PROCESSING PARAMETERS

---

NCI	IDWT	SLDBDOP	NDOP
0	0	100.0	32

NEAR-FIELD SCATTERING PARAMETERS

---

NUMQ	ITARGQ		
11	0		
XQ	YQ	ZQ	BCSQ
-3.50	6.06	0.01	2.0000
-3.75	6.50	0.01	2.0000
-4.00	6.92	0.01	2.0000
-4.25	7.36	0.01	2.0000
-4.50	7.79	0.01	2.0000

Figure C-7. Input File for Clutter Cancellation With Near-Field Scattering (Continued)

-4.75	8.23	0.01	2.0000
-5.00	8.66	0.01	2.0000
-5.25	9.09	0.01	2.0000
-5.50	9.53	0.01	2.0000
-5.75	9.96	0.01	2.0000
-6.00	10.39	0.01	2.0000

Figure C-7. Input File for Clutter Cancellation With Near-Field Scattering (Concluded)

	ADAPTIVE	QUIESCENT
$(J+N) / N$	0.000	0.000
$(C+N) / N$	0.000	0.000
$S / I$	17.251	12.480
$S / N$	17.251	12.480
$(S/I)/(S/I)$ a q	4.771	
$(S/I)/(S/N)$ a q	4.77	

Figure C-8. Output File 11 for Clutter Cancellation With Near-Field Scattering

# RADAR PARAMETERS

```

-----
NFR          DEFR          TIME_BW
1            3.5E06        5.25

FC           FREP          XMT_PWR
3200.0E06    25000.0      1000.0E03

PLATALT      VELNM
29000.0      388.77
  
```

# ANTENNA PARAMETERS

```

-----
NUMAZIM      NUMELEV      DEWL          DEWLELEV
168          26          0.50          0.50

NBAR         NBARELEV     SLLDB        SLDBELEV
2            2           57.0         57.0

ITAPER       THS          THS_EL       THSC1
0            22.5        1.4         180.00

ITPRSUB      NBARSUB      SLDBSUB
0            5           30.0

ISUBTPR      NSUBBAR      SUBSLDB
0            5           30.0

ITPRSUB2     NBARSUB2     SLDBSUB2
0            5           30.0

ISUBTPR2     NSUBBAR2     SUBSLDB2
0            5           30.0

TH_AZ3DB     TH_EL3DB     CANRATDB
1.00         80.00       130.00

IELPG        ITPRFILE
2            1
  
```

# CLUTTER PARAMETERS

```

-----
NCL          DTTHC        SIGMA_V
241          0.75        1.0E-10

GAMMA        ICLUT
-9.0         0
  
```

# JAMMING PARAMETERS

```

-----
NESI         IDCORRJ
0            0

TTHJ( 1 - 4 )
20.0E+00     00.0E+00     0.0E+00     0.0E+00

TTHJ( 5 - 8 )
00.0E+00     00.0E+00     0.0E+00     0.0E+00
  
```

Figure C-9. Input File for Elliptical Array Example

TTHJ( 9 - 12 )			
00.0E+00	00.0E+00	0.0E+00	0.0E+00
TTHJ( 13 - 16 )			
00.0E+00	00.0E+00	0.0E+00	0.0E+00
TTHJ( 17 - 20 )			
00.0E+00	00.0E+00	0.0E+00	0.0E+00
RNG_JAM( 1 - 4 )			
60.0E+00	60.0E+00	00.0E+00	00.0E+00
RNG_JAM( 5 - 8 )			
00.0E+00	00.0E+00	00.0E+00	00.0E+00
RNG_JAM( 9 - 12 )			
00.0E+00	00.0E+00	00.0E+00	00.0E+00
RNG_JAM( 13 - 16 )			
00.0E+00	00.0E+00	00.0E+00	00.0E+00
RNG_JAM( 17 - 20 )			
00.0E+00	00.0E+00	00.0E+00	00.0E+00
P( 1 - 4 )			
2.87E+06	2.35E+04	0.00E+00	0.00E+00
P( 5 - 8 )			
0.00E+00	0.00E+00	0.00E+00	0.00E+00
P( 9 - 12 )			
0.00E+00	0.00E+00	0.00E+00	0.00E+00
P( 13 - 16 )			
0.00E+00	0.00E+00	0.00E+00	0.00E+00
P( 17 - 20 )			
0.00E+00	0.00E+00	0.00E+00	0.00E+00
THJ_EL( 1 - 4 )			
00.0E+00	00.0E+00	00.0E+00	00.0E+00
THJ_EL( 5 - 8 )			
00.0E+00	00.0E+00	00.0E+00	00.0E+00
THJ_EL( 9 - 12 )			
00.0E+00	00.0E+00	00.0E+00	00.0E+00
THJ_EL( 13 - 16 )			
00.0E+00	00.0E+00	00.0E+00	00.0E+00
THJ_EL( 17 - 20 )			
00.0E+00	00.0E+00	00.0E+00	00.0E+00
NFR_J( 1 - 4 )			
1	1	1	1
NFR_J( 5 - 8 )			
1	1	1	1
NFR_J( 9 - 12 )			
1	1	1	1
NFR_J( 13 - 16 )			
1	1	1	1

Figure C-9. Input File for Elliptical Array Example (Continued)

NFR_J( 17 - 20 )			
1	1	1	1
DEFR_J( 1 - 4 )			
4.00E+06	0.00E+06	0.00E+06	0.00E+06
DEFR_J( 5 - 8 )			
1.00E+06	0.00E+06	0.00E+06	0.00E+06
DEFR_J( 9 - 12 )			
1.00E+06	0.00E+06	0.00E+06	0.00E+06
DEFR_J( 13 - 16 )			
1.00E+06	0.00E+06	0.00E+06	0.00E+06
DEFR_J( 17 - 20 )			
1.00E+06	0.00E+06	0.00E+06	0.00E+06
FC_J( 1 - 4 )			
1300.00E+06	1300.00E+06	1300.00E+06	1300.00E+06
FC_J( 5 - 8 )			
1300.00E+06	1300.00E+06	1300.00E+06	1300.00E+06
FC_J( 9 - 12 )			
1300.00E+06	1300.00E+06	1300.00E+06	1300.00E+06
FC_J( 13 - 16 )			
1300.00E+06	1300.00E+06	1300.00E+06	1300.00E+06
FC_J( 17 - 20 )			
1300.00E+06	1300.00E+06	1300.00E+06	1300.00E+06
PHIPLS_J( 1 - 4 )			
0.00	0.00	0.00	0.00
PHIPLS_J( 5 - 8 )			
0.00	0.00	0.00	0.00
PHIPLS_J( 9 - 12 )			
0.00	0.00	0.00	0.00
PHIPLS_J( 13 - 16 )			
0.00	0.00	0.00	0.00
PHIPLS_J( 17 - 20 )			
0.00	0.00	0.00	0.00
TARGET PARAMETERS			
-----			
TARGRNG	SIGMA_T	PHIPLSE	TARGALT
153.3150	1.00E-01	0.50	1000.0
(Range 1 = 150.5612 nmi ; range resolution = 0.0231 nmi)			
NOISE PARAMETERS			
-----			
F_N			
2.00			
LOSSES PARAMETERS			
-----			

Figure C-9. Input File for Elliptical Array Example (Continued)

L_S	L_T	ILOSS	
8.9	0.00	0	

GENERAL PROCESSING PARAMETERS

---

NP	IUSMTI	IADAPT	IELEM
1	0	0	1
IREADQC	IPRINTQC	IPRNTSIG	ICORR
0	0	0	0
NTAP	DTDLE	ITAC	
1	6.0E-07	2	

SUBARRAY PROCESSING PARAMETERS

---

NSUB_AZ	NEL_SUB	NOVRLAP
1	168	0
NSUB_EL	NEL_SUB2	NOVRLAP2
1	26	0

BEAM SPACE PROCESSING PARAMETERS

---

NBEAM	NLKB	NDFT
50	50	50

RECEIVE ANTENNA PATTERN PARAMETERS

---

NPTS	PASCN1	DPASCN	
1	0.000	0.001	
NPTS2	PASCN2	DPASCN2	IPLTF
1	-0.50	0.10	0
NPTS3	PASCN3	DPASCN3	
1	-1.000	0.002	

DOPPLER PROCESSING PARAMETERS

---

NCI	IDWT	SLDBDOP	NDOP
256	3	90.0	256

NEAR-FIELD SCATTERING PARAMETERS

---

NUMQ	ITARGQ		
0	0		
XQ	YQ	ZQ	BCSQ
-3.50	6.06	0.01	2.0000
-3.75	6.50	0.01	2.0000
-4.00	6.92	0.01	2.0000
-4.25	7.36	0.01	2.0000
-4.50	7.79	0.01	2.0000

Figure C-9. Input File for Elliptical Array Example (Concluded)



Figure 18 is obtained by plotting the quiescent clutter-plus-noise-to-noise ratio (CNR) (Column 2 of output file 16) versus frequency (Column 1 of output file 16), and varying the target range (*TARGRNG*) from 150.5612 to 153.7778 in steps of 0.0231. The curve of Figure 17 is obtained by plotting the amplitude of the elemental taper weights of input file 150 versus the antenna row and column indices. Note that for conciseness, input file 150 and output file 16 are not shown.

## C.6 ILLUSTRATIVE MCARM EXAMPLE

In Section 2.4, we showed how the simulation can be used for Rome Laboratory's MCARM Program. Figure C-10 shows the input file of the simulation for this example when the target range (*TARGRNG*) is 41.31 nautical miles and using non-adaptive processing (*IADAPT* = 0). The curves for Figures 19 and 20 are obtained by plotting the non-adapted CNR (Column 6 of output file 16) versus frequency (Column 1 of output file 16), and varying the target range (*TARGRNG*) from 41.3068 to 81.8036 in steps of 0.4050. The curves of Figures 21 and 22 are obtained by plotting the non-adapted signal-to-clutter-plus-noise ratio versus frequency and range. Note that conciseness, output file 16 is not shown. Figures 23 through 26 are obtained by running the simulation in the adaptive mode (*IADAPT* = 1) and having *NP* = 2, *NSUB\_AZ* = 12, *NEL\_SUB* = 1, *NSUB\_EL* = 2, and *NEL\_SUB* 2= 4.

# RADAR PARAMETERS

-----

NFR	DEFR	TIME_BW
1	1.00E06	100.0
FC	FREP	XMT_PWR
1250.0E06	2000.0	14.40E03
PLATALT	VELNM	
4921.5	219.65	

# ANTENNA PARAMETERS

-----

NUMAZIM	NUMELEV	DEWL	DEWLELEV
12	8	0.454167	0.5875
NBAR	NBARELEV	SLLDB	SLDBELEV
5	1	57.0	15.0
ITAPER	THS	THS_EL	THSC1
0	14.5	2.5	90.00
ITPRSUB	NBARSUB	SLDBSUB	
1	4	35.0	
ISUBTPR	NSUBBAR	SUBSLDB	
1	4	35.0	
ITPRSUB2	NBARSUB2	SLDBSUB2	
0	5	30.0	
ISUBTPR2	NSUBBAR2	SUBSLDB2	
0	5	30.0	
TH_AZ3DB	TH_EL3DB	CANRATDB	
13.0	12.80	60.00	
IELPG	ITPRFILE		
2	0		

# CLUTTER PARAMETERS

-----

NCL	DTHC	SIGMA_V
361	0.5	4.0E-10
GAMMA	ICLUT	
-9.0	1	

# JAMMING PARAMETERS

-----

NESI	IDCORRJ		
0	0		
TTHJ( 1 - 4 )			
00.0E+00	00.0E+00	0.0E+00	0.0E+00
TTHJ( 5 - 8 )			
00.0E+00	00.0E+00	0.0E+00	0.0E+00

Figure C-10. Input File for Illustrative MCARM Example

TTHJ( 9 - 12 )			
00.0E+00	00.0E+00	0.0E+00	0.0E+00
TTHJ( 13 - 16 )			
00.0E+00	00.0E+00	0.0E+00	0.0E+00
TTHJ( 17 - 20 )			
00.0E+00	00.0E+00	0.0E+00	0.0E+00
RNG_JAM( 1 - 4 )			
9.0E+00	60.0E+00	00.0E+00	00.0E+00
RNG_JAM( 5 - 8 )			
00.0E+00	00.0E+00	00.0E+00	00.0E+00
RNG_JAM( 9 - 12 )			
00.0E+00	00.0E+00	00.0E+00	00.0E+00
RNG_JAM( 13 - 16 )			
00.0E+00	00.0E+00	00.0E+00	00.0E+00
RNG_JAM( 17 - 20 )			
00.0E+00	00.0E+00	00.0E+00	00.0E+00
P( 1 - 4 )			
3.00E+04	2.35E+04	0.00E+00	0.00E+00
P( 5 - 8 )			
0.00E+00	0.00E+00	0.00E+00	0.00E+00
P( 9 - 12 )			
0.00E+00	0.00E+00	0.00E+00	0.00E+00
P( 13 - 16 )			
0.00E+00	0.00E+00	0.00E+00	0.00E+00
P( 17 - 20 )			
0.00E+00	0.00E+00	0.00E+00	0.00E+00
THJ_EL( 1 - 4 )			
32.0E+00	00.0E+00	00.0E+00	00.0E+00
THJ_EL( 5 - 8 )			
00.0E+00	00.0E+00	00.0E+00	00.0E+00
THJ_EL( 9 - 12 )			
00.0E+00	00.0E+00	00.0E+00	00.0E+00
THJ_EL( 13 - 16 )			
00.0E+00	00.0E+00	00.0E+00	00.0E+00
THJ_EL( 17 - 20 )			
00.0E+00	00.0E+00	00.0E+00	00.0E+00
NFR_J( 1 - 4 )			
1	1	1	1
NFR_J( 5 - 8 )			
1	1	1	1
NFR_J( 9 - 12 )			
1	1	1	1
NFR_J( 13 - 16 )			
1	1	1	1

Figure C-10. Input File for Illustrative MCARM Example (Continued)

NFR_J( 17 - 20 )			
1	1	1	1
DEFR_J( 1 - 4 )			
2.00E+06	0.00E+06	0.00E+06	0.00E+06
DEFR_J( 5 - 8 )			
1.00E+06	0.00E+06	0.00E+06	0.00E+06
DEFR_J( 9 - 12 )			
1.00E+06	0.00E+06	0.00E+06	0.00E+06
DEFR_J( 13 - 16 )			
1.00E+06	0.00E+06	0.00E+06	0.00E+06
DEFR_J( 17 - 20 )			
1.00E+06	0.00E+06	0.00E+06	0.00E+06
FC_J( 1 - 4 )			
1300.00E+06	1300.00E+06	1300.00E+06	1300.00E+06
FC_J( 5 - 8 )			
1300.00E+06	1300.00E+06	1300.00E+06	1300.00E+06
FC_J( 9 - 12 )			
1300.00E+06	1300.00E+06	1300.00E+06	1300.00E+06
FC_J( 13 - 16 )			
1300.00E+06	1300.00E+06	1300.00E+06	1300.00E+06
FC_J( 17 - 20 )			
1300.00E+06	1300.00E+06	1300.00E+06	1300.00E+06
PHIPLS_J( 1 - 4 )			
0.00	0.00	0.00	0.00
PHIPLS_J( 5 - 8 )			
0.00	0.00	0.00	0.00
PHIPLS_J( 9 - 12 )			
0.00	0.00	0.00	0.00
PHIPLS_J( 13 - 16 )			
0.00	0.00	0.00	0.00
PHIPLS_J( 17 - 20 )			
0.00	0.00	0.00	0.00
TARGET PARAMETERS			
-----			
TARGRNG	SIGMA_T	PHIPLSE	TARGALT
41.31	2.00E00	0.50	0000.0
NOISE PARAMETERS			
-----			
F_N			
2.50			
LOSSES PARAMETERS			
-----			

Figure C-10. Input File for Illustrative MCARM Example (Continued)

L_S	L_T	ILOSS
0.00	4.48	1

#### GENERAL PROCESSING PARAMETERS

NP	IUSMTI	IADAPT	IELEM
1	0	0	1
IREADQC	IPRINTQC	IPRNTEIG	ICORR
0	0	0	0
NTAP	DTDL	ITAC	
1	0.5E-06	2	

#### SUBARRAY PROCESSING PARAMETERS

NSUB_AZ	NEL_SUB	NOVRLAP
1	12	0
NSUB_EL	NEL_SUB2	NOVRLAP2
1	8	0

#### BEAM SPACE PROCESSING PARAMETERS

NBEAM	NLKB	NDFT
12	12	12

#### RECEIVE ANTENNA PATTERN PARAMETERS

NPTS	PASCN1	DPASCN	
1001	-1.00	0.002	
NPTS2	PASCN2	DPASCN2	IPLOTP
1	-0.50	0.10	0
NPTS3	PASCN3	DPASCN3	
1	0.04362	0.004	

#### DOPPLER PROCESSING PARAMETERS

NCI	IDWT	SLDBDOP	NDOP
200	3	100.0	200

#### NEAR-FIELD SCATTERING PARAMETERS

NUMQ	ITARGQ		
0	0		
XQ	YQ	ZQ	BCSQ
-3.50	6.06	0.01	2.0000
-3.75	6.50	0.01	2.0000
-4.00	6.92	0.01	2.0000
-4.25	7.36	0.01	2.0000
-4.50	7.79	0.01	2.0000

Figure C-10. Input File for Illustrative MCARM Example (Concluded)